

NDOT Research Report

Report No. 327-12-803

**Use of GEOGRID for Strengthening and
Reducing the Roadway Structural Sections**

January 2016

**Nevada Department of Transportation
1263 South Stewart Street
Carson City, NV 89712**



Disclaimer

This work was sponsored by the Nevada Department of Transportation. The contents of this report reflect the views of the authors, who are responsible for the facts and the accuracy of the data presented herein. The contents do not necessarily reflect the official views or policies of the State of Nevada at the time of publication. This report does not constitute a standard, specification, or regulation.

USE OF GEOGRID FOR STRENGTHENING AND REDUCING THE
ROADWAY STRUCTURAL SECTIONS

Final Report Submitted to
Nevada Department of Transportation

Nader Ghafoori, Ph.D., P.E.
Professor of Civil Engineering
AND
MohammadReza Sharbaf
Graduate Research Assistant
Department of Civil and Environmental Engineering and Construction
University of Nevada Las Vegas
4505 Maryland Parkway
Box 454015
Las Vegas, NV 89154-4015
Tel: (702) 895-2531
Fax: (702)895-3936
Email: nader.ghafoori@unlv.edu

January 2016

ABSTRACT

An experimental laboratory program to assess the effectiveness of biaxial and triaxial geogrid-reinforced flexible pavements to reduce roadway section was carried out. Six laboratory tests were conducted using a steel cylindrical mold with dimensions of 1.8 m (6 ft) in diameter and 2.1 m (7 ft) in height. The studied reinforced and unreinforced (without geogrid) sections consisted of a locally-obtained subgrade with a minimum thickness of 1.5 m (5 ft) and an asphaltic surface course of 7.6 cm (3 in). The base thickness of three tests was 30.5 cm (12 in) while for the other three tests used base thickness of 40.6 cm (16 in). A layer of biaxial or triaxial geogrid was placed at the mid-depth of aggregate base course for the tests with 40.6 cm (16 in) of aggregate base layer. For the tests which the base layer was 30.5 cm (12 in), the geogrid was placed at the subgrade-base interface. The instrumentations included pressure cells placed at different locations of the test sections, foil strain gauges installed on the ribs of geogrids, and LVDT placed on top of the loading system. These devices were connected to a data acquisition system. A hydraulic actuator provided 40 kN (9 kips) cyclic load through a 305 mm (12 in) circular steel plate at a frequency of 0.77 Hz. The repeated loading was continued for at least 3 million cycles for each test. Performances of biaxial-reinforced and triaxial-reinforced sections were compared with that of companion unreinforced sections.

Test results revealed that inclusion of both biaxial and triaxial geogrids in flexible pavement reduced the surface rutting and vertical stresses in the subgrade-base interface. For the studied geogrid-reinforced pavement sections, no tensile strain was experienced by the strain gauges installed on the ribs of the geogrids. The vertical pressure at the center of subgrade-base interface reduced by an average of 18 and 24% for biaxial and triaxial geogrid-reinforced pavement sections, respectively. Using the results of rutting depth, it was found that use of

geogrid increased the number of load applications by a factor of 1.5 to 7 depending on the test section and geogrid type, as well as rutting depth experienced at different loading applications. Using Base Course Reduction (BCR) method and the obtained rutting depth, inclusion of geogrid resulted in the base thickness reductions of 11 to 44 percent depending on the above-mentioned variables.

TABLE OF CONTENTS

ABSTRACT	II
TABLE OF CONTENTS	IV
LIST OF FIGURES	X
LIST OF TABLES.....	XIII
LIST OF EQUATIONS.....	XV
CHAPTER 1 INTRODUCTION.....	1
1.1. BACKGROUND.....	1
1.2. RESEARCH OBJECTIVES.....	1
1.3. CHAPTER BREAK DOWN.....	2
CHAPTER 2 LITERATURE REVIEW.....	3
2.1. GEOSYNTHETIC	3
2.1.1. Geosynthetic Definition	4
2.1.2. Functions of Geosynthetics.....	5
2.1.2.1. Reinforcement	6
2.1.2.1.1. Mechanisms involved in reinforcement function	7
2.1.2.2. Separation	8
2.1.2.3. Filtration	10
2.1.2.4. Lateral Drainage	12
2.1.2.5. Other Functions	12
2.1.3. Geonet.....	13
2.1.4. Geomembrane.....	14

2.1.5.	Geosynthetic Clay Liner	14
2.1.6.	Geocomposites.....	15
2.1.7.	Geotextile.....	16
2.1.7.1.	Geotextile production	17
2.1.7.2.	Functions of Geotextile	17
2.1.7.3.	Geotextile properties and test methods.....	19
2.1.8.	Geogrid	20
2.1.8.1.	Geogrid definition.....	21
2.1.8.2.	Geogrid Aperture.....	22
2.1.8.3.	Geogrid Production.....	24
2.1.8.4.	Geogrid Properties and Test Methods	25
2.1.8.5.	Function of Geogrid.....	25
2.1.8.5.1.	Lateral Confinement Mechanism	26
2.1.8.5.2.	Increase of the Bearing Capacity Mechanism	27
2.1.8.5.3.	Tension Membrane Mechanism	28
2.2.	PREVIOUS EXPERIMENTAL STUDIES USING GEOGRIDS.....	29
2.2.1.	Small- Scale Laboratory studies	30
2.2.1.1.	(Carroll, Walls, & Haas, 1987).....	30
2.2.1.2.	(Haas, Wall, & Carroll, 1988)	31
2.2.1.3.	(Al-Qadi, Brandon, Valentine, Lacina, & Smith, 1994).....	32
2.2.1.4.	(Montanelli, Zhao, & Rimoldi, 1997).....	32
2.2.1.5.	(Perkins S. , Geosynthetic Reinforcement of Flexible Pavements: Laboratory Based Pavement Test Sections, 1999)	33

2.2.1.6.	(Leng, Ju, & Gabr, 2002).....	34
2.2.1.7.	(Moghaddas-Nejad & Small, 2003).....	34
2.2.1.8.	(Perkins, et al., 2004).....	35
2.2.1.9.	(Nazzal, 2007)	35
2.2.1.10.	(Chen, Abu-Farsakh, & Tao, 2009).....	36
2.2.1.11.	(Abu-Farsakh & Chen, 2011)	37
2.2.1.12.	(Abu-Farsakh, Souci, Voyiadjis, & Chen, 2011)	38
2.2.1.13.	(Qian, Han, Pokharel, & Parsons, 2011)	38
2.2.2.	Large- Scale Field Investigation	39
2.2.2.1.	(Webster, 1993)	39
2.2.2.2.	(Cancelli & Montanelli, 1999).....	39
2.2.2.3.	(Perkins S. , Evaluation of geosynthetic reinforced flexible pavement systems using two pavement test facilities, 2002).....	40
2.2.2.4.	(Tingle & Webster, 2003).....	41
2.2.2.5.	(Aran, 2006).....	41
2.2.2.6.	(Helstrom, Humphrey, & Hayden, 2007)	42
2.2.2.7.	(Al-Qadi I. , Dessouky, Kwon, & Tutumluer, Geogrid in flexible pavements: validated mechanics, 2008).....	43
2.2.2.8.	(Duncan-Williams & Attoh-Okine, 2008).....	44
2.2.2.9.	(Henry, Clapp, Davids, Humphrey, & Barna, 2009).....	44
2.2.2.10.	(Cox, McCartney, Wood, & Curry, 2010).....	45
2.2.2.11.	(McCartney, Cox, Wood, & Curry, 2010).....	45
2.2.2.12.	(Al-Qadi I. , Dessouky, Tutumluer, & Kwon, 2011).....	46

2.2.2.13.	(Jersey, Tingle, Norwood, Kwon, & Wayne, 2012).....	47
2.2.2.14.	(Al-Qadi I. , Dessouky, Kwon, & Tutumluer, Geogrid-Reinforced Low- Volume Flexible Pavements: Pavement Response and Geogrid Optimal Location , 2012)	

CHAPTER 3	MATERIALS CHARACTERIZATION AND CYCLIC LOADING PLATE SYSTEM.....	49
3.1.	OVERVIEW	49
3.2.	PAVING MATERIALS CHARACTERISTICS.....	49
3.2.1.	Subgrade soil.....	49
3.2.2.	Base Course Aggregates	50
3.2.3.	Asphalt mixture.....	50
3.3.	GEOGRID INDEX AND MECHANICAL PROPERTIES	51
3.4.	MOLD DIMENSIONS AND CYCLIC LOADING SYSTEM.....	51
3.5.	INSTRUMENT SELECTION AND CALIBRATION	54
3.5.1.	Instrument for measuring vertical pressure.....	55
3.5.2.	Instrument for geogrid deformation measurement	57
3.5.3.	Instrument for asphalt surface deformation measurement.....	61
3.6.	DATA ACQUISITION SYSTEM.....	61
3.7.	TEST SECTION PREPARATION AND INSTRUMENTS INSTALLATION	61
3.7.1.	Test Section Preparation	61
CHAPTER 4	TEST RESULTS AND DISCUSSION.....	71
4.1.	OVERVIEW	71
4.2.	ASPHALT SURFACE DEFORMATION (RUTTING DEPTH).....	71

4.3.	VERTICAL STRESS DISTRIBUTION	74
4.4.	GEOGRID TENSILE STRAIN	79
CHAPTER 5 MODELING AND DESIGN METHODS.....		81
5.1.	SUMMARY	81
5.2.	MODELING OF FLEXIBLE PAVEMENTS	81
5.2.1.	Finite Element Modeling for Geogrid-Reinforced Flexible Pavements	82
5.2.1.1.	(Wathugala, Huang, & Pal, 1996)	82
5.2.1.2.	(Perkins, et al., 2004).....	82
5.2.1.3.	(Saad, Mitri, & Poorooshab, 2006)	83
5.2.1.4.	(Kwon, Development of a mechanistic model for geogrid reinforced flexible pavements, 2007)	84
5.3.	DESIGN METHODS USED FOR GEOGRID-REINFORCED PAVEMENTS	84
5.3.1.	Design Methods for Unpaved Roads	84
5.3.1.1.	The Giroud and Noiray Method	84
5.3.1.2.	The Giroud and Han Method.....	85
5.3.2.	Design Methods for Paved Roads.....	86
5.3.2.1.	AASHTO PP 46-01 (AASHTO R 50-09)	87
5.3.2.2.	Traffic Benefit Ratio (TBR)	88
5.3.2.3.	Base Course Reduction (BCR)	89
5.3.2.3.1.	BCR values based on rutting depth results	89
5.3.2.3.2.	BCR values based on vertical stresses results	92
5.3.2.1.	Effective Structural Capacity and Spectrapave4-PRO software	94
CHAPTER 6 CONCLUSIONS AND RECOMMENDATIONS		97

6.1. CONCLUSIONS 97

6.1.1. Test results 97

6.1.1.1. Rutting depth 98

6.1.1.2. Vertical stresses 98

6.1.1.3. Geogrid tensile strain..... 99

6.1.2. Design methods..... 99

6.1.2.1. Traffic Benefit Ratio..... 99

6.1.2.2. Base Course Reduction..... 100

6.1.2.3. Effective Base Layer Coefficient 101

6.2. RECOMMENDATIONS 101

APPENDIX I..... 103

APPENDIX II..... 105

APPENDIX III 111

APPENDIX IV 114

REFERENCES 119

LIST OF FIGURES

Figure 2.1: Reinforcement mechanisms induced by a geosynthetic layer used for base reinforcement (Zornberg & LaRocque, 2008):.....	9
Figure 2.2: Separation function of a geosynthetic layer placed between the base aggregate and a soft subgrade (Zornberg & LaRocque, 2008):.....	10
Figure 2.3: Filtration function provided by geotextile (Zornberg & LaRocque, 2008).....	11
Figure 2.4: Geosynthetic used for mitigation of crack propagation in pavement overlay (Zornberg & LaRocque, 2008)	13
Figure 2.5: Geonet (Tensar, RoadDrain™ Roadway Drainage System, 2015).....	14
Figure 2.6: Geomembrane (ArchiEXPO, 2015)	15
Figure 2.7: Geosynthetic clay liner (Hillier, 2008).....	15
Figure 2.8: Geotextile (USFabrics, 2015).....	16
Figure 2.9: Geogrid Component Nomenclature (Stadler, 2001).....	22
Figure 2.10: Uniaxial geogrid (Inversiones, 2011).....	23
Figure 2.11: Biaxial Geogrid (ArchiExpo, 2015)	23
Figure 2.12: Triaxial Geogrid (Staff, 2012).....	24
Figure 2.13: Interlock between aggregate and geogrid (Tensar, Rib Testing, 2015)	26
Figure 2.14: Lateral restraint mechanism and its components (Perkins S. W., 2001)	27
Figure 2.15: Increase of bearing capacity mechanism (Perkins S. W., 2001)	28
Figure 2.16: Tension membrane mechanism (Perkins S. W., 2001)	29
Figure 2.17: Design criteria for base course thickness proposed by (Carroll, Walls, & Haas, 1987) and (Webster, 1993).....	31
Figure 3.1: HMA particle size distributions	52

Figure 3.2: Test mold and loading system	54
Figure 3.3: Loading details	55
Figure 3.4: Subgrade pressure cells installation procedure	58
Figure 3.5: Base layer pressure cell installation	58
Figure 3.6: Foil strain gauge installation	60
Figure 3.7: Foil strain gauge soldering	62
Figure 3.8: Foil strain gauge protection	63
Figure 3.9: Geogrid installation	63
Figure 3.10: Dynamic loading system	64
Figure 3.11: Data acquisition system.....	64
Figure 3.12: Pavement test section schematics.....	68
Figure 3.13: Test section compaction and preparation	69
Figure 3.14: Geogauge testing	70
Figure 3.15: Loading plate system installation.....	70
Figure 4.1: Surface Deformation (Rutting depth).....	72
Figure 4.2: Surface Deformation of the 40.6 cm (16 in)-thick base pavement sections.....	73
Figure 4.3: Surface Deformation of the 30.5 cm (12 in)-thick base pavement sections.....	75
Figure 4.4: Vertical pressure the subgrade center point	75
Figure 4.5: Vertical pressure at the subgrade quarter radius off-center.....	76
Figure 4.6: Vertical pressure at the subgrade half radius off-center.....	77
Figure 4.7: Vertical pressure at the base layer center point.....	77
Figure 4.8: Average vertical pressure at different locations of the mold.....	79
Figure II.1: HMA layer coefficient.....	106

Figure II.2: Base layer coefficient	107
Figure IV.1: SpectraPave4-PRO software response to B16 test section	115
Figure IV.2: SpectraPave4-PRO software response to T16 test section.....	116
Figure IV.3: SpectraPave4-PRO software response to B12 test section	117
Figure IV.4: SpectraPave4-PRO software response to T12 test section.....	118

LIST OF TABLES

Table 2.1: Geosynthetic types and properties (Koemer, 1998; Shukla and Yin, 2006)	4
Table 2.2: Tests used to determine physical properties of geotextiles	19
Table 2.3: Tests used to determine mechanical properties of geotextiles.....	19
Table 2.4: Tests used to determine hydraulic, endurance and degradation properties of geotextiles	20
Table 2.5: Tests for geogrid properties	25
Table 3.1: Subgrade soil and base aggregate particle size distributions.....	50
Table 3.2: HMA properties	52
Table 3.3: Materials and dimension properties of BX1100 (Tensar, Tensar Biaxial BX grogrids, 2015)	53
Table 3.4: Materials and dimension properties of TX130s (Tensar, Tensar TriAx (TX) Gogrids, 2015)	53
Table 3.5: As- constructed lift properties of subgrade, base and asphalt layer	67
Table 4.1: Rutting depth comparison of reinforced test sections to unreinforced test sections....	73
Table 4.2: Permenent reduction of verical pressure: a comparison of reinforced and unreinforced pavement seicions	79
Table 5.1: Traffic Benefit Ratio for the studied test sections	88
Table 5.2: Comparison of TBR and C16/C12	89
Table 5.3: Base course reduction values for the studied pavement sections	92
Table 5.4: Pressure Benefit Ratio for the studied pavement sections.....	93
Table 5.5: Base Course Reduction percentages using PBR ratios.....	93

Table 5.6: Effective Layer Coefficients and Structural Numbers for studied for studied pavement sections..... 95

LIST OF EQUATIONS

Equation 2.1: Geosynthetic hydraulic permittivity	11
Equation 2.2: Geosynthetic transmissivity	12
Equation 2.3: Structural number	33
Equation 5.1: Structural Number	90
Equation 5.2: AASHTO 1998 ESAL.....	91
Equation 5.3: Resilient Modulus of Subgrade Soil.....	91

CHAPTER 1

INTRODUCTION

1.1. Background

Geosynthetic is defined as a planar product manufactured from a polymeric material that is used with soil, rock, or other geotechnical-related material as an integral part of civil engineering projects. Geosynthetics are available in a wide range of forms and manufactured using different processes and materials. Their market is growing steadily, and they are available worldwide because of their wide-range civil applications.

Geogrid is a major type of geosynthetics which has an open mesh grid structure. It can be used for soil reinforcement, separation, drainage and filtration in roads, airfields, railroads, embankments, earth retaining structures, reservoirs, canals, dams, and coastal protection. Uniaxial, biaxial, and triaxial geogrids are three common types of geogrid. Recently, geogrids have been widely used for soil reinforcement of paved and unpaved roads where weak soil condition exists.

1.2. Research Objectives

Road structure cross section is mostly composed of three components: subgrade, base course, and surface/wearing course. The main aim of this study was to determine the extent to which geogrid, could 1-decrease surface rutting, 2-lower vertical stresses experienced at subgrade-base interface, and 3-assist in reducing base course thickness once the studied paving sections were reinforced using biaxial or triaxial geogrid.

1.3. Chapter break down

In order to achieve the stated objectives, the findings of the study are divided into six chapters.

- Chapter 1 is devoted to the background related to geogrid reinforcement of flexible pavements, chapter break down of the report, and research significance of this investigation.
- Chapter 2 discusses the geosynthetic types and definition, geogrid properties and test methods, production methods for geogrid, function of geogrid in flexible pavements, and review of previous experimental studies on the use of geogrid in flexible pavements.
- Chapter 3 discusses the experimental program used herein including the paving materials characteristics, mold and loading system properties, instrumentation selection and installation, and pavement test section preparation.
- Chapter 4 reports on the findings of six tested pavement sections which includes asphalt surface deformation and vertical stress distribution.
- Chapter 5 discusses the design methods used for geogrid-reinforced paved and unpaved roads. Traffic Benefit Ratio (TBR) and Base Course Reduction (BCR) are two methods used to evaluate the findings of this study.
- Chapter 6 summarizes the results and findings of this study and suggests recommendations for future companion investigations.

CHAPTER 2

LITERATURE REVIEW

This chapter begins with definition of geosynthetic materials and discussion about their applications in civil projects. Afterward, geosynthetic materials types are introduced; followed by a closer look at geogrid and its properties. Finally, past related experimental studies are reviewed in two main categories of small-scale laboratory and large-scale field investigations.

2.1. Geosynthetic

Geosynthetics are widely used in construction industries and civil engineering. Because of their positive properties such as lightness, long-term durability, simplicity of installation, and non-corrosiveness, geosynthetics are now as prevalent as other civil engineering materials such as steel, concrete, and timber. In the word geosynthetic, the prefix “geo” intimate that the main function of geosynthetics is related to geotechnical engineering and geotechnical materials such as soil, sand, earth, and rock. The suffix “synthetics” implies that the geosynthetic materials are mostly produced from synthetic products.

Geosynthetics are grouped by material type, manufacturing method, and intended application. These groups include geotextiles, geonets, geomembranes, geosynthetic clay liners, geocomposites, and geogrids. General characteristics of these families are described in Table 2.1. In addition, each group of geosynthetic materials and its properties is discussed and considered separately in the following sections.


Generally speaking, five principal functions are known for geosynthetics: 1-separation, 2- enforcement, 3-drainage, 4-filtration, and 5-containment. Functions of geosynthetic materials are discussed in details in section 2.1.2.

Table 2.1: Geosynthetic types and properties (Koemer, 1998; Shukla and Yin, 2006)

Geosynthetic	Polymeric Materials	Structures	Application Areas	Major Functions
Geotextiles	Polypropylene (PP), Polyester (PET), Polyethylene (PE), Polyamide (PA)	Flexible, permeable fabrics	Retaining walls, slopes, embankments, pavements, landfills, dams	Separation, reinforcement, filtration, drainage, containment
Geogrids	PP, PET, high-density polyethylene (HDPE)	Mesh-like planar product formed by intersecting elements	Pavements, railway ballasts, retaining walls, slopes, embankments, bridge, abutments	Reinforcement, separation
Geonets	Medium- density polyethylene (MDPE), HDPE	Ney-like planar product with small apertures	Dams, pipeline and drainage facilities	Drainage
Geomembranes	PE, polyvinyl chloride (PVC), chlorinated polyethylene (CPE)	Impervious thin sheets	Containment ponds, reservoirs, and canals	Fluid barriers/ liner
Geocomposites	Depending on geosynthetics included	Combination of geotextiles and geogrids/ geonets, geomembranes and geogrids	Embankments, pavements, slopes, landfills, dams	Separation, reinforcement, filtration, drainage

2.1.1. Geosynthetic Definition

Based on the American Society for Testing and Materials (ASTM), a geosynthetic is defined as “a planar product manufactured from polymeric material used in soil, rock, earth, or other geotechnical engineering related materials as an integral part of a man-made project, structure, or system” (ASTM D4439-04, 2004). Geosynthetics are made of a wide range of various polymers such as polyester (PET), polypropylene (PP), polyvinyl chloride (PVC), polyethylene (PE), polyamide (PA), and polystyrene (PS). Geosynthetics could be used in

construction projects for many reasons such as economics, construction expediency, and functional superiority.

Geosynthetics are categorized in nine major groups: 1-geonet 2-geomembrane 3-geosynthetic clay liner 4-geocomposite 5-geotextile 6-geogrid 7-geopipe 8-geofoam, and 9-geocell. Among these categories, geonet, geomembrane, geosynthetic clay liners and geocomposites are discussed briefly in this section. In addition, Geotextile and Geogrid are explained in detail. Functions of geosynthetic materials are described at first, aimed to have a better understanding of the purpose of each of the geosynthetic materials.

2.1.2. Functions of Geosynthetics

Generally speaking, geosynthetic products have five major functions: separation, filtration, drainage, containment, and reinforcement. Brief descriptions of these functions are given below:

- Separation – Provide barrier to intermingling of dissimilar materials
- Filtration - Allow cross-plane fluid flow across the plane of the geosynthetic
- Drainage – Allow in-plane liquid flow within the plane of the geosynthetic
- Containment – Act as an impervious liquid or vapor barrier
- Reinforcement – Add tensile strength to a soil mass

Although typically designed and manufactured to perform one of these functions, a particular geosynthetic may actually perform multiple functions simultaneously. The functions of geotextile and geogrid are explained specifically in a related section.

In particularly, for road ways, geosynthetics could have 4 out of 5 mentioned functions. (Koerner, Designing with geosynthetics, 2015): Reinforcement, Separation, Filtration and Lateral Drainage (i.e., transmission). Each of these four functions is explained in the sections to follow.

2.1.2.1. Reinforcement

Base reinforcement is inclusion of a geosynthetic layer at the subgrade-base interface or within a base aggregate layer to increase the load-carrying or structural efficiency of a pavement section with a poor condition subgrade by transferring of load to the geosynthetic material. Reinforcement is the interactive improvement in pavement strength caused by geosynthetic inclusion. Reinforcement in pavement system has two benefits. It can 1-increase the service life of the pavement and/or 2-obtain same performance with a reduction in pavement layers thicknesses. Aggregate base layer reinforcement also increases the load capacity of the pavement, provides a safety factor for designed values, and increases the accuracy in the pavement design methods. The key mechanism related to this application is called confinement or lateral restraint (Holz, Christopher, & Berg, 1998).

Geosynthetic reinforcement benefits to the pavement system can be evaluated through a TBR or BCR ratio:

- Traffic Benefit Ratio (TBR) is defined as the ratio of the number of load applications on a reinforced pavement section to reach a specific rutting depth to the number of load applications on an unreinforced section, with the same properties, to reach the same defined rutting depth. TBR is sometimes termed Traffic Improvement Factor (TIF).

- Base Course Reduction (BCR) is defined as the percentage of reduction in the reinforced base course layer thickness from the unreinforced thickness, with the same material constituents, to reach the same defined failure state.

TBR and BCR ratios are specific to the geosynthetic properties, subgrade and course aggregate properties, failure criteria, geometry and loading details utilized in the test program. Thus, the applicability of the mentioned ratios (TBR and BCR) to project-specific geometry, materials, failure (or rehabilitation) criteria, and loading must be assessed independently. In addition, while previous studies has supported some of the design methods, long-term behavior of test sections designed based on these ratios is not available at this time and some confidence limits can be established.

In the following subsection, three mechanisms involved in geosynthetic reinforcement are explained in order to understand how geosynthetics could improve pavement properties over weak subgrades.

2.1.2.1.1. Mechanisms involved in reinforcement function

The reinforcement function is developed primarily through the following three mechanisms (Holz, Christopher, & Berg, 1998):

- I. Lateral restraint through interfacial friction between geosynthetic and aggregate. By applying load on an aggregate base layer, the aggregate tends to move laterally unless it is restrained by the subgrade or geosynthetic reinforcement. Poor condition subgrade soil provides little lateral restraint, which results in rutting development when the aggregate moves laterally. Interaction between the base course layer and the geosynthetic, transfers shear load from the base layer to a

tensile load in the geosynthetic (Perkins, Ismerik, Fogelson, Wang, & Cuelho, 1998). The geosynthetic being stiff in tension, can limit the extensional lateral strains in the aggregate base layer. Moreover, a geosynthetic layer confines the aggregate base layer, thereby increasing the mean stress and leading to improve its stiffness and shear strength. Frictional and interlocking characteristics between the subgrade and geosynthetic are required to recognize this mechanism. Particularly, for a geogrid, this implies that the geogrid apertures and subgrade soil particles distribution should be considered properly. A geotextile with good frictional capabilities can provide tensile resistance to lateral aggregate movement (Figure 2.1-a).

- II. Increased bearing capacity, i.e., by forcing the potential bearing surface failure plane to develop at alternate higher shear strength surface (Figure 2.1-b).
- III. Membrane type of support of the wheel loads (Figure 2.1-c). The tension membrane effect develops as a result of vertical strain causing a concave shape in the reinforcement layer. The tension developed in the geosynthetic can help to distribute the wheel load and reduce the vertical stress on the soil, but remarkable rutting depths are required to realize this mechanism.

2.1.2.2. Separation

Separation is the inclusion of a permeable geosynthetic layer at the interface between different materials (i.e. subgrade/base interface) so that the integrity and the functioning of both materials can remain intact or even be improved (Koerner & Soong, Analysis and design of veneer cover soils, 2005). In pavement design and applications, separation means the prevention

of subgrade soil intruding into base layer (or sub-base), and also prevention of aggregate base (or sub-base) contamination into the subgrade. For instance, a main cause of failure of sections constructed over weak subgrade is migration of the base course aggregate with the underlying poor-conditioned soil as shown in Figure 2.2. A geosynthetic layer can be placed at the subgrade-base interface to perform as a separator and prevent the subgrade and base course aggregate from being mixed (Figure 2.2).

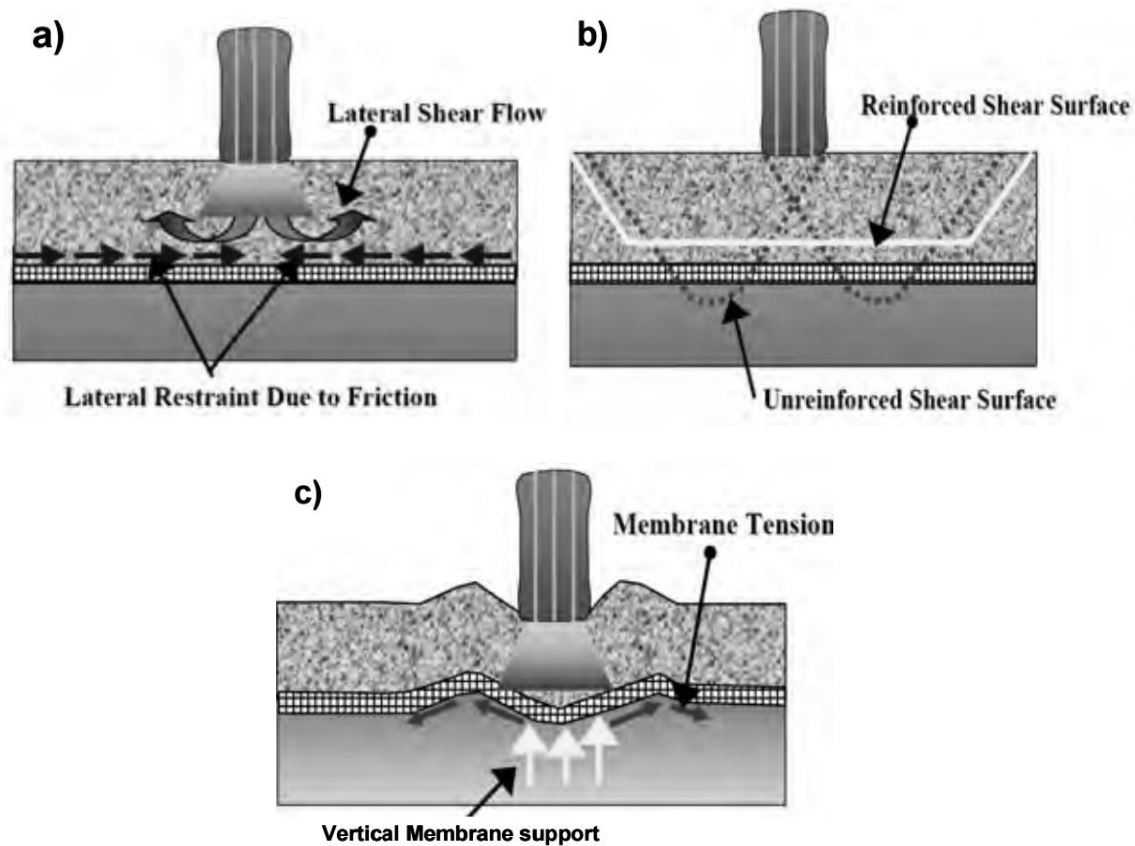


Figure 2.1: Reinforcement mechanisms induced by a geosynthetic layer used for base reinforcement (Zornberg & LaRocque, 2008):

(a) Lateral restraint; (b) Increased bearing capacity; (c) Membrane-type support

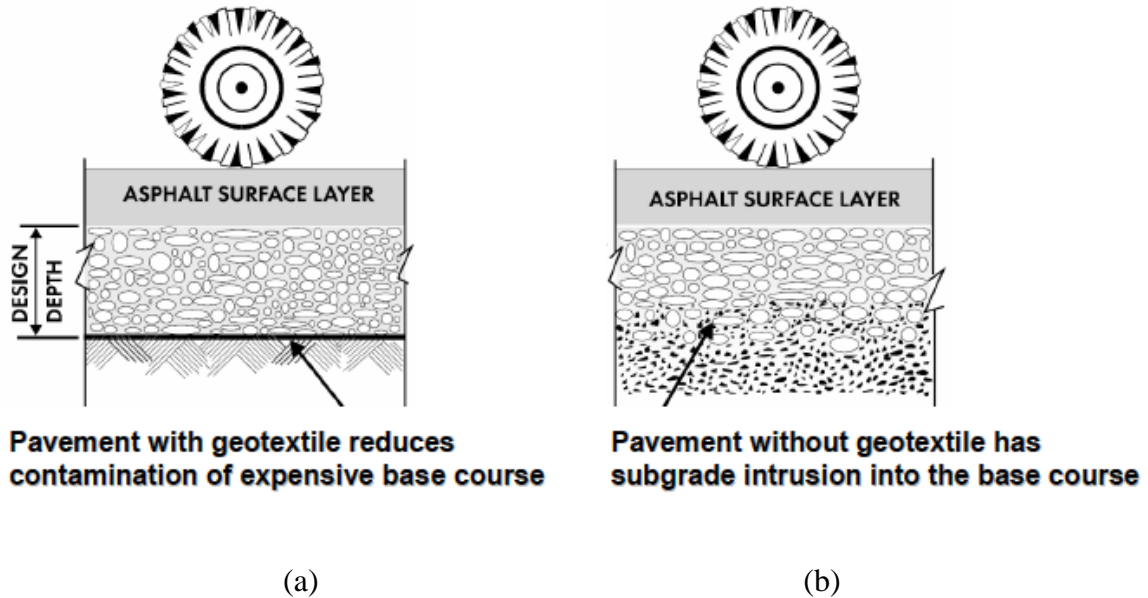


Figure 2.2: Separation function of a geosynthetic layer placed between the base aggregate and a soft subgrade (Zornberg & LaRocque, 2008):

(a) Test section with geotextile; (b) Test section without geotextile

2.1.2.3. Filtration

Filtration is defined as the equilibrium geosynthetic-to-soil system that allows for appropriate liquid flow with a little soil loss across the plane of the geosynthetic layer over a service lifetime compatible with the application under consideration (Koerner & Soong, Analysis and design of veneer cover soils, 2005). In other words, it is limiting the movement of soil particles, and at the same time allowing water to move from the filtered soil to the coarser soil adjacent to it during the performance life of the road structure.

A common application illustrating the filtration function is the use of a geosynthetic in a pavement edge drain as shown in Figure 2.3. The geosynthetic-soil system should achieve an balance that allows for adequate liquid flow under consideration. Whereas the flow of liquid is

perpendicular to the plane of the geosynthetic, filtration refers to the cross plane hydraulic conductivity or permittivity, which is defined as (Stormont, Henry, & Evans, 1997):

$$\psi = \frac{k_n}{t}$$

Equation 2.1: Geosynthetic hydraulic permittivity

ψ is the permittivity, k_n is the cross-plane hydraulic conductivity, and t is the geosynthetic thickness at a specified normal pressure. Comparison of the soil particle size to the geosynthetic aperture shape and size and 95% opening size of it, is another important property for soil retention design using geosynthetic (apparent opening size, AOS). The coarser sized particles eventually create a filter bridge that in turn retains the finer-sized particles, building up a stable upstream soil structure (Thompson, 2009).

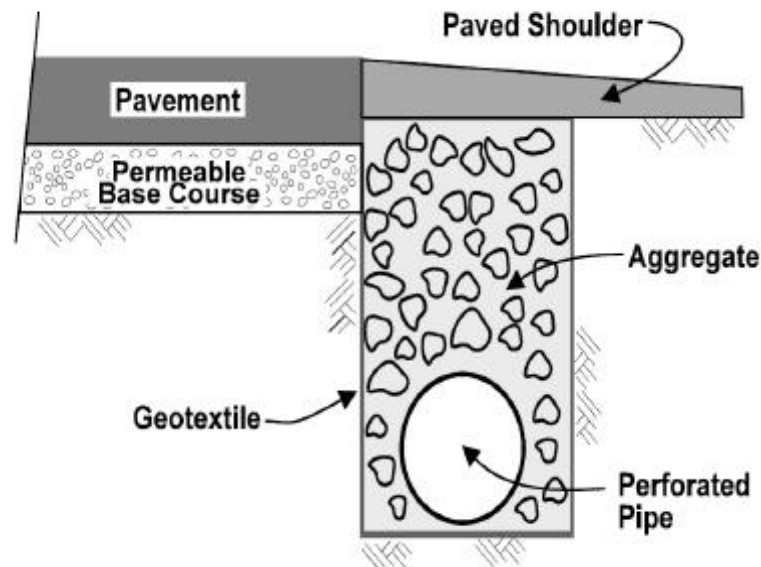


Figure 2.3: Filtration function provided by geotextile (Zornberg & LaRocque, 2008)

Speaking of functions of geosynthetics in pavement structures, lateral drainage is the forth function to be mentioned.

2.1.2.4. Lateral Drainage

Drainage defines as the ability of geosynthetics to provide a path for flow of water through the plane of the geosynthetic. As geotextile thickness decreases with increasing normal stress, the in-plane drainage of a geosynthetic is generally quantified by its transmissivity, which is defined as (Shukla, 2002):

$$\theta = k_p \times t$$

Equation 2.2: Geosynthetic transmissivity

θ is the transmissivity, k_p is the in plane hydraulic conductivity, and t is the geosynthetic thickness at a specified normal pressure.

2.1.2.5. Other Functions

Limitation of crack development (and sealing as secondary function) can be performed by a geosynthetic layer when used in the overlay of the pavement sections. Due to environmental stresses, the HMA layer is subjected to thermal cracking. A geosynthetic layer can acts as a stress relieving interlayer and dissipating stresses before the crack induces stresses in the overlay. Moreover, when a geosynthetic is impregnated with HMA or other polymeric mixes it becomes almost impermeable to both cross-plane and in-plane flow (Meccai & Al Hasan, 2004). As shown in Figure 2.4, the nonwoven geotextile can be placed on the existing pavement surface following the application of an asphalt tack coat. The geotextile has been reported not only to

prevent cracks in the overlay but also to act as a waterproofing membrane minimizing vertical flow of water into pavement structure (Button & Lytton, 2015).

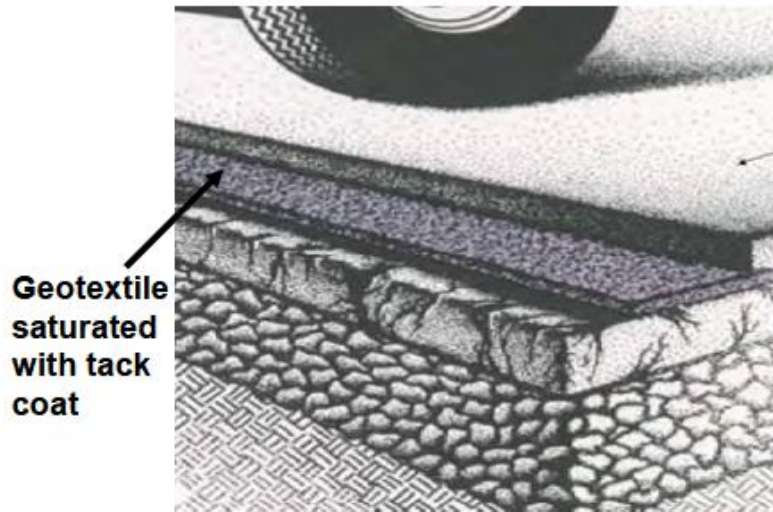


Figure 2.4: Geosynthetic used for mitigation of crack propagation in pavement overlay (Zornberg & LaRocque, 2008)

As alluded earlier, geosynthetics are categorized in nine groups of 1-geonet 2-geomembrane 3-geosynthetic clay liner 4-geocomposite 5-geotextile 6-geogrid 7-geopipe 8-geofoam and 9-geocell. Among these categories, geonet, geomembrane, geosynthetic clay liners and geocomposites are discussed briefly in this section. In addition, geotextile and geogrid are explained in-detail.

2.1.3. Geonet

A geonet is a specialized geosynthetic product that usually performs the drainage function. A geonet contains of integrally connected sets of parallel ribs overlying similar sets oriented at obtuse angles. This geometric orientation creates void space within the plane of the

product that allows easy movement of liquids or gases. Figure 2.5 shows a geonet produced by Tensar Company.

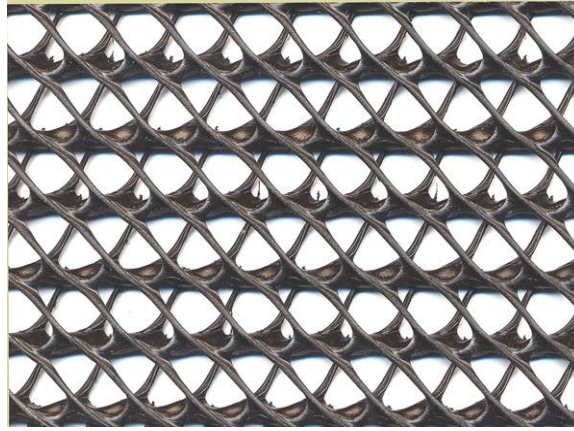


Figure 2.5: Geonet (Tensar, RoaDrain™ Roadway Drainage System, 2015)

2.1.4. Geomembrane

ASTM defines a geomembrane in two ways. First, “a geomembrane is a very low permeability synthetic membrane liner or barrier used with any geotechnical engineering related material in order to control fluid migration in a man-made project, structure, or system” (ASTM D4833 / D4833M-07(2013)e1, 2013). The second ASTM definition for a geomembrane is “an essentially impermeable geosynthetic composed of one or more synthetic sheets” (ASTM D4439-04, 2004). The most common geomembranes are extruded polymeric sheets. These products perform the primary function of liquid or vapor barrier. Figure 2.6 shows a geomembrane.

2.1.5. Geosynthetic Clay Liner

Geosynthetic Clay Liners are made of a layer of bentonite clay sandwiched between two non-woven geotextiles or a layer of bentonite clay glued to a geomembrane (Figure 2.7). As with

geomembranes, the primary function of a geosynthetic clay liner is to function as a liquid or vapor barrier.



Figure 2.6: Geomembrane (ArchiEXPO, 2015)



Figure 2.7: Geosynthetic clay liner (Hillier, 2008)

2.1.6. Geocomposites

Geocomposites are formed by the combination of one or more geotextiles, geonets, geogrids, or geomembranes. The functions of products within this family are product specific. Any one of the five primary functions discussed in Section 2.1.2 can be targeted using geocomposites (Koerner, *Designing with geosynthetics*, 2015).

2.1.7. Geotextile

A geotextile is a permeable geosynthetic layer comprised solely of textiles (ASTM D4439-04, 2004). Geotextiles are either woven or non-woven. These products resemble heavy fabrics and are typically very flexible and porous. A geotextile may perform one or more of the five primary functions discussed in section 2.1.2.

The idea of using textile in pavement structure goes back to the early Persian times when natural fibers were utilized to stabilize poor soils. It was not until the 1920's when the United States implemented a cotton textile for road construction. The introduction of synthetic fibers made road construction more feasible and beneficial. Some geotextile samples are shown in Figure 2.8.



Figure 2.8: Geotextile (USFabrics, 2015)

In the next subsections, the production methods of geotextiles are explained followed by their utilization, properties, and test methods.

2.1.7.1. Geotextile production

There are three ways a geotextile can be manufactured; they are knitted, woven, and non-woven. The distinction between woven and nonwoven is that a woven geotextile is produced by the interlacement of warp and weft yarns. These yarns may either be spun, multifilament, fibrillated, or of slit film. Nonwoven geotextiles are manufactured by mechanically interlocking or thermally bonding the fibers/filaments. This mechanical interlocking is attained through needle-punching, which is most applicable for civil engineering applications (Bhatia & Smith, 1996).

2.1.7.2. Functions of Geotextile

Although geosynthetic materials functions were discussed in section 2.1.2, the geotextile functions are discussed separately. These days, geotextiles are used in various projects for specific purposes. The most common use of geotextile is in road projects where used underneath paved and unpaved roads to separate, stabilize, reinforce, and filter (Giroud J.-P. , 1984). Each of these functions is discussed separately in the order mentioned.

Separation- There are several issues to consider when placing granular aggregates on top of fine-grained soils. Two such issues are fine-grained soils enter the void of the aggregate base and the aggregate punches into the fine grained soil. The first issue is a concern since it avoids adequate drainage and greatly reduces the strength of the aggregate layer which hastens road failure. The second issue is a concern since it decreases the effective thickness of the aggregate layer which also hastens road failure. Due to these concerns, geotextiles used for separation purposes are vital to maintain a long road life (Giroud J.-P. , 1984).

Stabilization- The effectiveness of the geotextile stabilization results from two factors. Firstly, the aggregate is compacted above the geotextile and individual stones are “seated” which leave imprints in the subgrade and geotextile. Because of this seating, the aggregates are fixed into a position, which stabilizes the aggregate base layer. The stabilization of the subgrade soil due to geotextile can change the soil failure mode from local shear to general shear. Due to this change in shear, an additional load is permitted before the soil strength is surpassed which allows for a reduced aggregate base layer. This is economically viable as it saves initial costs and reduces the maintenance required on the road (Giroud J.-P. , 1984).

Reinforcement- In regards to using a geotextile for reinforcement purposes, woven geotextile is considered more appropriate than nonwoven due to its higher tensile strength. The benefits of reinforcement are heavily reliant on the extent of system deformation permitted. Unpaved roads receive more benefits from the use of geotextiles since roads allow large amounts of deformation. Paved roads normally have low allowable deformations and do not receive as much benefit from reinforcement (Giroud J.-P. , 1984).

Filtration- Filtration by use of geotextile is provided by the geotextile’s defined openings that hold soil particles but permit the movement of fluids and has a similar purpose to that of separation. It should be noted that a geotextile that is a separator will not necessarily provide filtration. When there is a need for filtration, engineers must select an appropriate woven or nonwoven geotextile that will allow proper retention of soil particles and flow of water. The proper selection of geotextile will greatly enhance the performance of the pavement (Giroud J.-P. , 1984). Geotextiles that offer reinforcement, separation, and filtration simultaneously are classified under the application of stabilization (Morian, 2007).

2.1.7.3. Geotextile properties and test methods

Physical properties of the geotextiles generally serve as an index property and are not generally adopted directly in design. Table 2.2 shows common physical properties and their respective standards.

Table 2.2: Tests used to determine physical properties of geotextiles

Properties	Relevant standards
Specific gravity	ASTM D792 or D 1505
Mass per unit area (weight)	ASTM D5261 or ISO 9864
Thickness	ASTM D5199
Stiffness	ASTM D1388

The mechanical properties quantify the geotextiles' resistance to tensile stresses mobilized from applied loads or installation conditions. Some tests are performed with the geotextile in isolation while other tests are performed under the confinement of soil (often called performance tests). Table 2.3 summarizes tests available for quantification of mechanical properties of geotextiles.

Table 2.3: Tests used to determine mechanical properties of geotextiles

Tensile strength	Tear tests	Frictional behavior	Impact tests	Other tests
Grab tensile strength ASTM D4632	Trapezoidal test ASTM D4533	Direct shear device	Burst strength ASTM D3786	Compressibility
Narrow strip ASTM D751	Tongue tear test ASTM D751	Pullout tests	Puncture tests	Fatigue strength
Wide width ASTM D 4595	Elmendorf tear test ASTM D1424			Seam strength
Confined tensile strength				

The tests required to determine hydraulic, endurance and degradation properties of geotextiles are summarized in Table 2.4. A number of tests are available for each one of these categories. The hydraulic response of geotextiles under unsaturated conditions has been the focus of recent advances (Bouazza & Avalu, 2006). Some recent tests have been developed to accelerate the determination of endurance and degradation properties (e.g., creep) using time-temperature superposition methods (Zornberg & LaRocque, 2008).

Table 2.4: Tests used to determine hydraulic, endurance and degradation properties of geotextiles

Hydraulic properties	Endurance properties	Degradation properties
Porosity (nonwoven)	Installation damage	Temperature degradation
Percent open area (woven)	Creep response	Hydrolysis degradation
Apparent opening size	Confined creep response	Chemical degradation oxidative degradation
Permittivity	Stress relaxation	Radioactive degradation
Permittivity under load	Abrasion	Biological degradation
Transmissivity	Long-term clogging	Sunlight (UV)
Soil retention	Gradient ratio clogging	Synergistic effects
	Hydraulic conductivity ratio	General aging

2.1.8. Geogrid

In this section, the 6th and last class of geosynthetic materials is introduced. At the beginning of this section, geogrid is defined and various aperture types are shown. After that, the available methods for geogrid production are reviewed. In Section 2.1.8.4 properties and standard tests for geogrid evaluation are given, followed by geogrid benefits and most effective placement locations. At the end, the role of geogrid in flexible pavements is described.

2.1.8.1. Geogrid definition

Geogrids are geosynthetics formed with open apertures and grid-like configurations of orthogonal or non-orthogonal ribs. Koerner (1998) defines a geogrid as a “geosynthetic material consisting of connected parallel sets of tensile ribs with apertures of sufficient size to allow for strike-through of surrounding soil, stone, or other geotechnical material.” Extruding and drawing sheets of Polyethylene (PE) or Polypropylene (PP) plastic in one or two directions or weaving and knitting Polyester (PET) ribs are methods used to produce geogrids. Geogrids are designed mainly to satisfy the reinforcement function.

The ribs of a geogrid are defined as either longitudinal or transverse. The direction which is parallel to the direction that geogrid is fabricated on the mechanical loom is known as roll length direction, Machine Direction (MD), or longitudinal direction. On the other hand, the direction which is perpendicular to the mechanical loom and MD in the plane of geogrid, is known as Transverse Direction (TD) or cross machine direction. In other words, the longitudinal ribs are parallel to the manufactured direction (a.k.a. the machine direction); the transverse ribs are perpendicular to the machine direction. Some mechanical properties of geogrid such as tensile modulus and tensile strength are dependent on the direction which geogrid is tested. Also, geogrid installation in pavements is usually in a way that traffic path is parallel with the ribs produced in machine direction (Kwon, Tutumluer, & Al-Qadi, Validated mechanistic model for geogrid base reinforced flexible pavements, 2009).

In a geogrid, the intersection of a longitudinal rib and a transverse rib is known as a junction. Junctions can be created in several ways including weaving or knitting. Figure 2.9 shows a section of geogrid in plan view and labels the different grid components. Position of ribs and junctions could make various aperture types which are explained in the next section.

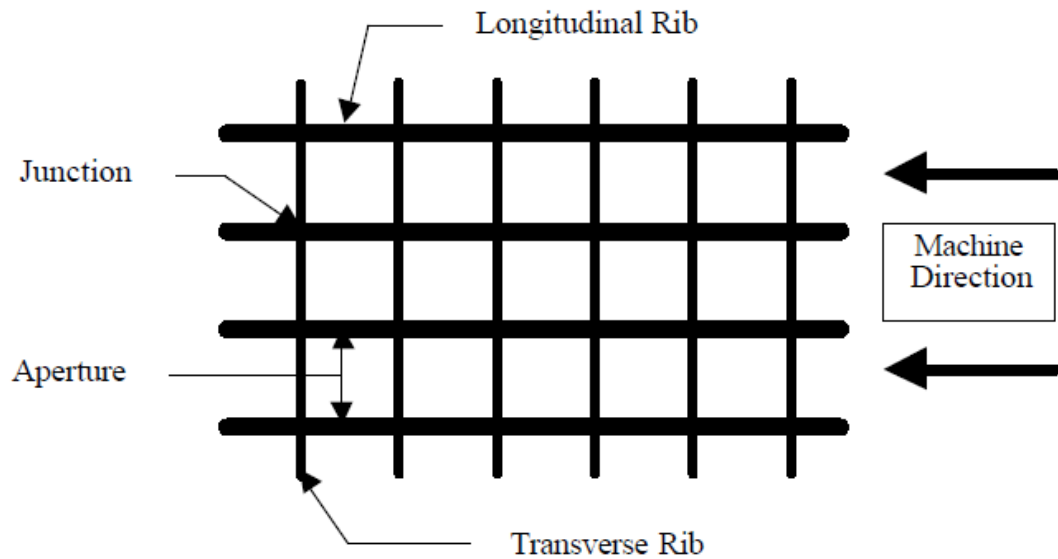


Figure 2.9: Geogrid Component Nomenclature (Stadler, 2001)

2.1.8.2. Geogrid Aperture

Geogrids can be categorized in three main groups based on their aperture: uniaxial, biaxial and triaxial. Uniaxial geogrid has a tensile strength in one direction. It is mainly used for reinforcing slopes, retaining walls, and embankments. Figure 2.10 shows uniaxial geogrid.

Biaxial geogrids have tensile strength in two dimensions and they are often used for reinforcement of pavements including unpaved roads, railroads, and flexible pavements. Dong et al. (Dong, Han, & Bai, 2010) revealed that biaxial geogrid cannot provide constant tensile strengths when subjected to tension in more than two directions, and it has tensile strengths in just two directions. This is one the limitations of biaxial geogrids. Figure 2.11 shows Biaxial Geogrid.

Figure 2.12 presents triangular aperture geogrid with ribs in three directions. This feature causes two benefits. First of all, the apertures allow soil particles to interact better with ribs.

Secondly, triaxial geogrid can provide uniform tensile strengths in all directions as compared with uniaxial and biaxial geogrids. This is because of the fact that triangular aperture geogrid has a more stable grid structure than rectangular aperture geogrids (Dong, Han, & Bai, 2011). However, triaxial geogrids are recently introduced to the market and their effects on the performance of reinforced pavements have not been well tested and evaluated. The question how geogrids are produced and have various aperture shapes is addressed in the next section.



Figure 2.10: Uniaxial geogrid (Inversiones, 2011)



Figure 2.11: Biaxial Geogrid (ArchiExpo, 2015)



Figure 2.12: Triaxial Geogrid (Staff, 2012)

2.1.8.3. Geogrid Production

In this section, the methods used to produce geogrid are introduced. Common geogrid types currently available in market include welded geogrid, extruded geogrid, and woven geogrid (Das, 2010). Extruded geogrid is produced from a polymer plate which is punched and drawn in either one or more ways. Various aperture types are shaped based on the way the polymer sheet is drawn. Drawing in one, two or three directions results in production of uniaxial, biaxial and triaxial geogrids, respectively (Koerner, *Designing with geosynthetics*, 2015).

Polypropylene (PP) or polyester (PET) fibers are generally used to produce woven geogrids. In most cases, these fibers are coated to increase the abrasion resistance of produced geogrid (Berg, Christopher, & Perkins, 2000). Manufacturing process of welded geogrid is by welding the joints of extruded polymer woven pieces.

Geogrids are also categorized in two main groups based on their rigidity. Geogrids made from polyethylene (PE) or polypropylene (PP) fibers are usually hard and stiff and they have a flexural strength more than 1,000 g-cm (ASTM D1388-14e1, 2014). Flexible geogrids, are often made from polyester (PET) fibers by using a textile weaving process. They usually have a

flexural strength less than 1,000 g-cm (Koerner, 1998). Geogrid test methods and properties are reviewed in the next section.

2.1.8.4. Geogrid Properties and Test Methods

The test methods involved to quantify properties of geogrids in laboratory are listed in Table 2.5.

Table 2.5: Tests for geogrid properties

Physical Properties	Mechanical Properties	Degradation properties
Structure	Single Rib test	Temperature effects
Junction type	Junction strength	Oxidation effects
Aperture size	Wide width tensile strength	Hydrolysis effects
Thickness	Shear test	Chemical effects
Mass per unit area	Pullout test	Radioactive effects
Flexural rigidity	Endurance properties	Biological effects
Stiffness	Installation damage	Sunlight (UV) effects
	Tension- Creep behavior	Stress- crack resistance

2.1.8.5. Function of Geogrid

In the prior sections, geogrid was defined and its properties and production methods were reviewed. Geosynthetic functions were also reviewed in 2.1.2 section. In the following paragraphs, the functions of geogrid in pavements are discussed.

While geotextiles can be used for separation, drainage and filtration, or reinforcement, geogrids are mainly used for reinforcement applications. Geogrids can also provide confinement

and partial separation. The confinement is developed through the interlocking mechanism between base course aggregate particles and geogrid openings, as shown in Figure 2.13.



Figure 2.13: Interlock between aggregate and geogrid (Tensar, Rib Testing, 2015)

The interlocking efficiency depends on base course aggregate particle distribution and the geogrid opening size and aperture. In order to achieve the best interlocking interaction, the ratio of minimum aperture size over D_{50} should be greater than three (Jewell et al., 1984). The effectiveness of interlocking depends on the in-plane stiffness of the geogrid and the stability of the geogrid ribs and junctions (Webster, 1993).

The reinforcement mechanisms in geogrid base reinforced pavement sections include lateral restraint (confinement), increased bearing capacity and tension membrane effect which are explained, respectively, in the next subsections.

2.1.8.5.1. Lateral Confinement Mechanism

Aggregate base layer lateral restraint is the fundamental mechanism for geogrid-reinforced pavements. As shown in Figure 2.14, the vertical load applied on the surface of the pavement would cause lateral spreading motion of the aggregate base materials. As the loading is applied on the surface of the roadway, tensile lateral strains are generated in the base layer

causing the aggregates moves out away from the loading. Geogrid reinforcement of pavement sections restrains these lateral movements and it is called lateral restraint. The phrase “lateral restraint” includes many components of geogrid reinforcement in pavements. First of all, it would restrain the lateral movement of granular base materials (Perkins S. , Mechanical response of geosynthetic-reinforced flexible pavements, 1999). Secondly, lateral restraint increases the stiffness of the base layer (Bender & Barenberg, 1978). Moreover, it reduces the shear stresses caused by the loading in the subgrade soil (Love, Burd, Milligan, & Houlsby, 1987). Finally, lateral restraint causes better load distribution on the subgrade soil (Palmeira & Milligan, 1989). Lateral restraint mechanism and its components are shown in Figure 2.14.

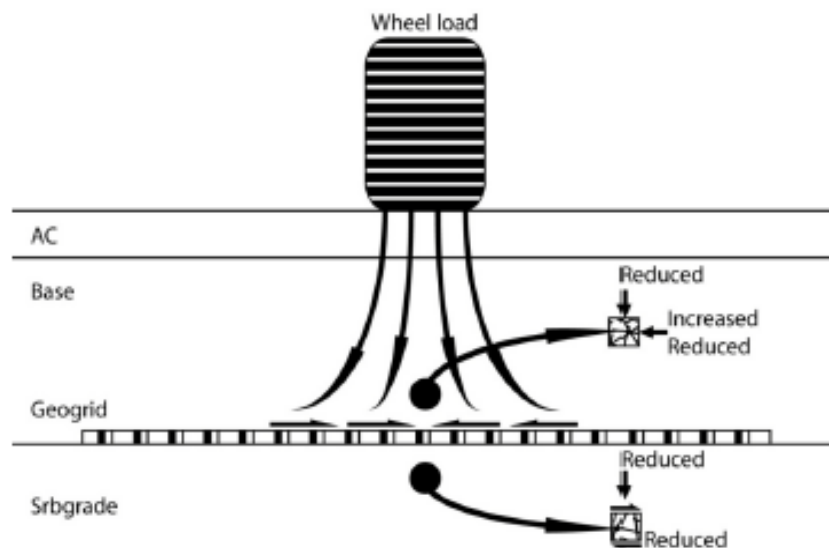


Figure 2.14: Lateral restraint mechanism and its components (Perkins S. W., 2001)

2.1.8.5.2. Increase of the Bearing Capacity Mechanism

By geogrid reinforcement of a pavement system, the failure envelope is shifted from the weak subgrade soil to the strong aggregate base layer. This mechanism is called increase of

(improved) bearing capacity and it's illustrated in Figure 2.15. Moreover, based on this mechanism the failure model of subgrade soil may change from punching failure to general failure by inclusion of geogrid in pavement. Therefore, the subgrade's failure model may change from punching failure without reinforcement to general failure with ideal reinforcement (Binquet & Lee, 1975).

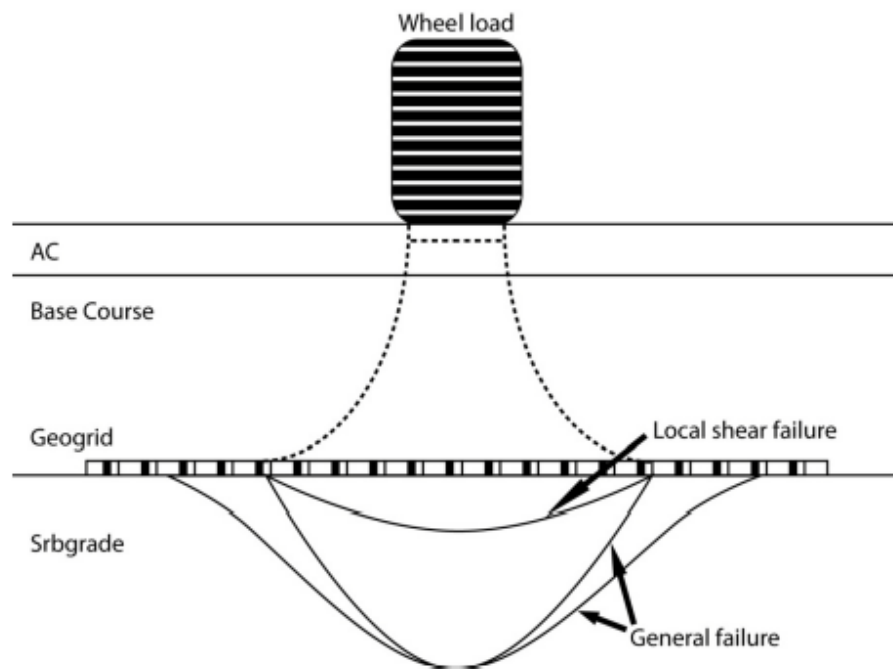


Figure 2.15: Increase of bearing capacity mechanism (Perkins S. W., 2001)

2.1.8.5.3. Tension Membrane Mechanism

The tension membrane effect develops as a result of vertical strains creating a concave shape in the tensioned geogrid layer, shown in Figure 2.16 (Giroud & Noiray, Geotextile-reinforced unpaved road design, 1981). The tension membrane force is not vertical, but its vertical component decreases the vertical pressure applied on the subgrade soil. Some sorts of movements must be provided to activate the tension membrane effect. For example, a rutting

depth is required to involve the tension membrane effect and increase the bearing capacity of the soil. For a heavy duty and strong geogrid a more significant mobilization, such as a remarkable rutting depth in needed to activate the tension membrane mechanism (Göbel, Weisemann, & Kirschner, 1994). In addition, for noticeable and great effect of this mechanism, the subgrade soil CBR should be less than 3% (Barksdale , Brown, & Chan, 1989).

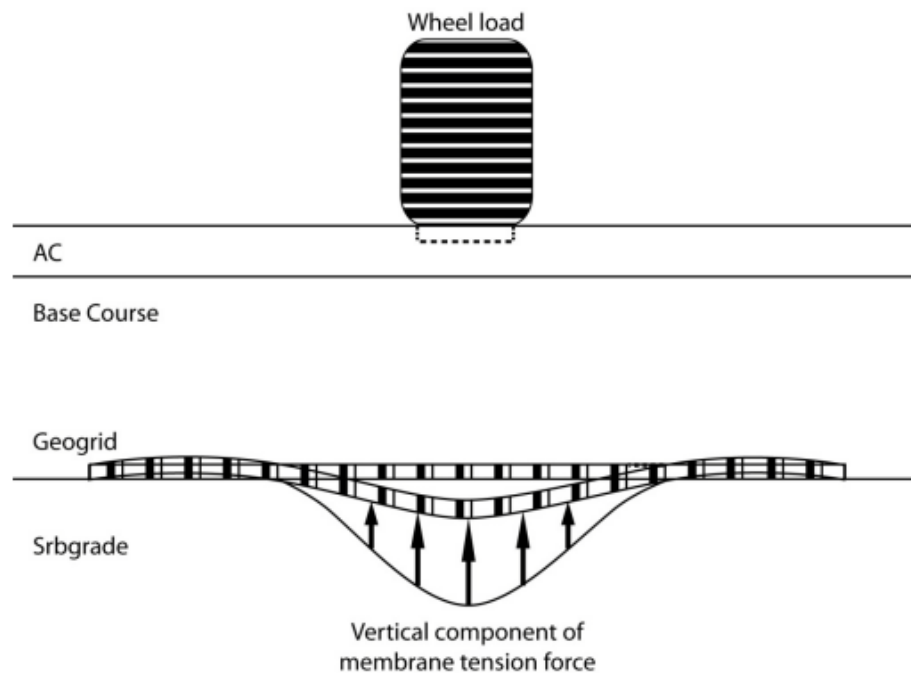


Figure 2.16: Tension membrane mechanism (Perkins S. W., 2001)

2.2. Previous Experimental Studies Using Geogrids

Geosynthetic materials were introduced in previous sections with an emphasis on geotextile and geogrid which are the most widely used ones. This section provides an extensive literature review on the lab-scale and large-scale investigations carried out on geogrid reinforcement in paved sections. Both field investigations and laboratory testing programs have

shown that geogrid reinforcement of flexible pavements would extend the service life of the roadway or decrease the pavement layers thicknesses with the same performance and service life.

2.2.1. Small- Scale Laboratory studies

Laboratory-scale studies on the effects of geogrid reinforcement on pavement performance are required to evaluate the benefits of geogrid inclusion and in order to conduct large-scale testing. Not only the lab-scale testing is cheaper and easier than the field investigation, but also the testing environment is more under control. Small-scale investigations have used monotonic or cyclic loading to examine the behavior of reinforced pavement sections.

2.2.1.1. (Carroll, Walls, & Haas, 1987)

By testing a couple of test sections using loading plate system, Abdelhalim et al. (Abd El Halim, Haas, & Chang, 1983) investigated the performance of geogrid reinforcement placed at subgrade-base interface under poor condition and strong subgrades. They revealed that geogrid-reinforced test sections took more loading cycles before the failure rutting depth of 20 mm (0.79 in) as compared to the unreinforced test section. Moreover, pretensioning of the geogrids at installation process did not show any remarkable benefits compared to ordinary installed geogrids. Based on this investigation (Abd El Halim, Haas, & Chang, 1983), other researchers (Carroll, Walls, & Haas, 1987) proposed a design method that suggested a conversion of unreinforced aggregate base layer thicknesses to equivalent base layer thicknesses for geogrid-reinforced sections, as presented in Figure 2.17. The point of inflection in Figure 2.17 shows the minimal thickness required. However, this design graph was developed based on experimental results of a single type of geogrid.

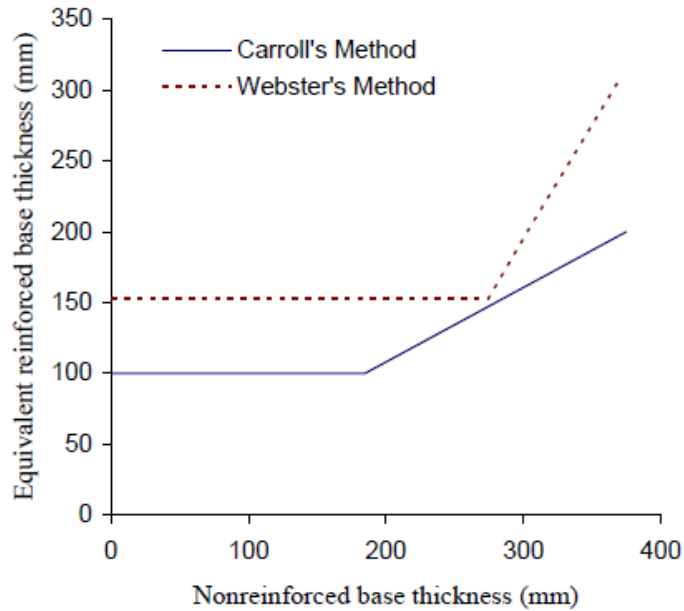


Figure 2.17: Design criteria for base course thickness proposed by (Carroll, Walls, & Haas, 1987) and (Webster, 1993)

2.2.1.2. (Haas, Wall, & Carroll, 1988)

Aimed to understand the benefits of geogrid inclusion in flexible pavements, an extensive test program was conducted in a 4.5×12×0.9 m (15×40×3 ft) box. Cyclic loading was performed through a 2.5 cm (1 in) thick circular shape steel plate with a diameter of 30.4 cm (12 in). Pavement test section properties such as subgrade stiffness, base course thickness, and location of the geogrid layer in pavement section, were different in the studied pavement sections. Rutting depth, vertical stress at the subgrade-base interface, and geogrid ribs tensile strains were measured throughout the tests. Haas et al. (Haas, Wall, & Carroll, 1988) revealed that inclusion of geogrid into the pavement test section increased the number of loading cycles by a factor of 3. By inclusion of geogrid in pavement system, base course layer thickness decreased by 25-50%. Subgrade-base interface was reported as the optimum location for geogrid reinforcement for thin

aggregate base layer sections. For a thick base layer pavement section, mid point of the base layer was suggested as the optimum location for geogrid placement.

2.2.1.3. (Al-Qadi, Brandon, Valentine, Lacina, & Smith, 1994)

Pavement test sections were prepared in a 3×2.1×1.8 m (10×7×6 ft) mold to represent a regular secondary road in the State of Virginia constructed on a poor condition subgrade. Various types of geotextiles and geogrids, different base course thicknesses, and different subgrade condition and strengths were used. Dynamic loading was performed on the surface of the pavement using a circular shape steel plate with diameter of 300 mm (12 in). Rutting depth of the surface asphalt layer was recorded through an array of LVDTs. Al-Qadi et al. (Al-Qadi, Brandon, Valentine, Lacina, & Smith, 1994) revealed that the geotextiles and geogrids significantly improved the performance of roadways constructed over a poor condition subgrade soil. The reinforcing mechanisms of geotextiles were different from geogrids, based on the tests results. They suggested that geotextile can provide separation between the soil and granular base materials, while geogrid cannot.

2.2.1.4. (Montanelli, Zhao, & Rimoldi, 1997)

Aimed to evaluate the influence of geogrid reinforcement in roadways, a lab-scale testing program using a cyclic plate system was carried out on test sections constructed on a subgrade soil with different CBRs of 1 to 18%. Intended to make use of the AASHTO design method, Montanelli et al. (Montanelli, Zhao, & Rimoldi, 1997) proposed a base layer coefficient ratio, also known as Base Course Reduction (BCR), which is the ratio of geogrid-reinforced to unreinforced aggregate base material coefficients. Based on experimental results, the BCR ratio varied from 1.5 to 2 depend on the subgrade strength (CBR value). The BCR ratio can be used to

calculate the structural number (SN) of the reinforced paved road to be used in AASHTO design method:

$$SN = a_1 D_1 + a_2 D_2 G$$

Equation 2.3: Structural number

In Equation 2.3, D_1 is the thickness of HMA layer and D_2 is base course layer thickness (both in inch unit). a_1 and a_2 are asphalt and aggregate base layers structural coefficients, respectively, used to specify the strength and structural capacity of pavement layers in unreinforced pavement sections. m_2 is the drainage coefficient of the aggregate course material and “G” is the base layer reinforcing coefficient (BCR). Geogrid-reinforced base layer thickness can be achieved as follows:

$$D_2 = \frac{SN - a_1 D_1}{a_2 G}$$

**2.2.1.5. (Perkins S. , Geosynthetic Reinforcement of Flexible Pavements:
Laboratory Based Pavement Test Sections, 1999)**

Perkins et al. (Perkins S. , Geosynthetic Reinforcement of Flexible Pavements: Laboratory Based Pavement Test Sections, 1999) carried out lab-scale tests on reinforced and unreinforced pavement sections that stimulate roadway materials, properties, and loading conditions in the field. A 2×2×1.5 m (79×79×59 in) reinforced concrete mold was used for the testing. 40 kN (9 kips) cyclic loads were applied through a 304 mm (12 in) diameter steel plate. Twenty test sections were prepared and tested. Variables in testing program was subgrade strength and materials, geosynthetic position, two types of geogrid and one type of geotextile, and base layer thickness. The pavement responses recorded in test set-up included strains

experienced by geosynthetics, rutting depth, stress and strain in subgrade soil, moisture content, and temperature in pavement sections. Geogrid-reinforced pavement sections with poor condition subgrade soil (CBR of 1.5 %) showed significant improvements. Minor benefit was observed for sections constructed on a stiff subgrade soil (CBR of 20%). The heavy-duty geogrid showed superior performance compared to the light-duty geogrid used in this investigation. Both geogrid-reinforced sections showed better performance than the geotextile-reinforced section. The geogrid location in the pavement section was found as a crucial element in evaluation of reinforced pavement system. Remarkably improved performance was detected when geogrid reinforcement layer was located at the mid-depth of aggregate base layer compared to the sections with geogrid installed at the subgrade-base interface.

2.2.1.6. (Leng, Ju, & Gabr, 2002)

Fourteen laboratory scale tests were carried out in a 1.5×1.5×1.35 m (59×59×53 in) box at North Carolina State University to investigate the properties of biaxial geogrid-reinforced aggregates constructed over a poor condition subgrade soil. Cyclic loading were performed through circular shape plate with diameter of 305 mm (12 in) with maximum applied pressure of 500 kPa (72 Psi). Rutting depth and vertical stress at the bottom of the base layer were recorded. The experimental results revealed that geogrid inclusion in test sections decreased the rutting depth and improved the stress distribution at the interface between subgrade and base.

2.2.1.7. (Moghaddas-Nejad & Small, 2003)

Moghaddas-Nejad and Small (Moghaddas-Nejad & Small, 2003) carried out triaxial compression test in drained condition on geogrid-reinforced fine gravel and sand. Geogrid was placed at the mid-depth of 200×400 mm (8×16 in) cylindrical sample. The experimental results

of this investigation revealed that for a specific confining stress, the improvement in rutting depth significantly increased with the increase of deviator stress, up to a peak point and then it started to decrease slowly. However, not any remarkable effects were observed by inclusion of geogrid on the resilient deformation of tested materials.

2.2.1.8. (Perkins, et al., 2004)

Perkins et al. (Perkins, et al., 2004) conducted cyclic triaxial tests on geogrid-reinforced and unreinforced granular base materials. The test sections were cylindrical with height of 60 cm (24 in) and diameter of 30 cm (12 in). The test samples were compacted in a firm compaction mold using a vibrating plate compactor. Four different kinds of geosynthetics were used in this study. Two types of geogrids, one type of geotextile and one class of geocomposite was placed at the mid depth of the test section. The results revealed that geosynthetic reinforcement of granular materials does not have any remarkable effects on the resilient modulus of unbound aggregates. However, significant improvements were observed in rutting depth of test specimens when they were reinforced with a layer of geosynthetic. These findings are similar to those observed by Moghaddas-Nejad and Small (Moghaddas-Nejad & Small, 2003). Perkins et al. (Perkins, et al., 2004) observed poor repeatability in rutting depth of reinforced test specimens by inclusion of different types of geosynthetics. They also reported that not any significant improvement was observed in reinforced test specimens until a friction angle of 30° was achieved.

2.2.1.9. (Nazzal, 2007)

Aimed to investigate the effects of geogrid reinforcement on resilient behavior and permanent deformation of limestone aggregates, a cyclic and monotonic loading test program was conducted. The aggregates had maximum grain size of 19 mm (3/4 in), uniformity

coefficient of 30, D_{10} of 0.18 mm, and a D_{60} of 6 mm. The crushed limestone aggregates were classified as GW-GC based on the Unified Soil Classification System (USCS). The maximum dry density of 0.172 gr/cm^3 (10.7 pcf), at the optimum moisture content of 7% was reported based on standard proctor test. Five different kinds of biaxial geogrids with different tensile strengths were used in this study.

Based on experimental results of this investigation, reported by Nazzal (Nazzal, 2007), the rutting depth of limestone aggregates decreased by inclusion of geogrid in cyclic loading test samples. Moreover, the stiffness and strength properties of limestone aggregates (shear strength, and secant elastic modulus) increased by geogrid reinforcement when monotonic loading was applied. Better performance was observed when geogrids with higher tensile strength were used. In addition, more remarkable improvements were found at higher levels of strain.

2.2.1.10. (Chen, Abu-Farsakh, & Tao, 2009)

The effectiveness of geogrid-reinforced aggregate base layer in paved sections on poor condition subgrade under cyclic plate load testing was studied by Chen et al. (2009). The performance of instrumentation sensors was also evaluated to improve future instrumentation programs. A test box with dimensions of $2.0 \times 2.0 \times 1.7 \text{ m}$ ($6.5 \times 6.5 \times 5.5 \text{ ft}$) was used to conduct the testing program. A 40-kN (9 kips) load at a frequency of 0.77 Hz was applied through a 305 mm (1 ft) circular plate. The instrumentations used included pressure cells, linear variable displacement transducers, foil strain gauges, and piezometers. The test results revealed that the inclusion of geogrid at the interface between subgrade and base layer can improve the performance of flexible pavement on weak subgrade (CBR of 0.5%). Moreover, the TBR can be increased up to 3.5 for a rutting depth of 25 mm (1 in). The test results also revealed that geogrid reinforcement has redistributed the applied load to a wider area, thus achieving an improved

stress distribution on the subgrade soil, which eventually reduced the permanent deformation of subgrade. Due to high number of cyclic loadings, the foil strain gauges are unsuitable for long-time continuous monitoring of strain development within geogrid.

2.2.1.11. (Abu-Farsakh & Chen, 2011)

In order to investigate the effects of geogrid reinforcement in flexible pavements, a cyclic loading palate test program was conducted. Pavement test sections were prepared inside a mold with dimensions of 2×2×1.7 m (6.5×6.5×5.5 ft). Cyclic loading was applied through a 2.5 cm (1 in) thick circular plate with diameter of 305 mm (1 ft). A hydraulic actuator provided 40 kN (9 kips) sinusoidal vertical loading, which applied a pressure of 550 kPa (80 Psi) on the surface of asphalt layer. These conditions simulates the standard single-axle dual tires force of 80-kN (18,000-lb). The subgrade soil was categorized as silty clay with Liquid Limit (LL) of 31 and Plasticity Index (PI) of 15. The base course layer was crushed limestone aggregates with D_{10} of 0.382 mm and D_{50} of 3.126 mm. Design level 2 super pave mixture with a thickness of 19 cm (7.5 in) was used as Hot Mixed Asphalt materials in this study. Aggregate base layer was reinforced with four different types of geogrids.

Based on experimental results of this study, geogrid reinforcement of base course layer remarkably decreased the surface rutting depth of pavement sections. By geogrid inclusion, the number of applied cyclic loadings increased by a factor of 15.3 at the rutting depth of 19.1 mm (3/4 in). More significant improvements were observed in rutting depth of the test sections reinforced with higher tensile strength geogrids. Upper one-third of the base course layer was suggested as the optimum location for geogrid reinforcement.

2.2.1.12. (Abu-Farsakh, Souci, Voyiadjis, & Chen, 2011)

A series of cyclic triaxial tests were conducted on geogrid-reinforced limestone aggregates test specimens. The limestone aggregates had a D_{10} of 0.28 mm (0.011 in) and D_{50} of 5 mm (0.2 in). One type of biaxial geogrid and one type of triaxial geogrid were used to reinforce the test sections. The results of this study revealed that geogrid reinforcement reduced the rutting depth of crushed limestone materials. These reductions were depended on geogrid properties such as aperture size, tensile modulus and also the location of geogrid in test section. Not any remarkable effect was observed on the resilient modulus of granular limestone materials by inclusion of geogrid.

2.2.1.13. (Qian, Han, Pokharel, & Parsons, 2011)

Qian et al. (2011) conducted a study to compare unreinforced and triaxial geogrid-reinforced base course layers over a poor condition subgrade. Test sections were constructed in a large geotechnical testing box with dimensions of 2×2.2×2 m (6.5×7×6.5 ft) at the University of Kansas and tested under cyclic loading. Throughout the tests, surface deformation and vertical stress at the subgrade-base interface were monitored. The test results revealed that triaxial geogrids reduced rutting depth and vertical stresses at the interface compared with an unreinforced base. The improvements were more significant by utilizing a heavier-duty geogrid. The back calculations from the measured vertical stresses at the subgrade-base interface revealed that the modulus ratio of base course to subgrade and the stress distribution angle decreased with an increase in the number of cycles. The rates of reduction in the stress distribution angle and the modulus ratio for the unreinforced base were faster than those for the reinforced bases.


2.2.2. Large- Scale Field Investigation

Laboratory-scale investigations are beneficial to initially and easily simulate geogrid-reinforced roadway sections. However, field-scale studies provide more relevant and actual results on the behavior of geogrid-reinforced pavement systems. In this chapter, an extensive literature review is conducted on field-scale geogrid inclusion in flexible pavements.

2.2.2.1. (Webster, 1993)

Aimed to provide a design criteria for geogrid-reinforced flexible pavements, a full scale testing program was conducted. Four lanes of paved roadway were constructed on a subgrade soil with CBR of 3 to 8%. The aggregate base layer thicknesses were 153, 254, 304, and 457 mm (6, 10, 12, and 18 in) at different test section locations. Based on the results of this study, Webster (Webster, 1993) proposed a design method which converts the unreinforced aggregate base layer thicknesses to geogrid-reinforced base layer thicknesses, as shown in Figure 2.17 (see Section 2.2.1.1). Comparison of the two proposed design curves suggested by two different studies, shows that how material properties and test program details were influential on the test results.

2.2.2.2. (Cancelli & Montanelli, 1999)

Aimed to compare the performance of woven geotextile and geogrid in flexible pavements, an extensive experimental program was conducted. Based on the results of this study, the aggregate base layer thickness reduced significantly by inclusion of geogrid in paved roads. Geogrids with higher tensile modulus showed better performance in reduction of the rutting depth. High strength geotextile was more effective in separation of base and subgrade materials than reinforcing the test section. The number of load applications increased by a factor of 200 at 

the rutting depth of 5 mm (0.2 in), by inclusion of geogrid in pavement system. Averagely, a TBR of 10 was suggested for geogrid-reinforced sections considering different types of geogrids and subgrade soil conditions. More remarkable improvements were observed when geogrid was used on a poor condition subgrade soil. The structural layer coefficient of base course layer increased to 1.5-2.0 by geogrid inclusion. The elastic strains recorded for geogrids were less than 0.2% in most of the reinforced test sections.

2.2.2.3. (Perkins S. , Evaluation of geosynthetic reinforced flexible pavement systems using two pavement test facilities, 2002)

The performance of geogrid and geotextile-reinforced pavement sections were compared in a full scale investigation conducted by Perkins (Perkins S. , Evaluation of geosynthetic reinforced flexible pavement systems using two pavement test facilities, 2002). Two different types of geogrid and one type of geotextile were placed at the subgrade-base interface. Each of the four test sections had a length of 9.91 m (32.5 ft) and a width of 3.18 m (10.4 ft). Base course and HMA layers had thicknesses of 350-mm (12 in) and 75-mm (3 in), respectively. The 40-kN loading was applied on the surface of the asphalt layer through a Heavy Vehicle Simulator. Asphalt surface rutting depth and stresses at the subgrade-base interface were recorded throughout the test. In addition, the strain values were recorded at different locations of pavement sections through strain coils.

The results of this study revealed that inclusion of all three types of geosynthetics significantly decreased the surface rutting depth. In addition, lower stress and strain values were experienced in reinforced pavement sections compared to those of unreinforced sections. Not any remarkable differences were observed between the performance of geogrid and geotextile layers.

2.2.2.4. (Tingle & Webster, 2003)

Four field-scale pavement sections were prepared to investigate the effects of geosynthetics on test section properties. The unreinforced section had a 50.8 cm (20 in) thick aggregate base course layer. Woven and nonwoven geotextile-reinforced sections had a base layer thickness of 38.1 cm (15 inch). Another pavement section was prepared with base layer thickness of 25.4 cm (10 inch) and reinforced with a layer of geocomposite (geogrid/nonwoven geotextile).

Tingle and Webster (Tingle & Webster, 2003) reported that the base aggregates were punched to the subgrade soil for about 3.8 cm (1.5 in) and the subgrade soil was intruded to the aggregates about 12.7 cm (5 in) at unreinforced section. However, subgrade rutting depth of zero was recorded for unreinforced section. When the test section was reinforced with woven geotextile, a rutting depth of 7.6 cm (3 in) was recorded on the subgrade and not any subgrade intrusion was recorded. Nonwoven geotextile-reinforced section showed a subgrade rutting depth of 7.6 cm (3 inch) and subgrade intrusion of 190 mm (7.5 in). Inclusion of geocomposite in roadway resulted in a subgrade rutting depth of 5.1 cm (2 inch). A base course reduction factor of 0.75 and 0.5 was suggested for geotextile and geocomposite-reinforced pavement sections, respectively.

2.2.2.5. (Aran, 2006)

Two roadway flexible pavements were constructed in 1986 and 1990 in order to study the long term performance of geogrid-reinforced sections. The test section prepared in 1986 had a base layer thickness of 25.4-cm (10 in) and the geogrid was placed the subgrade-base interface. The unreinforced section HMA layer thickness was 5 cm (2 in) more than the reinforced test

section. In the test section constructed in 1990, the base layer thickness was 10 cm (4 in) and the geogrid was placed at the middle or bottom of the aggregate base layer. The unreinforced test section had 15 cm (6 in) of lime-stabilized subgrade soil. The performance of the studied roadway sections were recorded in 1991, 2004, and 2005.

Long term evaluation of the results of this study revealed that geogrid-reinforced test section had the same performance with unreinforced section with 5-cm (2 in) thicker HMA layer. Moreover, improvements observed by geogrid inclusion in the studied sections were similar to unreinforced section with 15-cm (6 in) lime-stabilized subgrade. Improved behavior was observed when geogrid was used in thinner pavement sections.

2.2.2.6. (Helstrom, Humphrey, & Hayden, 2007)

Aimed to study the effects of geosynthetic reinforcement on flexible pavements, two series of test sections were prepared over a subgrade soil with standard penetration field blow of 7. Base course layer thickness was 300 mm (12 in) and 600 mm (24 in) for the first and second series of the test sections, respectively. Four different reinforced test sections were prepared at each of the test series. Geogrid reinforcement was placed at the subgrade-base interface and mid-depth of base course layer for the first two pavement sections. Another test section was reinforced with a layer of geogrid placed at the middle of aggregate base layer and a layer of drainage geocomposite placed at the subgrade-base interface. The last test section was prepared with a drainage geocomposite layer placed at the interface between subgrade and base course layers. All pavement sections had a 150 mm (6 in) thick HMA layer.

It was found that inclusion of geogrid and drainage composite layers in 304 mm (12 in) thick base layer pavements increased the base course structural coefficient by 5 and 17%,

respectively. However, not any remarkable results were observed for the test sections with base layer thickness of 600-mm (24-in). Inclusion of drainage geocomposite layers in pavement sections did not have any effects on pore water pressure in the subgrade soil. 18 to 83% of the long-term force in geogrid was created during base layer compaction and preparation. Helstrom et al. (Helstrom, Humphrey, & Hayden, 2007) suggested that geogrid and drainage composite inclusion in 300-mm (12-in) thick base layer pavements was equivalent to 25 to 75 mm (1 to 3 in) thicker base course layer.

2.2.2.7. (Al-Qadi I. , Dessouky, Kwon, & Tutumluer, Geogrid in flexible pavements: validated mechanics, 2008)

In order to study the improvements by inclusion of geogrid in low volume flexible pavements, nine field scale roadway sections were prepared on a subgrade soil with CBR of 4%. Three different aggregate base layer thicknesses of 202 mm (8 in), 304 mm (12 in), and 458 mm (18 in) were used to build the pavement sections. Two geogrid types were used and the HMA layer thickness was 75 mm (3 in) and 128 mm (5 in) for different test sections. Pavement responses were measured by 173 gauges installed in the test section to record rutting depth, stress, strain, moisture, temperature, and pore-water pressure. A cyclic loading of 44 kN was applied to simulate standard dual tire pressure.

Al-Qadi et al. (Al-Qadi I. , Dessouky, Kwon, & Tutumluer, Geogrid in flexible pavements: validated mechanics, 2008) revealed that inclusion of geogrid in pavement sections decreased the surface rutting depth of the studied test sections. Moreover, lower shear deformation in aggregate base layer was observed in geogrid-reinforced test sections. Subgrade-base interface was reported as the optimum location for geogrid reinforcement at thin aggregate

base layer sections. For a thick base layer pavement section, upper one third of the base layer was suggested as the optimum location for geogrid placement.

2.2.2.8. (Duncan-Williams & Attoh-Okine, 2008)

An experimental program to study the effects of geogrid reinforcement on strength properties of aggregate base materials was conducted. Unreinforced and geogrid-reinforced specimens were prepared inside a mold using different soil materials. The reinforcement layer was placed at the mid depth of the test specimen. Duncan et al. (Duncan-Williams & Attoh-Okine, 2008) revealed that geogrid reinforcement increased the CBR value of the soil.

2.2.2.9. (Henry, Clapp, Davids, Humphrey, & Barna, 2009)

Eight full scale pavement sections were prepared to study the properties of geogrid-reinforced flexible pavements with thick HMA and base course layers. Two HMA thicknesses (102 mm (4 in) and 152 mm (6 in)) and two base course layer thicknesses (300 mm (12 in) and 600 mm (24 in)) were involved amongst the roadway sections. The subgrade soil material was silt and reinforcement layer was placed at the interface between subgrade and base course layers for reinforced studied test sections. Subgrade soil had modulus of 109 MPa to 138 MPa based on Falling-Weight Deflectometer (FWD) test. However, required water was added to achieve the target modulus of 35 MPa. Elastic deformations and permanent rutting depth were recorded at the surface of HMA and subgrade-base interface through electromagnetic induction coils. Seven pressure cells were installed in each test section to record stresses throughout the test. Moreover, foil strain gauges were installed on the ribs of geogrid to measure flexural and longitudinal strains. Dynamic loading of 689.5 kPa was applied through a Heavy Vehicle Simulator on the surface of studied test sections.

Henry et al. (Henry, Clapp, Davids, Humphrey, & Barna, 2009) revealed that number of applied cyclic loadings increased by a factor of 1.3 to 1.4 by inclusion of geogrid in flexible pavement sections. However, not any remarkable improvements were observed in thick base (300 mm (12 in) and 600 mm (24 in)) and thick HMA layer (102 mm (4 in) and 152 mm (6 in)) test sections. Moreover, geogrid reinforcement did not decrease elastic vertical strain in any layers of the pavement system.

2.2.2.10. (Cox, McCartney, Wood, & Curry, 2010)

Cox et al. (Cox, McCartney, Wood, & Curry, 2010) conducted a research program to study the effects of geogrid reinforcement on rutting depth of flexible pavements. A Vibroseis (shaker) was used to apply cyclic loading on the surface of geosynthetic-reinforced pavement sections. A line of LVDTs were installed on the surface of test sections to record elastic deformations and permanent rutting depths. Based on experimental results of this study, lower rutting depths were observed for thicker base course layer pavements. Not any remarkable improvements were detected in pavement performance by geogrid reinforcement, possibly due to lack of enough strain in pavement section to mobilize the reinforcement layer.

2.2.2.11. (McCartney, Cox, Wood, & Curry, 2010)

This study investigated the response of full-scale geogrid-reinforced flexible pavements to static surface loading. Specifically, Static Plate Load (SPL) tests were conducted on a low-volume, asphalt pavement frontage road in Eastern Arkansas, USA. This site is consisting of sixteen 15 m (50 ft)-long sections including different geosynthetic types, two base course thicknesses, and control sections. Maximum deflections under a maximum static surface stress of 540 kPa (78 Psi) ranged from 2.5 to 4 mm (0.1 to 0.16 in). At least four unload-reload curves

were obtained for each section to dampen the effects of the visco-elastic response of the asphalt surface layer on the system stiffness. The range in tangent stiffness obtained from the third reload cycle for the pavement sections ranged from 495 to 905 kPa/mm during the winter (dry season), and 452 to 725 kPa/mm during the late spring (wet season). A smaller decrease in stiffness from the wet season to the dry season was observed for the reinforced sections. The trends in the stiffness values indicate logical trends with reinforcement type and base course thickness, showing that the SPL test is suitable for global characterization of the geosynthetic-reinforced sections. Three-layer elastic analyses using moduli determined using Spectral Analysis of Surface Waves (SASW) was found to be useful in quantifying the impact of geosynthetic reinforcement on the surface settlement. Although predicted elastic settlements were greater than measured settlements, the trends were close. The Poisson's ratios of the base course layers in each section (incorporating the geosynthetic reinforcement as a composite) were found to be a useful parameter to account for the effect of geosynthetic reinforcement on the base lateral confinement.

2.2.2.12. (Al-Qadi I. , Dessouky, Tutumluer, & Kwon, 2011)

In order to investigate the effectiveness of geogrid reinforcement in low-volume flexible roadways, and to identify the reinforcement mechanism involved in geogrid stabilized base course layers, a field-scale accelerated loading test program was carried out. Different HMA and base course layer thicknesses were used to construct pavement sections on a poor condition subgrade soil (CBR of 4%). More than 170 gauges were used to monitor the geogrid-reinforced and unreinforced test sections responses such as rutting depth, temperature, strains, moisture, pore-water pressure, and stresses throughout the test program. Cyclic loading was applied through an Accelerated Transportation Loading Assembly (ATLAS) which provided a dual-tyre

moving load of 44 kN (10 kips) at the speed of 8 km/h (5 mph). Lower loading speed was also utilized to compare different pavement sections responses.

Al-Qadi et al. (Al-Qadi I. , Dessouky, Tutumluer, & Kwon, 2011) revealed that inclusion of geogrid in flexible pavements reduced the surface rutting depth and delayed the surface cracking compared to unreinforced test sections. Moreover, vertical deflection and vertical stress at subgrade soil of geogrid-reinforced sections decreased by reducing the loading speed. Therefore, the most remarkable finding of this investigation was that geogrid reinforcement decreased the horizontal displacement of granular materials, specifically in loading directions. Researchers of this study reported that upper one-third of a relatively thick base course layer is the optimum place for geogrid layer. Also, the interface between subgrade and base course layer is the best placement for geogrid -reinforced pavement sections constructed over a poor condition subgrade soil.

2.2.2.13. (Jersey, Tingle, Norwood, Kwon, & Wayne, 2012)

A large-scale pavement section was prepared and subjected to traffic loading at the U.S. Army Engineer Research and Development Center to study the effectiveness of a geogrid layer that was utilized for base course layer reinforcement of a thin flexible pavement section. A geogrid-reinforced and two unreinforced pavement sections were prepared under controlled conditions. An accelerated traffic loading was applied on the surface of roadway sections. Pavement stiffness and permanent surface deformations were measured periodically throughout the testing. The results showed that the geogrid-reinforced pavement showed a better performance than the unreinforced control pavements. The results were used to develop traffic benefit ratios and effective base course structural coefficients to enable comparison of the pavement structures.

**2.2.2.14. (Al-Qadi I. , Dessouky, Kwon, & Tutumluer, Geogrid-Reinforced
Low-Volume Flexible Pavements: Pavement Response and Geogrid
Optimal Location , 2012)**

Al- Qadi et al. (Al-Qadi I. , Dessouky, Tutumluer, & Kwon, 2011) extended their previous researches to study the performance of a geogrid-reinforced low-volume flexible pavement constructed on a poor condition subgrade soil, and to investigate the optimum place for geogrid layer in pavement sections. Nine different test sections were prepared at Advanced Transportation Research and Engineering Laboratory (ATREL) of University of Illinois. More than 170 sensors were installed in test pavement sections to monitor the pavement response to dual tire accelerated loading. The results of this study showed that longitudinal and transverse shear deformations, significantly decreased by inclusion of geogrid in pavement sections.

CHAPTER 3

MATERIALS CHARACTERIZATION AND CYCLIC LOADING PLATE SYSTEM

3.1. Overview

In this chapter, materials characteristics used for the laboratory test set-up of the studied pavement sections are discussed. In addition, this section describes the experimental design, instrumentation selection and installation, test procedures, and data collection system.

3.2. Paving materials characteristics

The subgrade soil, base course aggregates and Hot-Mixed Asphalt (HMA) are the three types of materials used.

3.2.1. Subgrade soil

The subgrade soil utilized in this study was obtained from a local site representing common soil types in Southeastern Las Vegas. The soil is categorized as light brown silty, clayey sand with gravel (SC-SM) based on the Unified Soil Classification System (USCS). Subgrade soil had the **R-value of 40** and resilient modulus of 65.75 MPa (9536 Psi). The sieve analysis test was conducted prior to each of the six set-up tests to make sure the delivered soil had the same properties. The average particle size distribution for the subgrade soil is shown Table 3.1. Modified Procter tests (ASTM D1577-07, 2012) were carried out which produced an average maximum dry density of 2.03 gr/cm³ (127 PCF) corresponding to the optimum moisture content of 11%.

Table 3.1: Subgrade soil and base aggregate particle size distributions

Sieve size, mm	Passing, %	
	Subgrade soil	NDOT type 2 Class B requirements
37.5	100	100
25.0	93	100
19.0	89	90-100
12.5	83	-
9.5	79	-
6.3	72	-
4.75	68	35-65
2.36	61	-
2.00	57	-
1.18	52	15-40
0.6	49	-
0.425	46	-
0.3	43	-
0.15	39	-
0.075	33	2-10

3.2.2. Base Course Aggregates


Type 2 Class B crushed limestone aggregates, commonly used in Southern Nevada for paved roads, were used for aggregate base course layer (see NDOT Type 2 Class B gradation requirements in Table 3.1). The base aggregate was classified as Light Gray, Poorly Graded Gravel /Silt & Sand (GP-GM). The average Modified Proctor tests for the base course aggregate materials showed optimum moisture content of 8.5% and maximum dry density of 2.264 gr/cm³ (141 lb/ft³).

3.2.3. Asphalt mixture

The HMA type 2C plant-mix aggregate with rap, as designated by Nevada Department of Transportation, was prepared from a local asphalt plant and truck delivered to the laboratory testing site. It had a bitumen ratio of 4.4 and sand equivalent of 60. The LA abrasion loss was

equal to 24%. Other properties of the HMA are provided in Table 3.2. In addition, the particle distribution is shown in Figure 3.1.

3.3. Geogrid index and mechanical properties

 Rectangular (BX1100) and triangular (TX130S) aperture geogrids made of polypropylene, herein referred to as biaxial and triaxial geogrids, manufactured by Tensar Company were used in this study. Their material and dimensional properties are shown in Tables 3.3 and 3.4, respectively. Both geogrid types are of the same family. In other words, they have been produced through the same manufacturing process and only differ in the product design details. For this specific family of geogrid, they only differ in aperture shape and size, unit weight, mechanical properties, tensile modulus, and rib thickness.

3.4. Mold Dimensions and Cyclic Loading System

A cylindrical mold, shown in Figure 3.2-a, with a diameter of 1.8 m (6 feet) and a height of 2.1 m (7 feet) was prepared to house the studied test pavement sections. A hydraulic actuator with a force range of 40 kN (9 kips), was installed between the two I-beams of the crosshead (Figure 3.2-b). A cyclic loading was applied on the surface of the asphalt layer by a steel rod that fits into a hole on the loading plate. The loading plate was a 1.3 cm (0.5 in) thick circular steel plate with a diameter of 305 mm (12 inches). The applied load was kept constant at 40 kN (9 kips), which performed a pressure of 551 kPa (80 Psi) and model dual tires under an equivalent 80-kN (18,000-lb) single-axle load. The loading, as shown in Figure 3.3, had a linear load increase from 2.2 kN (0.5 kips) to 40 kN (9 kips) in 0.3 second, followed by a 0.2-second period where the load was held constant at 40 kN (9 kips), followed by a linear load decrease to 2.2 kN (0.5 kips) over

Table 3.2: HMA properties

Property	Value	Property	Value
Type material	Type 2C plantmix aggregate with rap	Liquid limit (before marination)	$\frac{3}{4}$ " : 16; $\frac{1}{2}$ " : 16; $\frac{3}{8}$ " : 15
Type asphalt	76-22NV	Plasticity index (before marination)	$\frac{3}{4}$ " : 2; $\frac{1}{2}$ " : 2; $\frac{3}{8}$ " : 2
Surface area m ² /kg (ft ² /lb)	6.23 (30.4)	LA Abrasion	24.0
Sand equivalent	60	VMA (Based upon calif. Sp. Gr.)	14.4 @4.4
Calif. Specific gravity	2.76	Original tensile strength (Psi)	120.5
Coarse Agg. bulk specific gravity	2.73	% retained strength	99
Fine agg. specific gravity	2.67	Bitumen ratio	4.4
		Resilient Modulus (ksi)	260

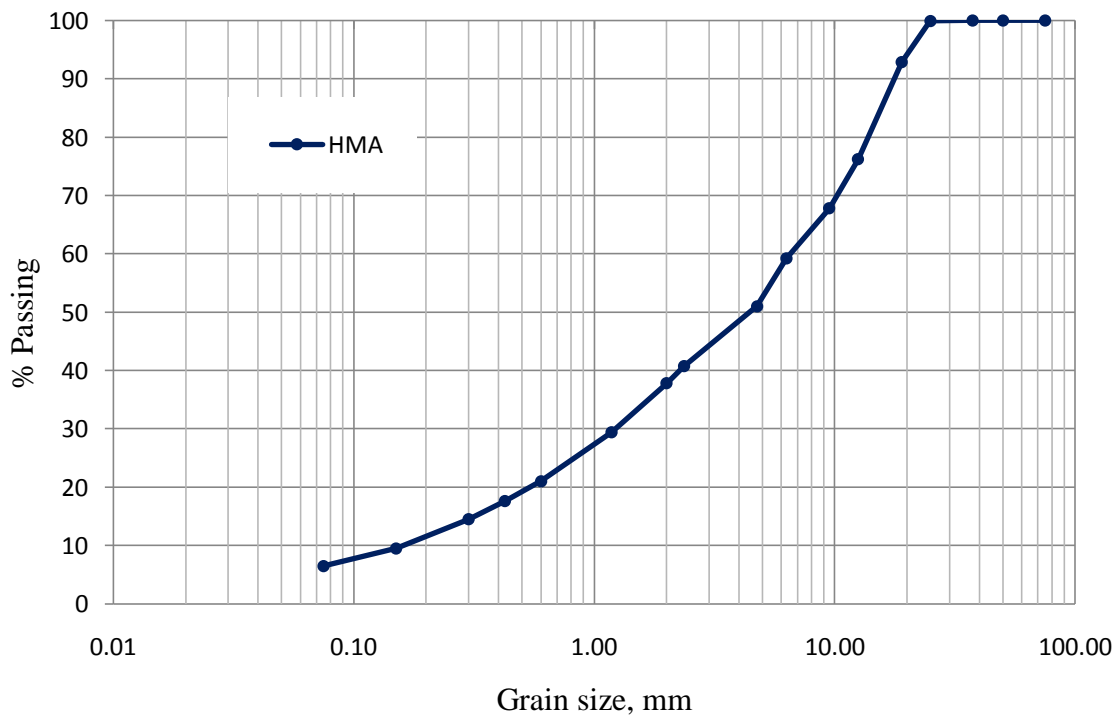


Figure 3.1: HMA particle size distributions

a 0.3-second period, and extended by a 0.5-second resting period of 2.2 kN (0.5 kips) before the next loading cycle resumed. This load pulse resulted in a frequency of 0.77 Hz.

Table 3.3: Materials and dimension properties of BX1100 (Tensar, Tensar Biaxial BX grogrids, 2015)

Index properties	Units	MD Values1	TD Values1
Aperture Dimensions	mm (in)	25 (1.0)	33 (1.3)
Minimum Rib Thickness	mm (in)	0.76 (0.03)	0.76 (0.03)
Load Capacity	Units	MD Values1	XMD Values1
True Initial Modulus in Use	kN/m	250	400
True Tensile Strength @2% Strain	kN/m	4.1	6.6
True Tensile Strength @5% strain	kN/m	8.5	13.4
Structural Integrity	Units	MD Values1	
Junction Efficiency	%	93	
Flexural stiffness	Mg-cm	250,000	
Aperture Stability	Kg-cm/deg	3.2	

Table 3.4: Materials and dimension properties of TX130s (Tensar, Tensar TriAx (TX) Gogrids, 2015)

Index Properties	Longitudinal	Diagonal	Transverse
Rib Pitch, mm (in)	33 (1.30)	33(1.30)	-
Mid-rib Depth, mm (inch)	-	1.5 (0.06)	1.2 (0.05)
Mid-rib Width, mm (inch)	-	0.6 (0.02)	0.7 (0.03)
Rib shape	Rectangular		
Aperture shape	Triangular		
Structural integrity			
Junction efficiency, %	93		
Aperture Stability, kg-cm/dg @ 5.0 kg-cm	3.0		
Radial stiffness at low strain, Kn/m @ 0.5 % strain	200		
Radial stiffness at low strain, lb/ft @ 0.5% strain	15,075		

3.5. Instrument selection and calibration

Intended to precisely compare the performance of the studied test sections reinforced with different types of geogrid and in order to identify the optimal test section properties for a given subgrade condition, the vertical stresses at the interface between the subgrade and base layer, as well as the strains experienced by the geogrid ribs were recorded. Moreover, the asphalt surface rutting depth was recorded throughout the six studied pavement sections. These measurements also allowed for understanding of the mechanisms taking place at the base-subgrade interface separately.

The selection of instrumentation was based on the data needed, cost effectiveness, reliability, and the information found in the literature. Each of these instrumentations is discussed in this chapter separately.



(a)

(b)

Figure 3.2: Test mold and loading system

(a) Mold and frame; (b) Loading plate system

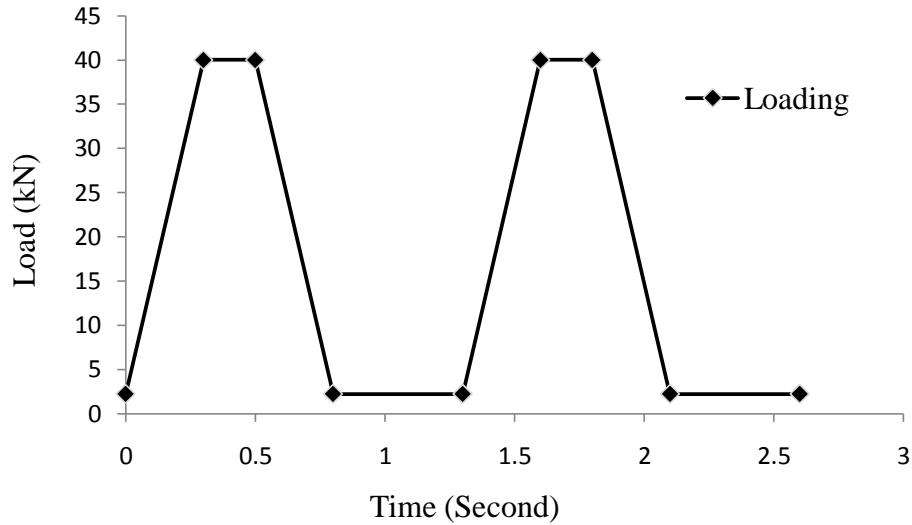


Figure 3.3: Loading details

3.5.1. Instrument for measuring vertical pressure

The vertical stress sensors were selected based on the pavement section properties and loading details in order to provide accurate and satisfactory measurements throughout the tests. The pressure cells should record the stress values at the base and subgrade layers without any interruption to the actual existing stress levels at the pavement section. Hydraulic pressure cells and the diaphragm (membrane) cells are two common types of earth pressure cells for recording the vertical pressure in granular materials.

The diaphragm cell is basically made of a strong circular membrane holding by a boundary ring. The diaphragm cell is installed in the subgrade soil and the membrane bends while the pressure is applied to the soil surface. The membrane movements are recorded by a strain gauge transducer installed inside the cell. The amount of membrane movement reflects the amount of pressure applied to the soil.

Hydraulic pressure cells are made of two concave circular shape steel plates welded together to create a cavity. The cavity is filled with a liquid and it is connected to a pressure transducer through a steel tube. The pressure transducer transforms the physical force of the fluid to electrical signals.

Hydraulic type pressure cells were selected to record the pressure values at the subgrade and aggregate base layers as one of the key responses of a flexible pavement system. The pressure cells were produced by Geokon Company (Geokon 3500) and generally had a diameter of 22.9 cm (9in). Customized hydraulic pressure cells with diameter of 15.2 cm (6 in) were ordered considering the test sections geometry in order to minimize any possible interruptions in the studied pavement sections. The installation of the pressure cells in the subgrade is discussed in the paragraph below.

Holes of the same form, but marginally larger than that of the earth pressure cells, were excavated to a specific depth with a hand trowel. Once, the bottom of each hole was flattened, the pressure cells were placed and leveled inside the holes, using a leveling device as shown in Figures 3.4-a and 3.4-b, before each hole was backfilled and compacted with the same subgrade soil materials. The amount of soil needed to backfill was estimated by removing the amount of soil occupied by the pressure cell, which was calculated by multiplying the density of the soil by the approximate volume of the pressure cell from the soil excavated. The installation process of the pressure cells are shown in Figure 3.4.

The pressure cell installed in the aggregate base layer was protected by embedding the pressure cell in a bag of fine sand, in order to avoid possible damages during compaction of base layer. A pressure cell protected and installed in the aggregate base layer is shown in Figure 3.5.

3.5.2. Instrument for geogrid deformation measurement

In order to evaluate mobilization and engagement of the geogrids installed in pavement sections, the strain amount in geogrid ribs were recorded throughout the tests. 8 foil strain gauges were placed in two directions of biaxial and triaxial geogrids away from the center of the mold at 15.2 cm (6 inches) intervals. The strain gauges were selected based on a lot of factors such as maximum possible strain values during the tests, number of repeated loadings, size, accuracy, temperature, and properties of the materials geogrids are made of.

With regard to consultations with foil strain gauge producers and a comprehensive literature review, EA-06-230DS-120 strain gauge produced by Vishay Micro-Measurements Inc. was chosen to use in this study. Mentioned strain gauges had a backing material made from 0.025 mm (0.001 in) tough, flexible cast polyimide. The measurement grid was constructed from a constantan alloy that was able to keep the strains of up to 5 percent. Strain gauges were precisely calibrated by the producer on a steel plate to obtain the gauge factor. The strain gauges had an electrical resistance of $120.0 \pm 0.15\%$ ohm, and gauge factor of $2.095 \pm 0.5\%$. The strain gauges had a length of 12.7 mm (0.5 in) and a width of 3.3 mm (0.13 in). They were installed on the ribs of biaxial and triaxial geogrids and connected to a three wire quarter bridge circuit. The circuit was connected to a data acquisition system. Installation, soldering and protection of the strain gauges are discussed in the paragraphs to follow.



(a)

(b)



(c)

(d)

Figure 3.4: Subgrade pressure cells installation procedure

(a) Positioned the pressure cells in their location; (b) Checked pressure cells to be level; (c) Installation of a pressure cell in subgrade; (d) Final look of the pressure cells installed



(a)

(b)

Figure 3.5: Base layer pressure cell installation

(a) Protected pressure cell for installation of base layer;
 (b) Installed pressure cell at the subgrade-base interface

Strain gauges were set up on the surface of the ribs of the geogrid in order to measure the bending and tensile strains in geogrid. A small drop of the adhesive was applied to the center of the sanded rib (Figure 3.6-a), and the gauge was transferred to the center point using a process, designed to prevent contamination from getting on the surface of the gauge. The top of the gauge (the side with the measurement grid) was carefully positioned on the sticky side of a piece of tape using sterile tweezers. Then the sticky side of the tape was transferred to the geogrid surface (gauge facing up but covered with tape), the gauge was aligned and centered, and slight pressure was applied until adhesive fully covered the contact area between the back of the gauge and the surface of the geogrid. A small spring clamp was used to apply pressure in order to make sure a strong attachment of the strain gauge to the geogrid's rib took place. After the adhesive had cured, the clamps were removed and the tape was slowly peeled back at nearly a 180 angle to avoid damaging (or pulling up) the gauge. Any excess adhesive that extended over the rib was carefully trimmed using a razor blade, without damaging the material or the gauge. The gauge was inspected to ensure proper alignment and adhesion. The same procedure was repeated for external terminals. Final configuration of two strain gauges installed on the ribs of triaxial geogrid is shown in Figure 3.6-b.

For the wiring and soldering of the strain gauges, cable conductors and wires were positioned and secured to the geogrid with a cable tie before soldering the transmission cable to the external terminal. Tiny wires were used to solder the strain gauges to the terminals followed by soldering of the main wires to the terminals as shown in Figure 3.7-a. The final installation configuration is shown in Figures 3.7-b and 3.7-c.



(a) (b)
Figure 3.6: Foil strain gauge installation

(a) Adhesive applied on the ribs of geogrid; (b) Installation of foil strain gauges and terminals

All foil strain gauges needed protection. For this purpose, non-conductive silicone was applied liberally on all electrical components in the area of the install to form a protective (but ductile) cover around the gauges, terminals, and wires as shown in Figure 3.8-a. Subsequently, thin electrical tape was wrapped around the nodes and ribs to fully seal the electrical connection (Figure 3.8-b). Care was taken to minimize the amount of protection in the grid opening in order to avoid influencing the interaction with the soil. The resistance of the gauge was verified at the end to make sure the installation and protection process did not damage the strain gauge. As shown in Figure 3.8-c, a plastic hose was used to protect the wires from any possible damages during compaction and testing. The final configuration of a protected strain gauge is shown in Figure 3.8-d.

After installation, soldering, wiring, and protections of the strain gauges, the geogrid was cut in a circular shape, as shown in Figure 3.9-a, with a diameter of 180.4 cm (5 feet 11 inch which was 1 inch smaller than the mold diameter). The wires were passed through two plastic pipes on the sides of the mold and the geogrid was installed inside the mold as shown in Figure 3.9-b.

3.5.3. Instrument for asphalt surface deformation measurement

To monitor test section loading responses, a Linear Variable Displacement Transformer (LVDT) was part of the loading actuator and was used to record the HMA surface deflection. This displacement transducer was part of the loading system and was placed on top of the loading plate (Figure 3.10-a). The asphalt surface deformation (rutting depth) was recorded throughout the test by RMCTools software provided by the hydraulic loading system company (Figure 3.10-b).

3.6. Data acquisition system

Instruments were connected to a data acquisition system to collect, store, and plot the collected data at a rate of 10 Hz. An in-house programme for data acquisition was developed using Labview software. The instruments were only activated during load application. The data acquisition system is shown in Figure 3.11.

3.7. Test Section Preparation and Instruments Installation

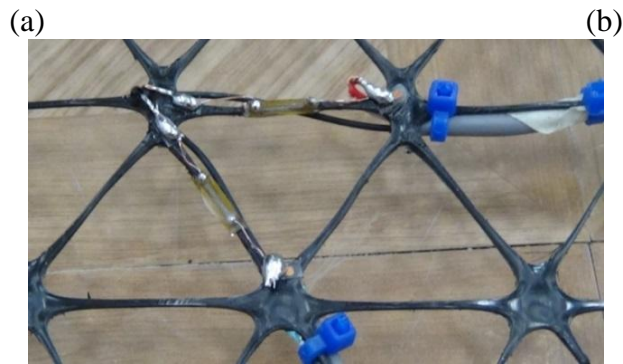
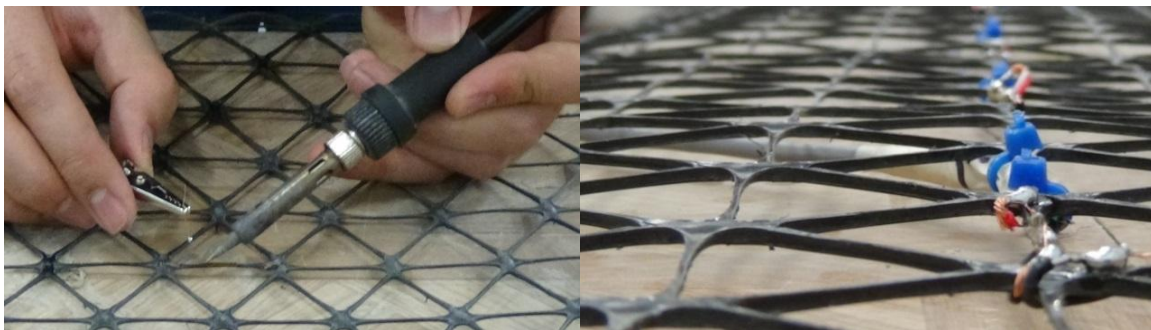
All the studied pavement sections were prepared with care in order to make sure they have the same and a uniform compaction level.

Discussed instrumentations were installed in the studied pavement sections. Accurate installation of the gauges guarantees a reliable measurement throughout the test.

3.7.1. Test Section Preparation

Six pavement test sections were prepared. The first section was unreinforced with a 40.6 cm (16 inch) thick base layer. The second and third test sections were reinforced with biaxial and triaxial geogrid layers, respectively, positioned at the mid-depth of the 40.6 cm (16 inch) thick

aggregate-base layer. The fourth test section was unreinforced consisted of a 30.5 cm (12 inch) base layer. Fifth and sixth test sections with the same thickness of base layer, were biaxial and triaxial geogrid-reinforced and the reinforcement was placed at the interface of subgrade and base layers. The six pavement test sections are schematically shown in Figure 3.12. The test codes consist of a letter and two digit numbers. The letters C, B and T represents the words, Control, Biaxial and Triaxial respectively. And the two digit number shows the thickness of aggregate base layer in inches. For example, the test code B12 belongs to the test section reinforced with a biaxial geogrid and 12 inches (30.5 cm) of aggregate base layer. The same coding system is used throughout this study.



(c)

Figure 3.7: Foil strain gauge soldering

- (a) Soldering of foil strain gauges; (b) Wiring of the gauges and terminals; (c) Two strain gauges installed and soldered on geogrid ribs



(a)

(b)

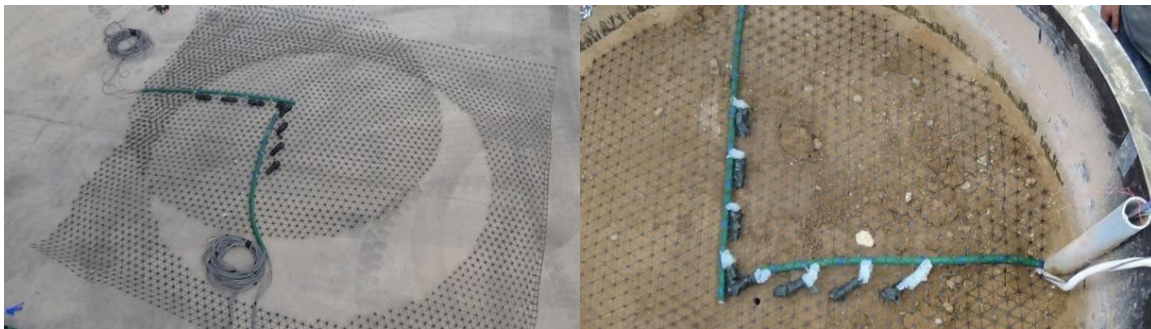


(c)

(d)

Figure 3.8: Foil strain gauge protection

(a) Applying silicon to protect the gauges; (b) Electrical tape applied for protection purposes;
 (c) Protection of wires; (d) Final look of a protected foil strain gauge



(a)

(b)

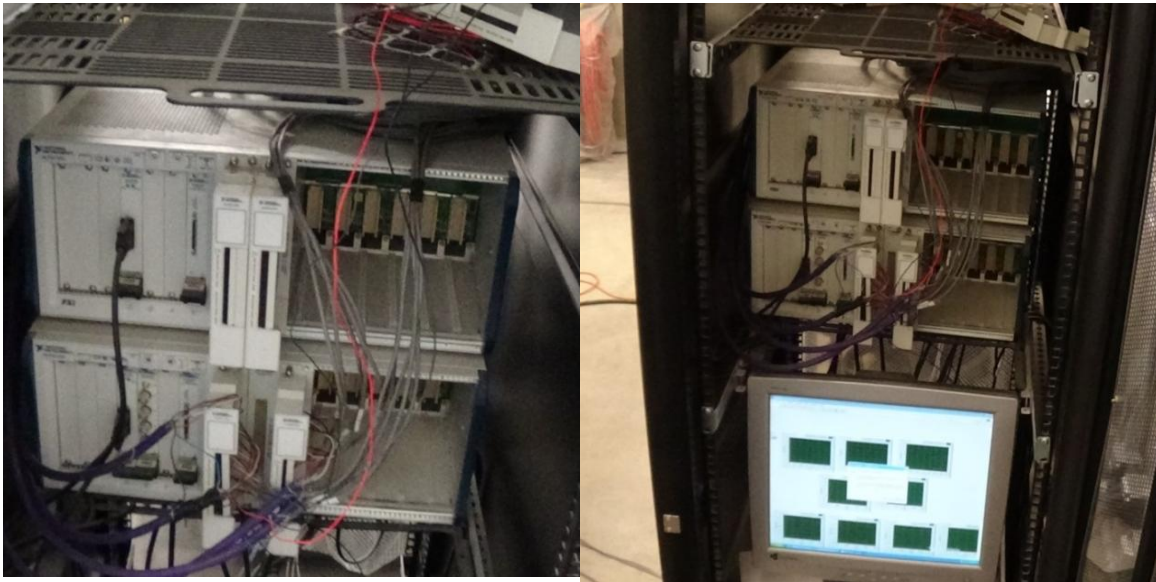
Figure 3.9: Geogrid installation

(a) Cutting the geogrid in a circular shape; (b) A geogrid layer installed inside the mold



(a) (b)
Figure 3.10: Dynamic loading system

(a) Loading plate system control device; (b) Asphalt surface deformation measurement instrument



(a) (b)

Figure 3.11: Data acquisition system

(a) Data acquisition system modules; (b) LabView software monitoring the instruments while tests are running

As for the construction of pavement sections, the silty clay subgrade was first placed and compacted in multiple equal lifts inside the steel mold (Figure 3.13-a and 3.13-b). The loose thickness of each lift was 22.9 cm (9 inches) which resulted in a 12.7 cm (5 inches) thickness of compacted soil. The subgrade soil was compacted at a water content of 11.2% to the compaction level of 95% corresponding to the Modified Proctor test (maximum dry density of 2.03 gr/cm^3 (127 PCF) at the optimum moisture content of 11%). The subgrade was prepared by using a tiller to mix the silty clay and water. Then, the silty clay was rake-leveled and compacted using a compaction rammer to a predetermined height to achieve the desired density. At the completion of subgrade preparation, the pressure cells were placed 5.1 cm (2 inches) below the subgrade-base interface at the distances of 0, 22.8 and 45.7 cm (0, 9 and 18 inches) away from the center of the mold as shown in Figure 3.4-d. Another pressure cell was placed 5.1 cm (2 inches) above the interface in the base course layer at the center of the mold. The pressure cells installation and protection process were described in Section 3.5.1. Table 3.5 shows subgrade's moisture content and resulting compaction density for the six pavement test sections.

The base course layer was prepared by placing crushed limestone in two 10 inches (or 8 inches) loose lifts, mixed with the desired optimum water content, and compacted to the final thickness of 8 inches (or 6 inches) resulting in an average density of 2.15 gr/cm^3 (134 pcf) which corresponded to nearly 95% of the optimum density using Modified Proctor Compaction. The geogrid was installed at the center of base course layer between the two compacted lifts for the first three test sections with 40.6 cm (16 inch) of base thickness and at the subgrade-base interface for the last three test sections with 30.5 (12 inch) thick base layer (Figure 3.13-c and 3.13-d).

The HMA was truck delivered, spread over the area of the test mold, rake-leveled, and immediately compacted to the predetermined height of 7.6 cm (3 inches) using a vibratory plate compactor at the level of 95% of optimum density of 2.603 gr/cm³ (162.5 pcf). The asphalt preparation and compaction process are shown in Figure 3.13-e and 3.13-f.

Geogauge tests were carried out, as shown in Figure 3.14, after compaction of each lift to ensure the required compaction level and moisture content is achieved. Shown in Table 3.5 are Geogauge test results for the subgrade, base, and HMA layers.

Table 3.5: As- constructed lift properties of subgrade, base and asphalt layer

Test No.	Test Section	Subgrade Moisture Content (%)	Subgrade Density gr/cm ³ (PCF)	Subgrade Compaction effort (%)	Base Moisture Content (%)	Base Density gr/cm ³ (PCF)	Base Compaction Effort (%)	HMA Density gr/cm ³ (PCF)	HMA Compaction Effort (%)
1	C16	11.40	1.86 (115.8)	91.40	4.10	2.13 (133.3)	94.30	2.34 (144.3)	93.10
2	B16	12.50	1.81 (113)	89.20	4.20	2.18 (135.9)	96.15	2.39 (148.2)	95.61
3	T16	11.34	1.83 (114.2)	90.10	3.90	2.09 (130.7)	92.51	2.30 (146.9)	94.79
4	C12	13.20	1.82 (113.8)	89.80	3.80	2.18 (136.1)	96.27	2.39 (145.9)	94.10
5	B12	11.8	1.87 (117)	92.35	4.6	2.15 (134.2)	94.98	2.36 (145.3)	93.75
6	T12	13.1	1.82 (113.4)	89.5	5.35	2.17 (135.4)	95.78	2.38 (145)	93.7

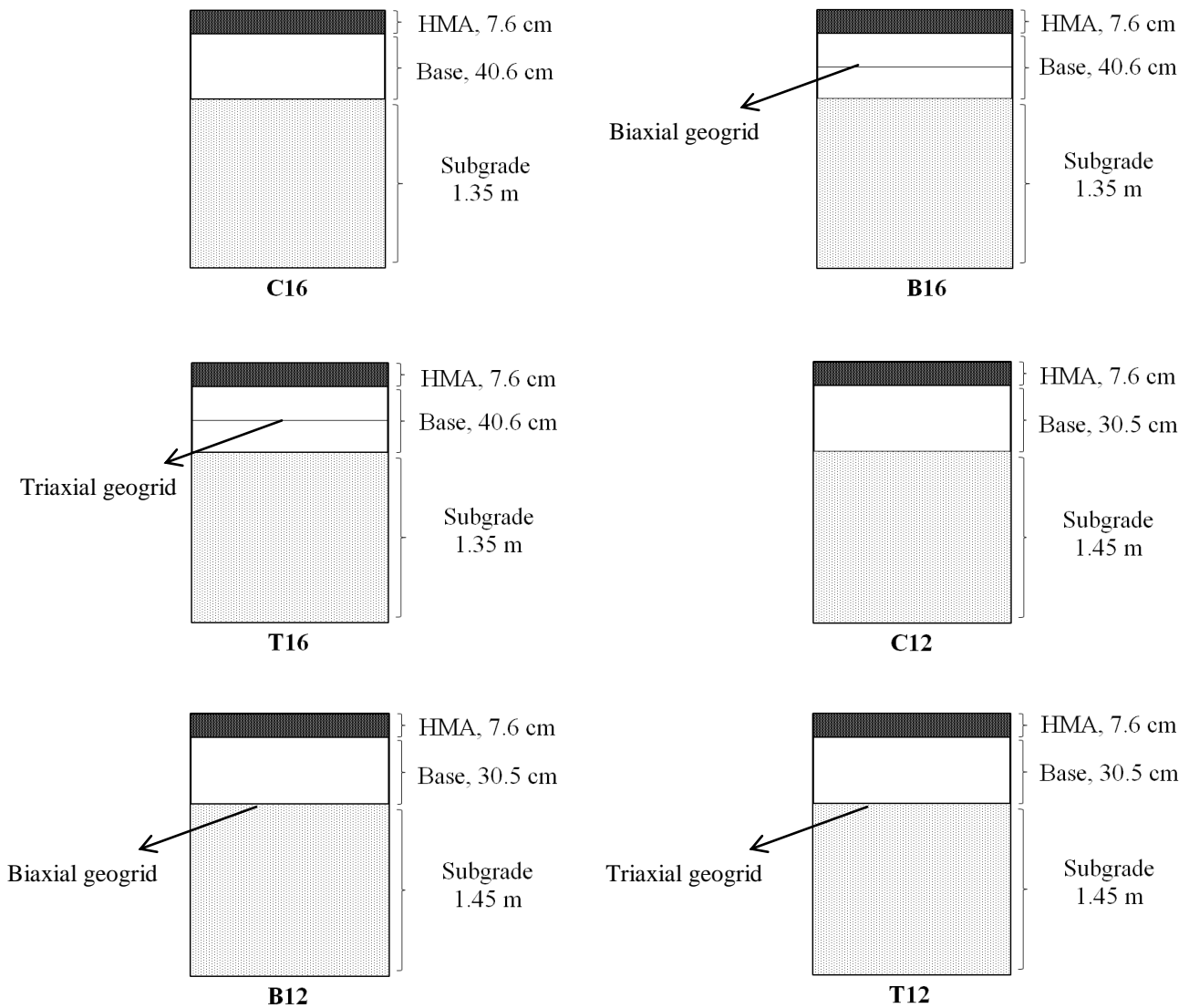


Figure 3.12: Pavement test section schematics

The loading plate system and the displacement transducer were then installed on top of the prepared pavement section as shown in Figure 3.15. All sensors were connected to a data acquisition system and the results were recorded throughout the repeated loading for at least 3 million cycles.



(a)

(b)



(b)

(d)



(c)

(d)

Figure 3.13: Test section compaction and preparation

(a) Dumping soil inside the mold; (b) Compaction of subgrade soil; (c) Spreading coarse aggregate over the subgrade; (d) Compaction of aggregate base; (e) Hot mix asphalt delivery; (f) Compaction of HMA



(a)

(b)

Figure 3.14: Geogauge testing

(a) Subgrade soil compaction level and moisture measurement; (b) Hot mix asphalt compaction level and moisture measurement



(a)

(b)

Figure 3.15: Loading plate system installation

(a) Moving the loading plate system after test section preparation; (b) Installation of the loading system

CHAPTER 4

TEST RESULTS AND DISCUSSION

4.1. Overview

This chapter presents the results of testing and analyses performed for the six pavement sections described in Section 3.7.1. Differences in performance between the two aggregate base layer thicknesses, as well as the two geogrid types are discussed. As explained in Chapter 3, the two aggregate base layer thicknesses and the two geogrid types were selected to ensure that the experimentation was generalized.

4.2. Asphalt surface deformation (Rutting Depth)

Figure 4.1 illustrates the development of asphalt surface deformation (rutting depth) for accelerated load tests, up to 3 million repeated loading for the different tested pavement sections. The permanent surface deformation was recorded by the LVDT placed on top of the loading plate attached to the loading system. Generally speaking, the rutting depth increased with increases in the number of loading cycles for all studied pavement sections. The rutting depth increased at a faster rate up to the first 0.5 million loading cycles; however, the rate of increase in rutting depth decreased with additional increases in the number of loading cycles. The unreinforced sections displayed higher surface deflections as compared to those of the reinforced pavement sections. Use of triaxial geogrid was more effective than biaxial geogrid in reducing both surface rutting and vertical stresses at the interface between base and subgrade.

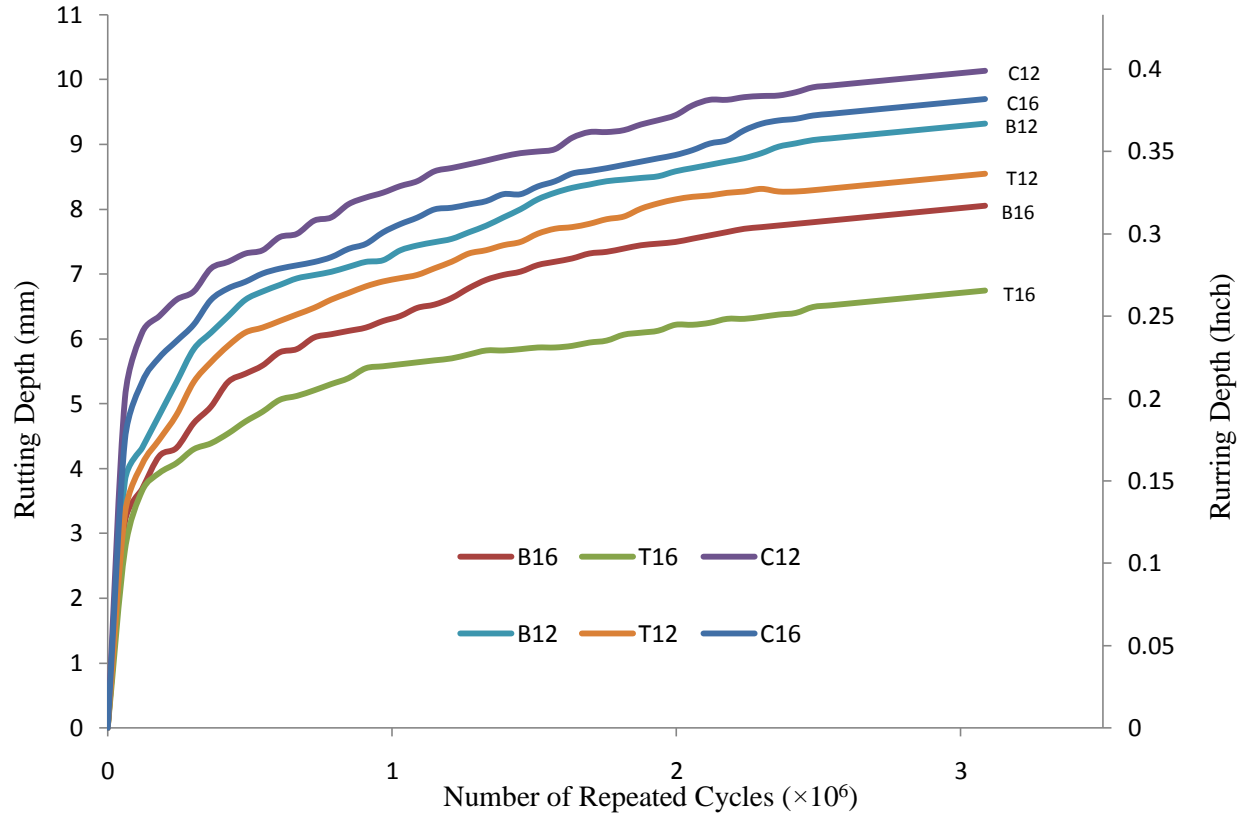


Figure 4.1: Surface Deformation (Rutting depth)

The results of the accelerated load tests, up to 3 million repeated loading for the 40.6 cm (16 in) thick base test sections, are graphically presented in Figure 4.2. As can be seen, the surface deformation of the biaxial geogrid-reinforced pavement section was less than the reference test section throughout the test. The biaxial-reinforced section displayed lower surface deflections, as compared to that of the unreinforced section, by approximately 21, 18, 15, 16, 17, and 17.1% at the loading cycles of 0.5, 1, 1.5, 2, 2.5 and 3 million, respectively (Table 4.1). The triaxial geogrid-reinforced test section showed a better performance than both the biaxial-reinforced and the unreinforced pavement sections. By using triaxial geogrid, the rutting depth decreased by nearly 31, 28, 30, 30, 31, and 30% at 0.5, 1, 1.5, 2, 2.5 and 3 million strokes, respectively; as compared to unreinforced pavement section. The asphalt surface deformation of

triaxial-reinforced test section was approximately 13, 12, 18, 18, 17, and 16% lower than the biaxial-reinforced test section at 0.5, 1, 1.5, 2, 2.5, and 3 million cycles, respectively.

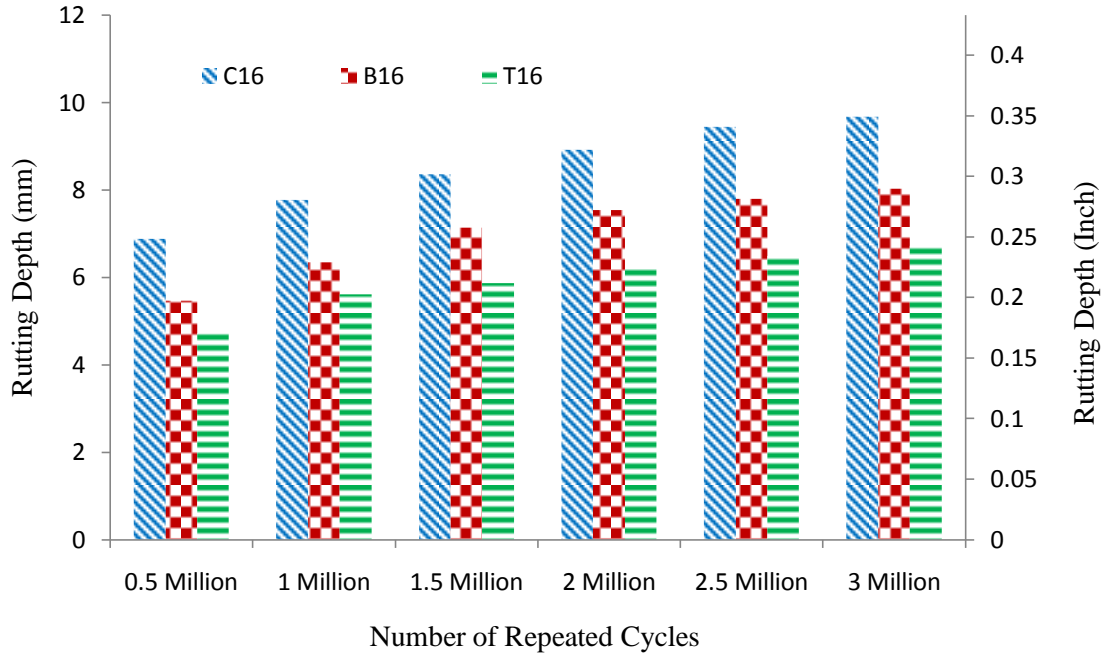


Figure 4.2: Surface Deformation of the 40.6 cm (16 in)-thick base pavement sections

Table 4.1: Rutting depth comparison of reinforced test sections to unreinforced test sections

Pavement Section	Number of loading cycles							
	0.1×10^6	0.25×10^6	0.5×10^6	1×10^6	1.5×10^6	2×10^6	2.5×10^6	3×10^6
C16	---	---	---	---	---	---	---	---
B16	-31.0%	-27.7%	-20.7%	-18.3%	-14.6%	-15.4%	-17.5%	-17.1%
T16	-31.4%	-31.6%	-31.4%	-27.8%	-29.8%	-30.3%	-31.3%	-30.5%
C12	---	---	---	---	---	---	---	---
B12	-29.2%	-19.2%	-9.7%	-11.8%	-8.3%	-10.1%	-8.2%	-8.1%
T12	-33.3%	-26.9%	-16.7%	-17.1%	-14.3%	-14.7%	-16.1%	-15.7%

Figure 4.3 illustrated the asphalt surface deformation of the 30.5 cm (12 inch)-thick base layer pavement sections. The rutting depth of biaxial-reinforced test section was lower than that of the unreinforced test section. The surface deformation of biaxial geogrid-reinforced test section was 10, 12, 8, 10, 8 and 8% smaller than that of the unreinforced section at 0.5, 1, 1.5, 2, 2.5 and 3 million strokes, respectively. The rutting depth of the triaxial geogrid-reinforced test section was smaller than unreinforced and biaxial-reinforced sections. When triaxial geogrid was used, the surface deformation decreased by 17, 17, 14, 15, 16 and 16% at 0.5, 1, 1.5, 2, 2.5 and 3 million loading cycles, respectively, as compared to unreinforced test section. Also, triaxial geogrid-reinforced pavement section rutting depths decrease by 7.7, 5.6, 6.5, 5.2, 8.6, and 8.4% at 0.5, 1, 1.5, 2, 2.5 and 3 million strokes respectively when compared to that of the biaxial-reinforced test section.

4.3. Vertical Stress distribution

The results of the vertical pressures, generated from the installed pressure cells in the subgrade center point, quarter radius off-center, and half radius off-center for the six tested pavement sections are shown in Figure 4.4, 4-5, and 4-6, respectively. The vertical stresses obtained from the pressure cell installed at the aggregate base layer center point are presented in Figure 4.7. As can be seen, irrespective of the test section properties and the location of the pressure cells, the magnitude of vertical stresses remained steady throughout the 3 million cyclical loading.

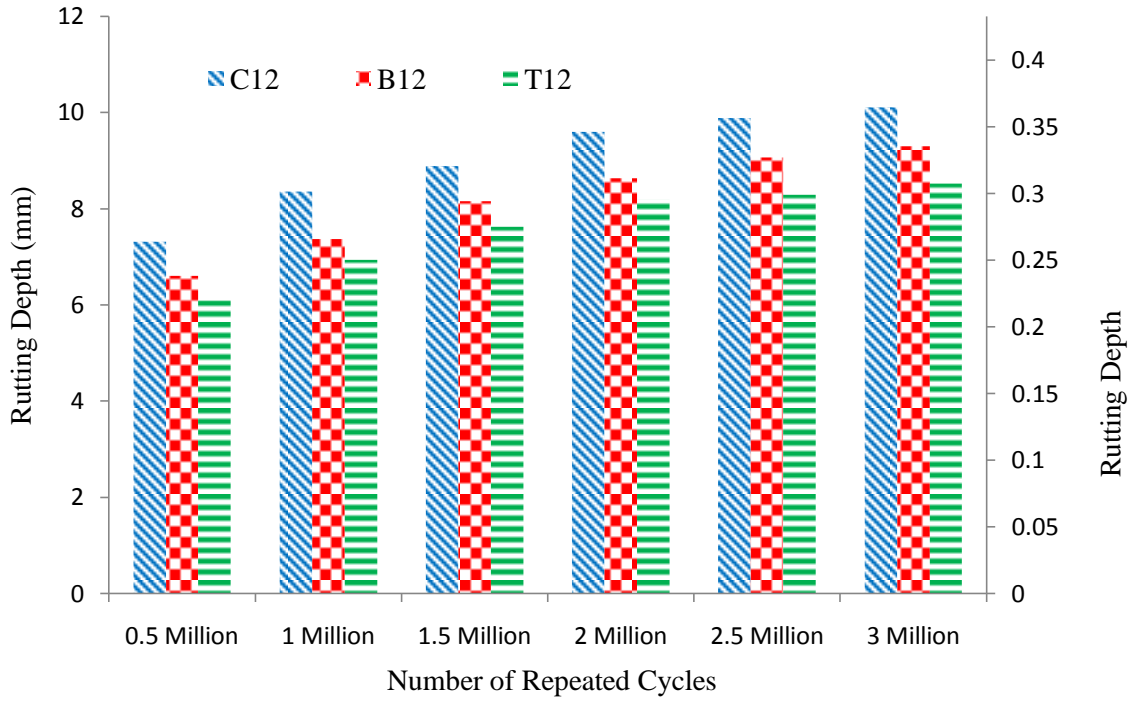


Figure 4.3: Surface Deformation of the 30.5 cm (12 in)-thick base pavement sections

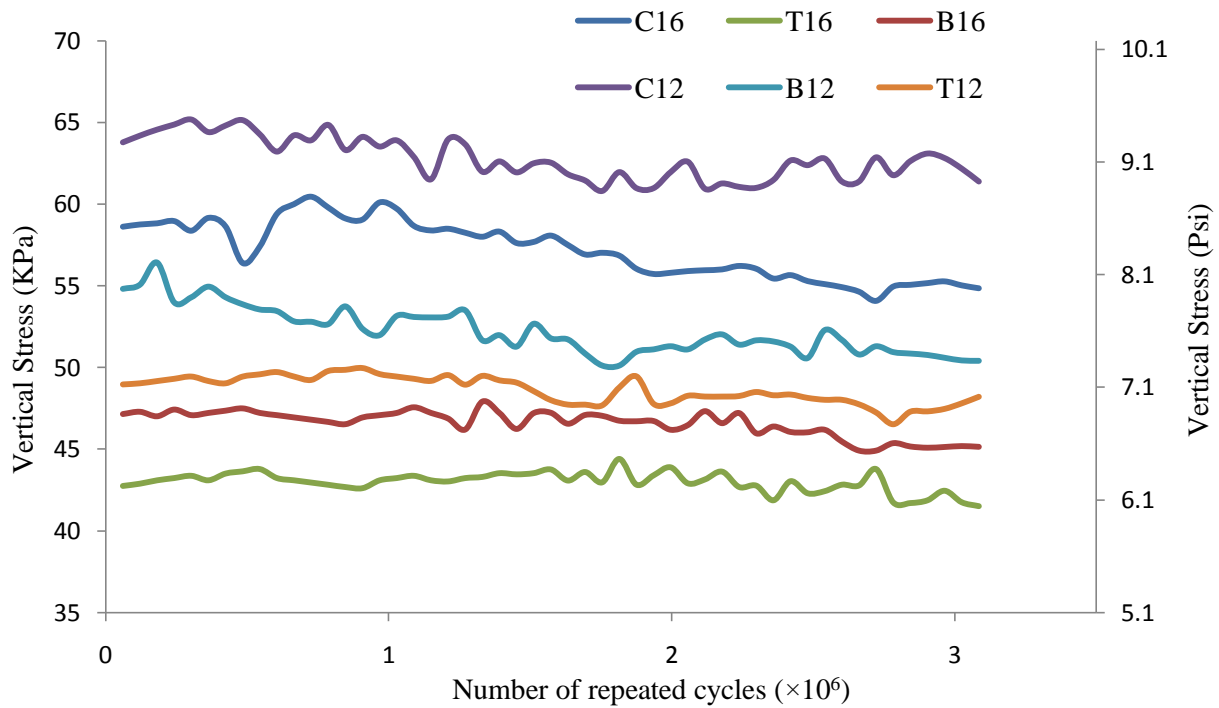


Figure 4.4: Vertical pressure the subgrade center point

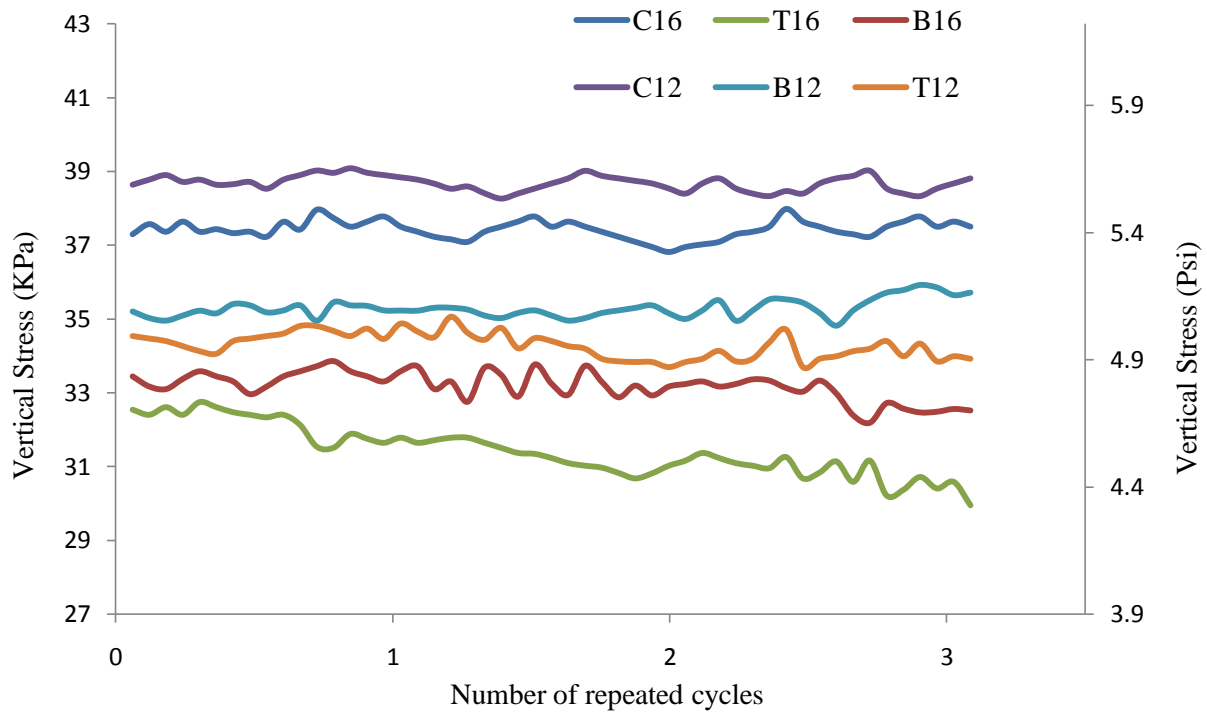


Figure 4.5: Vertical pressure at the subgrade quarter radius off-center

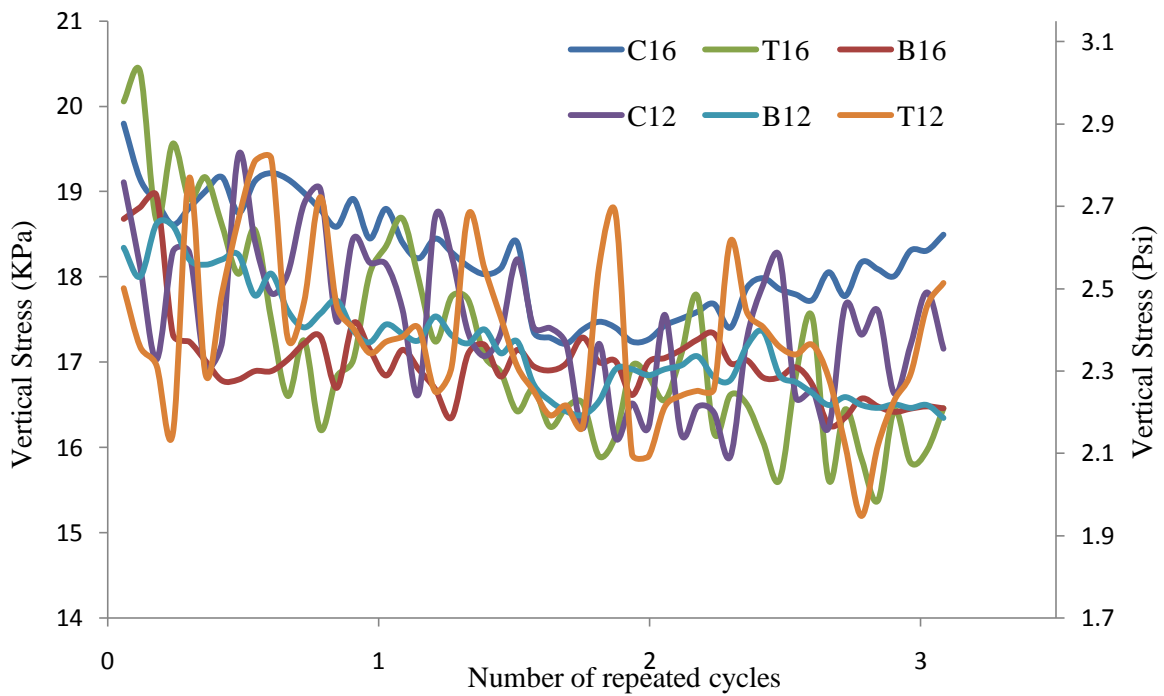


Figure 4.6: Vertical pressure at the subgrade half radius off-center

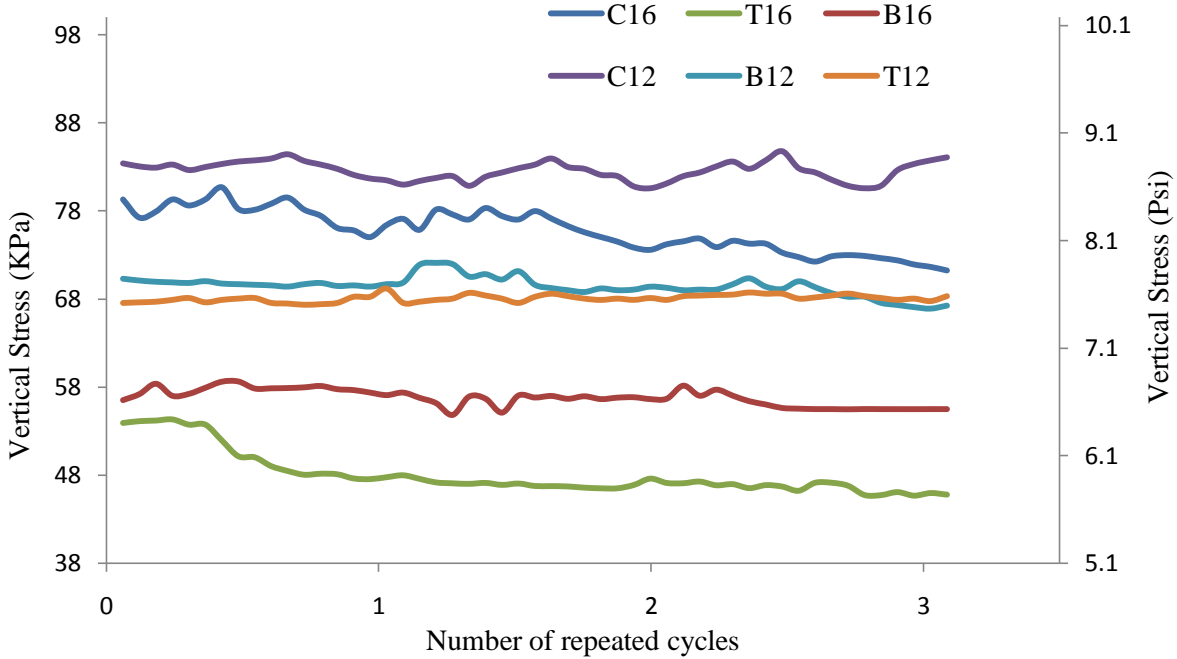


Figure 4.7: Vertical pressure at the base layer center point

The vertical stress distribution at the subgrade/base interface is presented in Figure 4.8. The stresses measured are the average of vertical stresses after 3 million loading cycles. As can be seen, the stress at the center of base layer is more than that of the subgrade for all studied pavement test sections. Also, the pressure in the subgrade soil center is more than quarter radius off-center and quarter radius off-center in more than the half radius off-center. In addition, irrespective of the aggregate base layer thickness, the magnitude of the pressure for biaxial geogrid-reinforced test section is less than unreinforced test section in all designated locations. Triaxial geogrid-reinforced test sections, showed lesser pressure values in all locations as compared to unreinforced test section and biaxial geogrid-reinforced test section for both base layer thicknesses.

As reported in Table 4.2, by reinforcing the C16 test section (base thickness of 40.6 cm (16in)) with biaxial geogrid, the average vertical stresses at base center, subgrade center, quarter radius off-center, and half radius off center reduced by 26, 19, 11, and 7%, respectively. The reductions in the vertical stresses of the triaxial geogrid-reinforced pavement section were 37, 25, 16 and 6% when compared to the unreinforced test section. Additionally, the reduction in average vertical stresses in triaxial-reinforced section were 11, 6, and 5% more than that of the biaxial-reinforced test section at base center, subgrade center, and quarter radius off-center.

When comparing the average vertical pressures of the C12 test section (base thickness of 30.5 cm (12 in)) with the biaxial geogrid-reinforced test section, at the base center, subgrade center, quarter radius off-center, and half radius off-center, decreases of 20, 17, 9, and 2%, respectively, were found. A comparison of the vertical stresses at base center, subgrade center, subgrade quarter radius off-center and half radius off-center between the triaxial geogrid-reinforced and unreinforced test section revealed that the vertical stresses reduced by 21, 23, 11 and 1% respectively. On the other hand, the reductions in average vertical pressure of the triaxial-reinforced section were 1, 6, and 2% more than that of biaxial-reinforced test section at base center, subgrade center, and quarter radius off-center, respectively.

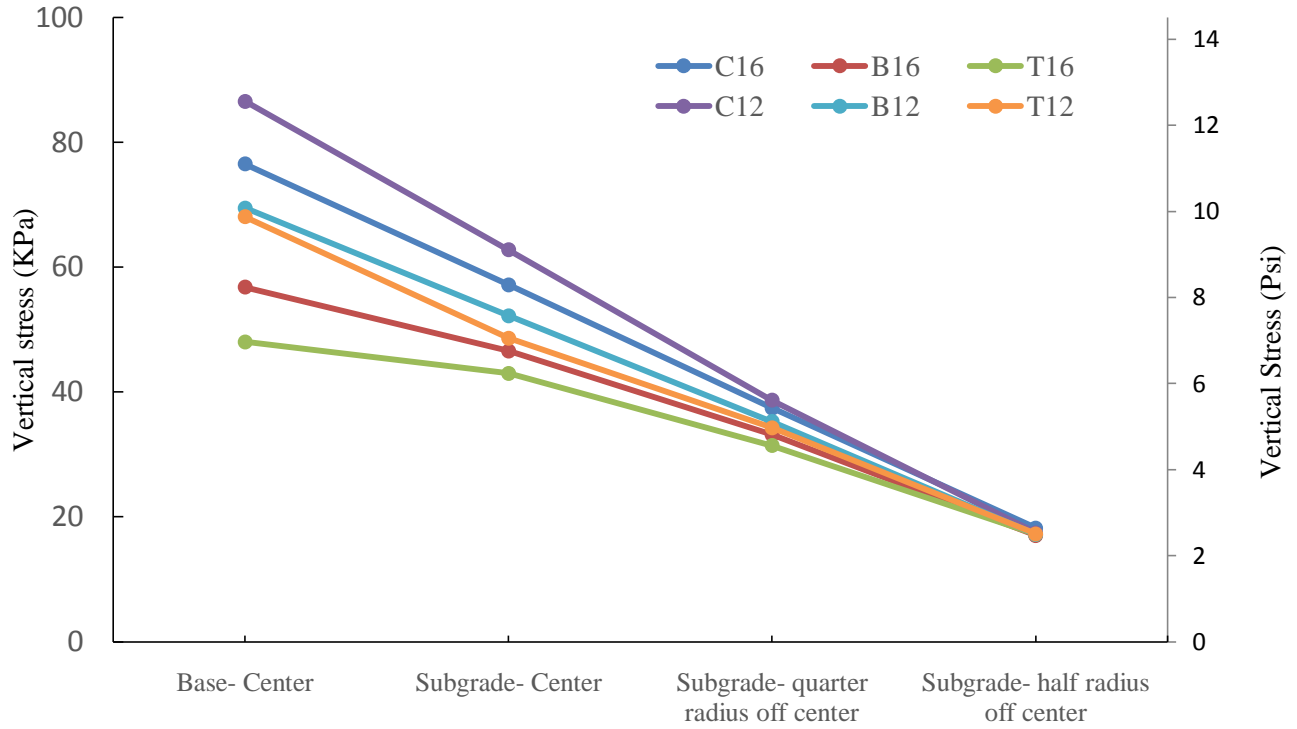


Figure 4.8: Average vertical pressure at different locations of the mold

Table 4.2: Permanent reduction of vertical pressure: a comparison of reinforced and unreinforced pavement sections

Test Pavement section	Base-Center	Subgrade-Center	Subgrade-Quarter radius off center	Subgrade-half radius off center
C16	---	---	---	---
B16	-26%	-19%	-11%	-7%
T16	-37%	-25%	-16%	-6%
C12	---	---	---	---
B12	-20%	-17%	-9%	-2%
T12	-21%	-23%	-11%	-1%

4.4. Geogrid Tensile Strain

Foil strain gauges were installed on the ribs of geogrid in order to record the deformation of geogrid's ribs under cyclic loading. Negligible readings were recorded during the first

500,000 cycles and then slowly diminished throughout the remaining repeated loading. This behavior was observed in all geogrid-reinforced test sections. At the completion of testing and upon demolding, foil strain gauges were connected to the data acquisition system and reexamined for the expected performance. The foil strain gauges were found to be in good working conditions. This implies that, due to the strong base and subgrade soil as used in this study, the amount of vertical pressure was insufficient to induce noticeable strains at the level where geogrids were installed.

CHAPTER 5

MODELING AND DESIGN METHODS

5.1. Summary

The main function of a pavement system is to take the loading applied by vehicles and distribute it to a wider area and safely transfer it to the subgrade soil. Regularly, flexible pavements are made of Hot Mix Asphalt (HMA) and base course layers build on top of the subgrade granular materials. Pavement design guides are developed to find the most optimal and economical combination of HMA and base course layer thicknesses, , taking into account the subgrade's strength and properties and the loading details to be carried throughout the service life of roadways.

This chapter discusses numerical modeling and design methods of geogrid-reinforced flexible pavements. Furthermore, design methods used in unpaved roads are reviewed briefly. Moreover, analytical design methods are used to evaluate the results of this investigation.

5.2. Modeling of Flexible Pavements

Paved road's key responses such as vertical pressure and vertical strain at the interface of subgrade and base layer, vertical pressure and vertical strain at the interface of asphalt and base layers, and tensile strains at the asphalt-base interface are important for pavement design and performance prediction. New numerical modeling methods can be used to predict critical responses of a flexible pavement system.

5.2.1. Finite Element Modeling for Geogrid-Reinforced Flexible Pavements

Finite Elements (FE) simulation is a strong method to study the behavior of geogrid-reinforced paved roadway sections. In this method, geogrid reinforcement layer is considered as a continuous membrane in pavement structure, in spite of the fact that geogrid has a mesh-like structure with openings. This assumption, limits FE modeling to consider lateral confinement mechanism provided by geogrid reinforcement to granular base materials, discussed in Chapter 2.

5.2.1.1. (Wathugala, Huang, & Pal, 1996)

Wathugala et al. (Wathugala & Desai, 1993) used ABAQUS software to develop axisymmetric finite element models to study the behavior of geosynthetic-reinforced paved sections with reinforcement located at subgrade-base interface. They used elasto-plastic Drucker-Prager modeling for HMA and base course layers. Hierarchical Single Surface (HiSS) model was utilized for subgrade soil simulation. Lower surface deformation for pavement system was anticipated with use of heavy duty geogrids. More significant improvements in pavement performance were observed by use of elasto-plastic modeling compared to linear elastic simulation.

5.2.1.2. (Perkins, et al., 2004)

Perkins et al. developed design criteria for geogrid-reinforced paved sections using Mechanistic-Empirical Pavement Design Guide. Two-dimensional axisymmetric finite element models, as one of the ME design components for unreinforced paved roads, were developed in ABAQUS software by following the guidelines suggested for nonlinear response models (Uzan, 2004). The authors could not develop a unique response model for reinforced paved roads to

explain the improvement by geogrid inclusion, but they suggested a multi-step modeling procedure to address the compaction level and surface loading effects on the confinement level of the base course layer by inclusion of geogrid in paved roads. In this simulation, geogrids were considered as a linear elastic membrane. Contacts were allocated to the up and down faces of the reinforcement layer and the neighboring pavement layers, based on the Coulomb friction model. The multi-step finite element modeling showed that shear stresses at layers interfaces increase with an increase in compaction level and traffic loading cycles. The shear stresses observed at layers interfaces contribute to the lateral confinement of aggregate base layer. Similar predicted results in rutting depth was observed between the data obtained from testing program and the results of developed finite element models based on critical pavement responses.

5.2.1.3. (Saad, Mitri, & Poorooshab, 2006)

Saad et al. (Saad, Mitri, & Poorooshab, 2006) used ADINA software to develop a dynamic 3 dimensional finite element model to predict geogrid-reinforced flexible pavements behavior. The soil granular layer was simulated by the modified CamClay model and the aggregate base layer was simulated through the elastoplastic Drucker-Prager simulation. Both HMA and geogrid layers were considered as a linear elastic membrane. A triangular wave shape dynamic loading with the duration of 0.1 second was performed to the pavement model. The interface between the geosynthetic and the pavement layers was assumed to be fully bounded. A parametric study was performed in order to investigate the factors that could influence the effectiveness of geosynthetic reinforcement such as aggregate base materials thickness and quality, and subgrade soil strength.

5.2.1.4. (Kwon, Development of a mechanistic model for geogrid reinforced flexible pavements, 2007)

Kwon developed an axisymmetric FE model to investigate the benefits of geogrid reinforcement in paved roads. The asphalt layer was simulated as isotropic elastic straight layer. A nonlinear, stress-dependent simulation was developed for the aggregate base course and soil layers. Anisotropy of the aggregate base materials was reflected on the modeling procedure. The geogrid layer was modeled through membrane elements with finite thicknesses. A remarkable aspect of the simulation is consideration of "locked-in" horizontal remaining stresses in geogrid's adjacent pavement layers, which models the improvements of geogrid reinforcement developed by construction and loading. The remaining stress was implementing to the base layer on top of the geogrid as a primary condition. The finite element simulations were regulated and approved by field studies carried out as accelerated pavement testing programs.

5.3. Design Methods used for geogrid-reinforced pavements

Several design methodologies have been proposed for geogrid-reinforced paved and unpaved roads since the late 1970s. Unpaved methods include: Giroud and Noiray (1981), and Giroud and Han (2004); and paved methods are AASHTO R50-09 and a software developed by Tensar named SpectraPave4 Pro. A short review of these methods is presented below. Moreover, the geogrid-reinforced pavement design methods are used to evaluate the results of this study.

5.3.1. Design Methods for Unpaved Roads

5.3.1.1. The Giroud and Noiray Method

Giroud and Noiray (Giroud & Noiray, Geotextile-reinforced unpaved road design, 1981) used the tensioned membrane theory to evaluate the effects of the tensile strength of the

geotextile on required aggregate base layer thickness. The subgrade they considered in the study was a soft, saturated clay material that is undrained. The aggregate base material had a minimum CBR of 80%. Moreover, this method considered a rectangular contact area and a steady stress distribution angle. In order to approximate the vertical stress at the subgrade-base interface, a stress distribution method was proposed. Henry (Henry K. S., 1999) compared the Barenburg et al. and Giroud and Noiray design methods and reported the differences.

5.3.1.2. The Giroud and Han Method

Giroud and Han (Giroud & Han, Design method for geogrid-reinforced unpaved roads. I: Development of design method, 2004) suggested an equation to determine the required aggregate base layer thickness of geogrid-reinforced unpaved sections constructed over an undrained, cohesive granular materials. Giroud and Has method considers more parameters than other available design procedures for geogrid-reinforced unpaved roads. Geosynthetic type and properties, the aperture size and shape of the geogrid, the stability modulus of the geogrid, the aggregate base course modulus, the modulus of the subgrade soil, the traffic loading details, the tire pressure, the wheel load, subgrade's undrained shear strength, and the rutting depth are some of the parameters used in this method. Different bearing capacity factors were recommended for unreinforced, geotextile-reinforced, and geogrid-reinforced base course layers.

Not like the Giroud and Noiray method, the Giroud and Han method considers the effects of the aggregate base layer stiffness, which has relationship with the CBR of the aggregate base material. Moreover, the new method considers the tire contact area as a circular shape. These features are some of the improvements of the Giroud and Han method as compared to the previous methods. Consideration of base layer stiffness in design method is consistent with the findings of a research conducted by Knapton and Barber (Knapton & Barber, 1979), which

concluded that the aggregate base material CBR value is an important factor in the number of loading cycles an unpaved road can resist. Another major difference between the Giroud and Han method and the Giroud and Noiray method is the inclusion of the stress distribution angle in design procedure. In the Giroud and Noiray procedure, the stress distribution angle was fixed and steady, but in the Giroud and Han method, the stress distribution angle varies based on the number of loading cycles, the aggregate base layer thickness, the radius of the contact area, and the geosynthetic type and properties. These features make this design approach more accurate and realistic.

5.3.2. Design Methods for Paved Roads

As paving material costs increase, thickness reduction and cost savings using geogrids become more attractive options for many road construction projects. However, the absence of appropriate design methodologies limits contractors and state highway agencies to use geogrid as reinforcement in paved roads. There is a lack of documentation on general test data illustrating the beneficial field performance of geogrid reinforcement in flexible pavements. Not all types or brands of geogrids have the same characteristics, suggesting that the performance of geogrids is somewhat product specific. Current available geogrids design procedures are both product specific and specific to the conditions under which pavement test sections were carried out.

The current geogrid-reinforced pavement design methods are based on empirical design method with traffic benefit ratio (TBR). The TBR-based design approach, such as the AASHTO Recommended Practice PP46-01 (Berg & Association, 2000), provides a simple but limited approach to quantifying geogrid performance benefits for various design scenarios.

5.3.2.1. AASHTO PP 46-01 (AASHTO R 50-09)

The American Association of State Highway and Transportation Officials (AASHTO) has provided guidance on the use of geosynthetics in paved roads. Now in the form of a Standard Practice document (AASHTO, R50-09, 2009), clear trend is provided about evaluation of performance benefit of geosynthetic reinforcement in paved roads. In Section 3 of this standard practice document, AASHTO state that “Because the benefits of geosynthetic-reinforced pavement structures may not be derived theoretically, test sections are necessary to obtain benefit quantification.” Within Section 5 of the same document, it is stated that their design procedures “use experimentally derived input parameters that are often geosynthetic specific” and “users of this document are encouraged to affirm their design with field verification of the reinforced pavement performance.”

It is clear that AASHTO is supporting a radical departure from the current “state of practice” for the design of geosynthetic-reinforced flexible pavements. In the same document, they later state that “traffic benefit ratio (TBR) and base course reduction factor (BCR) are the parameters that need to be quantified through full scale testing.”

Evaluation of the improvements by geogrid reinforcement in flexible pavements is based on pavement trials conducted in both small-scale and full-scale field testing. Research summaries from previous investigations were provided in Chapter 2 of this report. Within AASHTO R 50-09 and it’s predecessor, PP 46-01 a single Traffic Benefit Ratio (TBR) or Base Course Reduction (BCR) value method is used to account for the benefit derived from geogrid-reinforcement of flexible pavement structure. AASHTO R 50-09 and PP 46-01 provide no guidance on how to carry out a study to arrive at TBR/BCR range. In addition, variations in pavement structure geometry and loading conditions are noticeably missing. Furthermore, these guidelines do not

delineate the applications of subgrade stabilization and base course reinforcement. Based on AASHTO R 50-09 standard, TBR and BCR are used to account for the benefits of geogrid reinforcement in this study.

5.3.2.2. Traffic Benefit Ratio (TBR)

The improvement to the pavement system provided by geogrid reinforcement can be directly measured by a Traffic Benefit Ratio (TBR), which is defined by Berg et al. as follows: “A ratio of the number of load cycles on a reinforced section to reach a defined failure state to the number of load cycles on an unreinforced section, with the same geometry and material constituents, to reach the same defined failure state (Berg, Christopher, & Perkins, 2000).”

The traffic benefit ratio (TBR) is used to evaluate the benefit of geogrid base reinforcement in this study. Calculated TBRs for the different unreinforced and reinforced test sections at the rutting depths of 4, 5, 6, 7, 8, and 9 mm are summarized in Table 5.1. More details on TBRs calculations process is provided in Appendix I.

Table 5.1: Traffic Benefit Ratio for the studied test sections

Rutting Depth, mm (in)	Test Pavement Section					
	C16	B16	T16	C12	B12	T12
4 (0.16)	1.0	3.0	4.0	1.0	-	-
5 (0.20)	1.0	3.0	5.0	1.0	3.0	4.0
6 (0.24)	1.0	3.0	7.5	1.0	3.0	4.0
7 (0.28)	1.0	2.7	-	1.0	2.2	3.0
8 (0.31)	1.0	2.6	-	1.0	1.7	2.2
9 (0.35)	-	-	-	1.0	1.5	-

Number of repeated loading cycles for unreinforced test sections to reach to 4, 5, 6, 7, 8, and 9 mm of rutting depth is shown in Table 5.2. The C16/C12 ratios shown in the Table are number of loading cycles applied on unreinforced test section with 40.6 cm base thickness (C16)

reaching to a specific rutting depth to the number of loading cycles applied on unreinforced test section with 30.5 cm base layer (C12) reaching to the same surface deformation. A comparison of C16/C12 ratios and TBRs for different rutting depths is documented in Table 5.2. As can be seen in this table, all calculated traffic benefit ratios for the specific rutting depth is more than the C16/C12 ratios. This implies that the 40.6 cm (16 in) base thickness of unreinforced pavement section can be reduced to 30.5 cm (12 in) base thickness when it is reinforced with biaxial or triaxial geogrid.

Table 5.2: Comparison of TBR and C16/C12

Rutting Depth mm (inch)	Loading cycles		Ratio C16/C12	TBR	
	C16	C12		B12	T12
4 (0.16)	60,500	-	-	-	-
5 (0.20)	121,000	60,500	2	3.0	4.0
6 (0.24)	242,000	121,000	2	3.0	4.0
7 (0.28)	544,500	363,000	1.5	2.2	3.0
8 (0.31)	1,149,500	847,000	1.36	1.7	2.2
9 (0.35)	2,117,500	1,573,000	1.35	1.5	-

5.3.2.3. Base Course Reduction (BCR)

Base Course Reduction Factor (BCR) essentially quantifies the amount of component thickness reduction that can take place in a geogrid-reinforced pavement layer with no loss of performance.

5.3.2.3.1. BCR values based on rutting depth results

With the TBR values found in the previous section and shown in Table 5.1, a simple analysis, using AASHTO 1993 pavement design procedure, is utilized to evaluate the impact of geogrid reinforcement on base course thickness reduction. The reinforced Equivalent Standard Axle Loads ($ESAL_r$) are calculated by dividing the unreinforced $ESAL_u$ by the TBR value. The

ESAL_r values can be used to back calculate the structural number and then, the new base course depth. By dividing the reinforced base course to unreinforced base course thicknesses, the base course reduction factor is calculated. More details on the design method is provided in the following paragraphs and a sample calculation is described in Appendix II.

In the AASHTO 1993 Pavement Design Procedure, the structural number (SN) is considered to determine the overall structural capacity of a roadway pavement section. The SN for paved section design is calculated from the following equation (AASHTO, AASHTO Guide for Design of Pavement Structures, 1993):

$$SN = a_1 D_1 + a_2 D_2 m_2$$

Equation 5.1: Structural Number

In Equation 5.1, D_1 and D_2 are the asphalt and aggregate base layers thicknesses, respectively (inch). a_1 and a_2 are layer structural coefficients for the asphalt and aggregate base layer, respectively. m_2 is the drainage coefficient of the base course and it was assumed 1.0 in this investigation because the test sections were laboratory controlled. The layer coefficients a_1 and a_2 are obtained (Van Til, McCullough, Vallerga, & Hicks, 1972) from the resilient modulus of materials reported in Chapter 3. More details on layer coefficient selection are available in Appendix II.

The obtained structural number is utilized to calculate the total number of load applications (18-kip (80-kN) single-axle load) using the following equation (AASHTO, AASHTO Guide for Design of Pavement Structures, 1993):

$$\log W_{t18} = 9.36 \log(SN + 1) - 0.20 + \frac{\log \left[\frac{\Delta PSI}{4.2 - 1.5} \right]}{0.4 + \frac{1094}{(SN + 1)^{5.19}}} + 2.32 \times \log M_r - 8.07$$

Equation 5.2: AASHTO 1998 ESAL

In equation 5.2, W_{t18} is the number applications (18-kip (80 kN) single-axle load) before requiring the resurfacing maintenance; ΔPSI is initial design serviceability index minus design terminal serviceability index (ΔPSI of 1.5 was used in this investigation). M_r is resilient modulus of the subgrade soil which is calculated from the equation suggested by Nevada Department of Transportation ((NDOT), 2011):

$$M_r = 145 \times 10^{0.0147 \times R\text{-Value} + 1.23}$$

Equation 5.3: Resilient Modulus of Subgrade Soil

Based on the subgrade R-value presented in Chapter 3 (R-value = 40), the subgrade resilient modulus is 9,536 Psi. The $ESAL_r$ is calculated for all test pavement sections and the results are shown in Table 5.3. Same as the TBR, Base Course Reduction factor could be defined for a specific rutting depth. As can be seen in Table 5.3, the BCRs attributed to the triaxial geogrid reinforcement are more than that of the biaxial geogrid reinforcement for both 40.6 and 30.5 cm base layer thicknesses. In other words, irrespective of the base layer thickness and geogrid location in paved section, triaxial geogrid is more effective than the biaxial geogrids in the reduction of the base layer thickness.

Table 5.3: Base course reduction values for the studied pavement sections

Reinforcement type	Test Pavement Section	Rutting Depth, mm (Inch)	TBR	ESAL _r	Base Layer Thickness	Base Course Reduction Factor	Base Course Reduction Percentage
Unreinforced 40.6 cm (16 Inch)-thick base	C16	-	1	2,176,581	16	-	-
Biaxial Reinforced 40.6 cm (16 Inch)-thick base	B16	4 (0.16)	3	725,527	11.78	0.74	26.4
	B16	5 (0.20)	3	725,527	11.78	0.74	26.4
	B16	6 (0.24)	3	725,527	11.78	0.74	26.4
	B16	7 (0.28)	2.7	806,141	12.15	0.76	24.1
	B16	8 (0.31)	2.6	837,146	12.28	0.77	23.2
Triaxial Reinforced 40.5 cm (16 Inch)-thick base	T16	4 (0.16)	4	544,145	10.8	0.68	32.5
	T16	5 (0.20)	5	435,316	10.08	0.63	37.0
	T16	6 (0.24)	7.5	290,211	8.825	0.55	44.8
Unreinforced 30.6 cm (12 Inch)-thick base	C12	-	1	774,005	12	-	-
Biaxial Reinforced 30.6 cm (12 Inch)-thick base	B12	5 (0.20)	3	258,002	8.48	0.71	29.3
	B12	6 (0.24)	3	258,002	8.48	0.71	29.3
	B12	7 (0.28)	2.2	351,820	9.41	0.78	21.6
	B12	8 (0.31)	1.7	455,297	10.22	0.85	14.8
	B12	9 (0.35)	1.5	516,003	10.63	0.89	11.4
Triaxial Reinforced 30.5 cm (12 Inch)-thick base	T12	5 (0.20)	4	193,501	7.66	0.64	36.2
	T12	6 (0.24)	4	193,501	7.66	0.64	36.2
	T12	7 (0.28)	3	258,002	8.48	0.71	29.3
	T12	8 (0.31)	2.2	351,820	9.41	0.78	21.6

5.3.2.3.2. BCR values based on vertical stresses results

A concern may be raised on the use of geogrid in strong soil, such as the one available in nearly all locations throughout Nevada. If chosen to use pressure variations between unreinforced and geogrid-reinforced section, a new term called “Pressure Benefit Ratio (PBR)”

can be introduced. PBR is defined as the ratio of average vertical stresses at the center of subgrade layer for geogrid-reinforced pavement sections to the equivalent unreinforced test sections. For this study, PBR for geogrid-reinforced pavement sections are shown in Table 5.4.

Table 5.4: Pressure Benefit Ratio for the studied pavement sections

Test section	PBR
B16	1.23
T16	1.33
B12	1.20
T12	1.29

Same as Base Course Reduction (BCR) method discussed in Section 5.3.2.3, PBR ratios are utilized to perform a simple analysis using AASHTO 1993 pavement design guide. Reinforced equivalent standard axle loads are calculated by dividing the unreinforced number of passes by PBR ratio. Similar to the example presented in Appendix II, base course reduction percentages using PBR ratios for the four reinforced studied pavement sections were calculated. The results are shown in Table 5.5.

Table 5.5: Base Course Reduction percentages using PBR ratios

Test Pavement section	PBR	ESAL	Base layer thickness	Base Course Reduction Factor	Base course reduction percentage
C16	1	2,176,581	16	1	---
B16	1.23	1,769,578	15.136	0.946	5.40
T16	1.33	1,636,527	14.82	0.26	7.38
C12	1	774,005	12	1	---
B12	1.2	619,204	11.23	0.936	6.42
T12	1.29	609,453	11.18	0.932	6.83

As can be seen in Table 5.5, using PBR values, base course reduction percentages remained approximately between 5 and 8% for the studied biaxial and triaxial geogrid-reinforced sections.

5.3.2.1. Effective Structural Capacity and Spectrapave4-PRO software

The test section properties and results were used to calculate an effective layer coefficient for the base course layer of geogrid-reinforced test sections using the AASHTO Pavement Design Guide. The effective base course structural coefficient represents an adjustment to the standard base course coefficient which accounts for the actual passes sustained by the test section and the actual base course thickness. Same as BCR method, TBR values are used to calculate the reinforced W_{118} , and reinforced structural numbers. While in BCR method the new SN was used to calculate the reduced base layer thickness, the resulted SN in this method is used to calculate the effective base layer coefficient with the same thickness. Thus, the effective base course structural coefficient is higher for the geogrid-reinforced pavement. Calculation details and procedures are presented in Appendix III. The resulted values are summarized in Table 5.6.

A pavement design procedure is presented in the SpectraPave4-PROTM software developed by Tensar Company. This software was first released in 1998 and has been updated regularly. This software contains procedures for both unpaved and paved road sections. The SpectraPave4-PRO User's Manual states that the pavement optimization design module complies with AASHTO R-50, Standard Practice for Geosynthetic Reinforcement of the Aggregate Base Course of Flexible Pavement Structures.

Table 5.6: Effective Layer Coefficients and Structural Numbers for studied for studied pavement sections

Reinforcement type	Test Section	Rutting Depth, mm (Inch)	HMA		Aggregate Base Course			Effective Structural Number	SpectraPave4 Base Effective Layer Coefficient
			Thickness, cm (in)	Layer Coefficient	Thickness, cm (in)	Effective Layer Coefficient	Drainage Coefficient		
Unreinforced 40.6 cm (16 Inch)-thick base	C16	-	7.6 (3)	0.34	40.6 (16)	0.12	1	2.94	0.12
	B16	4 (0.16)	7.6 (3)	0.34	40.6 (16)	0.159	1	3.556	0.124
	B16	5 (0.20)	7.6 (3)	0.34	40.6 (16)	0.159	1	3.556	
	B16	6 (0.24)	7.6 (3)	0.34	40.6 (16)	0.159	1	3.556	
	B16	7 (0.28)	7.6 (3)	0.34	40.6 (16)	0.155	1	3.492	
B16	8 (0.31)	7.6 (3)	0.34	40.6 (16)	0.153	1	3.468		
Triaxial Reinforced 40.6 cm (16 Inch)-thick base	T16	4 (0.16)	7.6 (3)	0.34	40.6 (16)	0.170	1	3.74	0.165
	T16	5 (0.20)	7.6 (3)	0.34	40.6 (16)	0.179	1	3.876	
	T16	6 (0.24)	7.6 (3)	0.34	40.6 (16)	0.196	1	4.148	
Unreinforced 30.5 cm (12 Inch)-thick base	C12	-	7.6 (3)	0.34	30.5 (12)	0.12	1	2.46	0.16
	B12	5 (0.20)	7.6 (3)	0.34	30.5 (12)	0.163	1	2.976	0.135
	B12	6 (0.24)	7.6 (3)	0.34	30.5 (12)	0.163	1	2.976	
	B12	7 (0.28)	7.6 (3)	0.34	30.5 (12)	0.150	1	2.82	
	B12	8 (0.31)	7.6 (3)	0.34	30.5 (12)	0.140	1	2.7	
B12	9 (0.35)	7.6 (3)	0.34	30.5 (12)	0.135	1	2.64		
Triaxial Reinforced 30.5 cm (12 Inch)-thick base	T12	5 (0.20)	7.6 (3)	0.34	30.5 (12)	0.176	1	3.126	0.18
	T12	6 (0.24)	7.6 (3)	0.34	30.5 (12)	0.176	1	3.126	
	T12	7 (0.28)	7.6 (3)	0.34	30.5 (12)	0.163	1	2.9736	
	T12	8 (0.31)	7.6 (3)	0.34	30.5 (12)	0.150	1	2.82	

In fact, the SpectraPave4-PRO flexible pavement design module follows the empirically based 1993 AASHTO Guide for Design of Pavement Structures. The design approach uses enhanced layer coefficients to account for the benefits of the geogrid. Tensar mentioned “these coefficients are based on extensive testing (laboratory, field, accelerated, etc.) and over 30 years of field performance.” These coefficients are specific to the selected Tensar biaxial and triaxial geogrids and are functions of the technical specifications of the geogrid, thickness of the asphalt layer, thickness of the aggregate base course, and subgrade strength. The enhanced layer coefficients for the test pavement sections are shown in Table 5.6. More details on software input and output data are presented in Appendix IV.

CHAPTER 6

CONCLUSIONS AND RECOMMENDATIONS

6.1. Conclusions

As stated earlier, this investigation was intended to determine the extent to which geogrid could 1-decrease surface rutting, 2-lower vertical stresses experienced at subgrade-base interface, and 3-assist in reducing base course thickness of the studied flexible pavement sections reinforced with biaxial or triaxial geogrid.

Six laboratory tests were conducted using a steel cylindrical mold. The base thickness of three tests was 30.5 cm (12 in), whereas base thickness of 40.6 cm (16 in) was used for the remaining three tests. A layer of biaxial or triaxial geogrid was placed at the mid-depth of aggregate base course for the tests with 40.6 cm (16 in) of base layer. For the tests which the base layer was 30.5 cm (12 in), the geogrid was placed at the subgrade-base interface. A hydraulic actuator provided 40 kN (9 kips) sinusoidal vertical load through a 305 mm (12 in) circular steel plate at a frequency of 0.77 Hz. The repeated loading was continued for at least 3 million cycles for each test. Performances of biaxial-reinforced and triaxial-reinforced sections were compared with that of companion unreinforced sections. AASHTO design method (AASHTO, R50-09, 2009) was used to evaluate the results. TBR and BCR ratios were calculated for the reinforced test sections. The main results and conclusions of the study are described below.

6.1.1. Test results

The results of the laboratory program included rutting depth, vertical stresses, and geogrid tensile strain for the six tested pavement sections.

6.1.1.1. Rutting depth

- The inclusion of geogrid reduced the rutting depth of the studied pavement sections. Irrespective of the base layer thickness and number of load repetition, use of triaxial geogrid was more effective than biaxial geogrid in reducing surface rutting of flexible pavements.
- Use of biaxial and triaxial geogrids in the mid-depth of a 40.6 cm (16 in) aggregate base layer resulted in 17 and 30%, respectively, lower rutting depth at 3 million loading cycles.
- After 3 million loading cycles, the rutting depth of the studied pavement sections approximately decreased by 8 and 16% when the pavement section with 30.5 cm (12 in) base layer thickness was reinforced with biaxial and triaxial geogrids, respectively.

6.1.1.2. Vertical stresses

- Irrespective of the test section properties and the location of the pressure cells, the magnitude of vertical stresses remained fairly steady throughout 3 million loading cycles.
- Independent of the aggregate base layer thickness, the stresses experienced at the subgrade and base layer for biaxial geogrid-reinforced test sections were less than that of unreinforced test sections. Triaxial geogrid-reinforced test sections, showed lesser pressure values in all locations as compared to unreinforced and biaxial geogrid-reinforced test sections for both base layer thicknesses.

- By reinforcing the C16 test section with biaxial geogrid, the average vertical stresses at base center, subgrade center, quarter radius off center, and half radius off center, reduced by 26, 19, 11, and 7%, respectively. These reductions for the triaxial geogrid-reinforced pavement section were 37, 25, 16 and 6% when compared to those of companion unreinforced test section.
- The average vertical stresses at base center, subgrade center, quarter radius off center, and half radius off center of the test section with 30.5 cm (12 in) of aggregate base layer decreased by 20, 17, 9, and 2%, respectively, for biaxial geogrid-reinforced section. These reductions were by 21, 23, 11, and 1%, respectively, when triaxial geogrid was used.

6.1.1.3. Geogrid tensile strain

- Negligible to no tensile strain readings were recorded at the level where geogrids were installed in all studied test sections.

6.1.2. Design methods

Traffic Benefit Ratio (TBR), Base Course Reduction (BCR) using rutting depth and subgrade center point pressure values, and Effective Base Layer Coefficient were used to evaluate the results of this study.

6.1.2.1. Traffic Benefit Ratio

TBR is defined as the ratio of the number of load cycles of a geogrid-reinforced section to the number of load cycles of an unreinforced section for a given rutting depth.

- TBRs of triaxial geogrid-reinforced test sections were more than biaxial geogrid-reinforced test sections at both studied base layer thicknesses. Triaxial geogrid-reinforced sections produced higher TBRs than those recorded for the biaxial geogrid-reinforced pavement sections.
- Comparison of TBRs and C16/C12 ratios revealed that the 40.6 cm (16 in) base thickness of unreinforced pavement section can be reduced to 30.5 cm (12 in) base thickness when it is reinforced with biaxial or triaxial geogrid.
- The Traffic Benefit Ratio (TBR) of 3, 7.5, 3, and 4 was recorded for the B16, T16, B12, and T12 test sections, respectively, at the rutting depth of 6 mm.

6.1.2.2. Base Course Reduction

Base Course Reduction Factor (BCR) essentially quantifies the amount of component thickness reduction that can take place in a geogrid-reinforced pavement layer with no loss of performance. AASHTO 1993 pavement design guide was performed to have a simple analysis to assess the impact of geogrid reinforcement on base layer thickness reduction.

- Triaxial geogrid was found to be more effective than biaxial geogrid in reducing base layer thickness.
- Considering the TBR corresponding to 6 mm (0.24 in) rutting depth, the 40.6 cm (16 in) thickness of aggregate base layer of unreinforced pavement sections can be reduced by 26 and 45% when reinforced with biaxial and triaxial geogrids, respectively. Similarly, the base thickness of C12 test section can be reduced by 29 and 36%.

- Based on the average stress reductions in the subgrade center point of geogrid-reinforced pavement sections, a Pressure Benefit Ratio (PBR) was defined and utilized to calculate base layer reduction percentages. PBR of the studied biaxial and triaxial geogrid-reinforced sections were averagely 1.22 and 1.31, respectively. Using the obtained PBRs, the base course layer thickness of biaxial and triaxial geogrid-reinforced pavement sections reduced by nearly 5 to 8%.

6.1.2.3. Effective Base Layer Coefficient

By reinforcing the test sections with biaxial and triaxial geogrids, an effective layer coefficient can be used. The effective base course structural coefficient represents an adjustment to the standard base course coefficients used in AASHTO 1993 design method. Similar to other two previously mentioned design methods, effective structural numbers suggested for triaxial geogrid-reinforced sections were more than the companion biaxial geogrid-reinforced sections.

- While the real structural number for the aggregate base materials in this study was 0.12, the average effective structural number for biaxial and triaxial geogrid-reinforced base layers were 0.16 and 0.18, respectively, for 40.6 (16 in) thick base layer sections.
- The effective structural coefficient averagely increased to 0.15 and 0.17 when biaxial and triaxial geogrids, respectively, were used to reinforce the 30.5 cm (12 in) thick aggregate base layer test sections.

6.2. Recommendations

This study has been focused on the laboratory evaluation of biaxial and triaxial geogrid-reinforced flexible pavements. Based on the findings of this investigation, the following

recommendations are made for the future studies on the inclusion of geogrid in flexible pavements:

- Laboratory study of geogrid-reinforced flexible pavement sections with base layer thicknesses of less than 30.5 cm (12 in).
- Large scale field study to obtain correlations between field and laboratory results.
- Laboratory and field studies for biaxial and triaxial geogrid-reinforced unpaved sections.

APPENDIX I

As described in Chapter 5, the Traffic Benefit Ratio is defined as the ratio of the number of passes necessary to reach a given rutting depth for a section containing reinforcement and the number of passes necessary to reach the same rutting depth for an unreinforced section with the same base thickness and subgrade properties. TBR calculation process for the studied pavement sections is explained here and the results are shown in Table I-1.

The first column of Table I-1 is rutting depths of 4, 5, 6, 7, 8, 9, and 10 mm. For each test section, number of loading cycles applied to reach to a specific rutting depth was provided. By dividing the reinforced section's number of loadings to unreinforced number of the loadings required to reach to a specific rutting depth, Traffic Benefit Ratio was obtained. For example, test section B12, which is a biaxial-reinforced section with base layer thickness of 30.5 cm (12 in), required 786,500 loading cycles for the rutting depth of 7 mm. The unreinforced test section with the same base thickness, which is C12, needed 363,000 loading cycles for the rutting depth of 7 mm. Hence, TBR of B12 test section at the rutting depth of 7 mm was 786,500 divided by 363,000 which is 2.2 (see table I-1, column B12).

Table I.1: TBR calculation

Rutting Depth	C16		B16		T16		C12		B12		T12	
	No. of cycles	No. of cycles	TBR	No. of cycles	TBR	No. of cycles	No. of cycles	TBR	No. of cycles	TBR	No. of cycles	TBR
4mm	60,500	181,500	3.0	242,000	4.0	---	60,500	---	121,000	---	---	---
5mm	121,000	363,000	3.0	605,000	5.0	60,500	181,500	3.0	242,000	4.0	---	---
6mm	242,000	726,000	3.0	1,815,000	7.5	121,000	363,000	3.0	484,000	4.0	---	---
7mm	544,500	1,452,000	2.7	---	---	363,000	786,500	2.2	1,089,000	3.0	---	---
8mm	1,149,500	2,964,500	2.6	---	---	847,000	1,452,000	1.7	1,875,500	2.2	---	---
9mm	2,117,500	---	---	---	---	1,573,000	2,420,000	1.5	---	---	---	---
10mm	---	---	---	---	---	2,783,000	---	---	---	---	---	---

APPENDIX II

Base Course Reduction Factor (BCR), for B12 test section at the rutting depth of 7 mm is calculated here as an example for the BCRs provided in Table 5.3.

As mentioned in Section 5.3.2.3, in order to calculate the BCR of a geogrid-reinforced test section (B12), W_{t18} for the unreinforced section with the same base layer thickness (C12) was calculated as the first step.

The total number of 18-kip (80-kN) single-axle load applications was estimated by Equation 5-2 suggested by (AASHTO, AASHTO Guide for Design of Pavement Structures, 1993):

$$\log W_{t18} = 9.36 \log(SN + 1) - 0.20 + \frac{\log \left[\frac{\Delta PSI}{4.2 - 1.5} \right]}{0.4 + \frac{1094}{(SN + 1)^{5.19}}} + 2.32 \times \log M_r - 8.07$$

In the above equation, W_{t18} is the total number of 18-kip (80 kN) single-axle load applications, and ΔPSI is the difference between the initial design serviceability index and the design terminal serviceability index which is assumed 1.5 in this study. M_r is resilient modulus of the subgrade soil which is obtained from Equation 5-3 suggested by NDOT:

$$M_r = 145 \times 10^{0.0147 \times R\text{-Value} + 1.23}$$

R-value of the subgrade soil is 40. The resilient modulus of the subgrade soil (M_r) is

$$M_r = 145 \times 10^{(0.0147 \times 40) + 1.23} = 9536 \text{ psi}$$

The Structural Number (SN) used in Equation 5-2, is defined as:

$$SN = a_1 D_1 + a_2 D_2 m_2$$

Where D_1 and D_2 are the thickness of the HMA and base layer in inch unit, which is 3 and 12 inches, respectively, for the C12 test section. a_1 , layer coefficient for the HMA layer, is 0.34 based on the correlation suggested by (Van Til, McCullough, Vallerga, & Hicks, 1972) shown in Figure II-1.

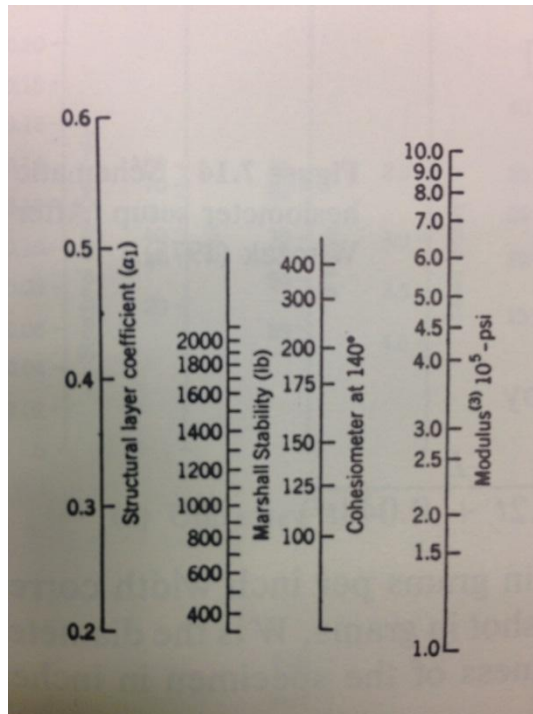


Figure II.1: HMA layer coefficient

According to HMA properties provided in Table 3.3, the modulus of HMA was 260 Ksi, and based on the above correlation, the structural coefficient (a_1) became 0.34.

a_2 is the layer coefficient of the aggregate base layer. The correlation of CBR and layer coefficient for untreated base layers, suggested by (Van Til, McCullough, Vallerga, & Hicks, 1972), is used to calculate a_2 (Figure II-2).

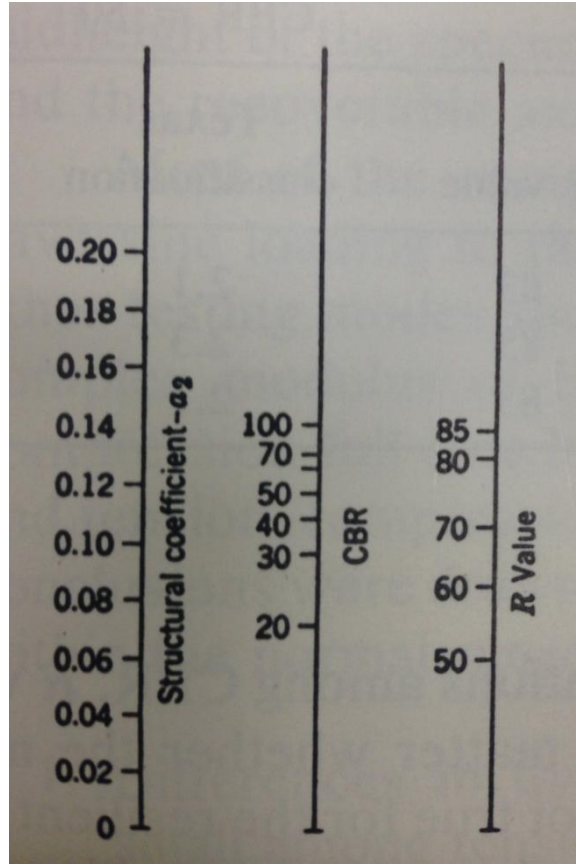


Figure II.2: Base layer coefficient

The R-value of the aggregate base is 77 (Table 3.2) and above correlation, suggested a_2 of 0.12 for the base layer.

m_2 is the drainage coefficient of the base course and it was assumed 1.0 in this investigation because the test sections were laboratory controlled.

Having D_1 , D_2 , a_1 , a_2 , and m_2 values available and using Equation 5-1, the Structural Number for C12 test section is calculated:

$$SN = a_1 D_1 + a_2 D_2 m_2 = 0.34 \times 3 + 0.12 \times 12 \times 1 = 2.46$$

Now W_{t18} for C12 test section can be calculated:

$$\begin{aligned} \log W_{t18} &= 9.36 \log(2.46 + 1) - 0.20 + \frac{\log \left[\frac{1.5}{4.2 - 1.5} \right]}{0.4 + \frac{1094}{(2.46 + 1)^{5.19}}} + 2.32 \times \log 9536 - 8.07 \\ &= 5.8887 \\ &\rightarrow W_{t18} = 10^{5.8887} = 774,005 \end{aligned}$$

Meaning that, the unreinforced test section with base layer thickness of 30.5 cm (12 in) could have 774,005 18-kip (80 kN) single-axle load applications before the resurfacing maintenance is required.

Calculation of BCR for B12 test section at the rutting depth of 7 mm was the goal of this example. Traffic Benefit Ratio for the B12 test section at rutting depth of 7 mm is 2.2, as shown in Table 5.1. By dividing the W_{t18} of C12 test section by the TBR value of B12 test section, the reinforced W_{t18} ($ESAL_r$) was obtained:

$$\frac{774,005}{2.2} = 351,820$$

Reinforced W_{t18} values was used to back calculate the structural number and then, the new base course depth.

$$\log 351,820 = 5.5463$$

Using Equation 5-2:

$$5.5463 = 9.36 \log(SN + 1) - 0.20 + \frac{\log \frac{1.5}{4.2 - 1.5}}{0.4 + \frac{1094}{(SN + 1)^{5.19}}} + 2.32 \times \log(9536) - 8.07$$

$$\rightarrow SN = 2.1490$$

So the structural number for the reinforced test section was 2.1490. The layer coefficients for the HMA and base layer were 0.34 and 0.12, respectively. The HMA thickness was 3 inches and the drainage coefficient (m_2) was 1.0. Having all these values, the reinforced base layer thickness was evaluated through Equation 5-1:

$$SN = a_1 D_1 + a_2 D_2 m_2 \rightarrow 2.1490 = 0.34 \times 3 + 0.12 \times x \times 1 \rightarrow x = 9.41 \text{ in}$$

Therefore, the base layer thickness for the reinforced test section was 9.41 inches which is shown in Table 5.3. By dividing the reinforced base layer thickness to the unreinforced base layer thickness, the Base Course Reduction (BCR) Factor was obtained:

$$\frac{9.41}{12} = 0.78$$

In other words, by reinforcing the C12 test section with biaxial geogrid, the base layer thickness can be reduced from 12 to 9.41 inches. The base course reduction percentage can also be calculated:

$$\frac{(12 - 9.41)}{12} = 21.6 \%$$

Same calculation process was carried out for all other test sections and rutting depths. The results are shown in Table II-1.

Test Section	Rutting Depth	TBR	Wt	Log(Wt)	Mr	ΔPSI	SN	a ₁	D ₁ (in)	a ₂	m ₁	D ₂ (in)	Base Course Reduction	Reduction Percentage
C16	-	1	2,176,581	6.33777	9536	1.5	2.94	0.34	3	0.12	1	16	---	---
B16	4mm	3	725,527	5.86065	9536	1.5	2.433	0.34	3	0.12	1	11.775	0.74	26.41
B16	5mm	3	725,527	5.86065	9536	1.5	2.433	0.34	3	0.12	1	11.775	0.74	26.41
B16	6mm	3	725,527	5.86065	9536	1.5	2.433	0.34	3	0.12	1	11.775	0.74	26.41
B16	7mm	2.7	806,141	5.90641	9536	1.5	2.477	0.34	3	0.12	1	12.145	0.76	24.09
B16	8mm	2.6	837,146	5.92280	9536	1.5	2.494	0.34	3	0.12	1	12.28	0.77	23.25
T16	4mm	4	544,145	5.73571	9536	1.5	2.316	0.34	3	0.12	1	10.8	0.68	32.50
T16	5mm	5	435,316	5.63880	9536	1.5	2.229	0.34	3	0.12	1	10.075	0.63	37.03
T16	6mm	7.5	290,211	5.46271	9536	1.5	2.079	0.34	3	0.12	1	8.825	0.55	44.84
C12	-	1	774,005	5.88874	9536	1.5	2.46	0.34	3	0.12	1	12	---	---
B12	5mm	3	258,002	5.41162	9536	1.5	2.038	0.34	3	0.12	1	8.48	0.71	29.33
B12	6mm	3	258,002	5.41162	9536	1.5	2.038	0.34	3	0.12	1	8.48	0.71	29.33
B12	7mm	2.2	351,820	5.54632	9536	1.5	2.149	0.34	3	0.12	1	9.41	0.78	21.58
B12	8mm	1.7	455,297	5.65829	9536	1.5	2.246	0.34	3	0.12	1	10.22	0.85	14.83
B12	9mm	1.5	516,003	5.71265	9536	1.5	2.296	0.34	3	0.12	1	10.63	0.89	11.42
T12	5mm	4	193,501	5.28668	9536	1.5	1.939	0.34	3	0.12	1	7.66	0.64	36.17
T12	6mm	4	193,501	5.28668	9536	1.5	1.939	0.34	3	0.12	1	7.66	0.64	36.17
T12	7mm	3	258,002	5.41162	9536	1.5	2.038	0.34	3	0.12	1	8.48	0.71	29.33
T12	8mm	2.2	351,820	5.54632	9536	1.5	2.149	0.34	3	0.12	1	9.41	0.78	21.58

APPENDIX III

For demonstration purpose, the calculation process used to obtain the effective base layer coefficient of the B12 test section at rutting depth of 7 mm is presented in Appendix III. The calculation of the effective structural coefficient was same as BCR method. At first, the W_{t18} for C12 test section was needed. With the same explanation provided in Appendix II, W_{t18} for C12 test section was 774,005.

The TBR for B12 test section at the rutting depth of 7 mm is 2.2 (Table 5.1). Therefore, the reinforced W_{t18} became:

$$774,005 \times 2.2 = 1,702,811$$

Reinforced W_{t18} values were used to back calculate to determine the structural number and then, the new base layer coefficient.

$$\log 1,702,811 = 6.2312$$

$$6.2312 = 9.36 \log(SN + 1) - 0.20 + \frac{\log \frac{1.5}{4.2 - 1.5}}{0.4 + \frac{1094}{(SN + 1)^{5.19}}} + 2.32 \times \log(9536) - 8.07$$

$$\rightarrow SN = 2.8177$$

Therefore, the structural number for the reinforced test section was determined to be 2.8177. The layer coefficient for the HMA is 0.34. The HMA and base layer thicknesses are 3 and 12 inches, respectively, and the drainage coefficient (m_2) is 1.0. Having all these values, the effective base layer coefficient can be calculated through Equation 5-1:

$$SN = a_1D_1 + a_2D_2m_2 \rightarrow 2.8177 = 0.34 \times 3 + x \times 12 \times 1 \rightarrow x = 0.15$$

Hence, the effective base layer coefficient for the B12 test section was 0.15. In other words, by reinforcing the C12 test section with a layer of biaxial geogrid, the base layer coefficient increased from 0.12 to 0.15.

A similar calculation process was carried out for other test sections and rutting depths. The results are shown in Table III-1.

	Rut depth	TBR	Wt18	Log(Wt)	Mr	Δ PSI	SN	D ₁ (in)	a ₁	D ₂ (in)	m ₂	Effective layer coeff.
C16	---	1	2,176,581	6.33777	9536	1.5	2.94	3	0.34	16	1	0.12
B16	4mm	3	6,529,742	6.8149	9536	1.5	3.556	3	0.34	16	1	0.1585
B16	5mm	3	6,529,742	6.8149	9536	1.5	3.556	3	0.34	16	1	0.1585
B16	6mm	3	6,529,742	6.8149	9536	1.5	3.556	3	0.34	16	1	0.1585
B16	7mm	2.7	5,876,768	6.76914	9536	1.5	3.492	3	0.34	16	1	0.1545
B16	8mm	2.6	5,659,110	6.75275	9536	1.5	3.468	3	0.34	16	1	0.153
T16	4mm	4	8,706,323	6.93983	9536	1.5	3.74	3	0.34	16	1	0.17
T16	5mm	5	10,882,903	7.03674	9536	1.5	3.876	3	0.34	16	1	0.1785
T16	6mm	7.5	16,324,355	7.21284	9536	1.5	4.148	3	0.34	16	1	0.1955
C12	---	1	774,005	5.88874	9536	1.5	2.46	3	0.34	12	1	0.12
B12	5mm	3	2,322,015	6.36587	9536	1.5	2.976	3	0.34	12	1	0.163
B12	6mm	3	2,322,015	6.36587	9536	1.5	2.976	3	0.34	12	1	0.163
B12	7mm	2.2	1,702,811	6.23117	9536	1.5	2.82	3	0.34	12	1	0.15
B12	8mm	1.7	1,315,809	6.11919	9536	1.5	2.7	3	0.34	12	1	0.14
B12	9mm	1.5	1,161,008	6.06484	9536	1.5	2.64	3	0.34	12	1	0.135
T12	5mm	4	3,096,020	6.4908	9536	1.5	3.126	3	0.34	12	1	0.1755
T12	6mm	4	3,096,020	6.4908	9536	1.5	3.126	3	0.34	12	1	0.1755
T12	7mm	3	2,322,015	6.36587	9536	1.5	2.974	3	0.34	12	1	0.1628
T12	8mm	2.2	1,702,811	6.23117	9536	1.5	2.82	3	0.34	12	1	0.15

APPENDIX IV

The SpectraPave4-PRO software inputs are aggregate base and HMA layers thicknesses, layer coefficients, subgrade resilient modulus, and geogrid type. The output of the software is the effective layer coefficient. The biaxial geogrid utilized in this study (BX1100), was available to be chosen as “BX Type 1” in the software, but unfortunately the triaxial geogrid (TX130s) was not recognized by the program. However, the properties of “TX5” category in SpectraPave4-PRO, was similar to TX130s geogrid and it was chosen instead. The software input and output data are shown in Figures IV-1 through IV-4. As can be seen, the software suggested base layer coefficient of 0.124 for the test sections with 40.6 cm (16 in) of base layer thickness and biaxial geogrid reinforcement. Also, base layer coefficient of 0.165 was proposed for triaxial geogrid-reinforced test sections with the same base layer thickness. Figure IV-3 illustrates the software response to biaxial geogrid reinforcement of 30.5 cm (12 in) thick base layer pavements. The software suggested effective layer coefficient of 0.135. SpectraPave4-PRO suggested layer coefficient of 0.18 for triaxial geogrid-reinforced sections with 30.5 cm (12 in) base layer thickness. All these values are also shown in Table 5.4 and compared with the calculated effective layer coefficients.

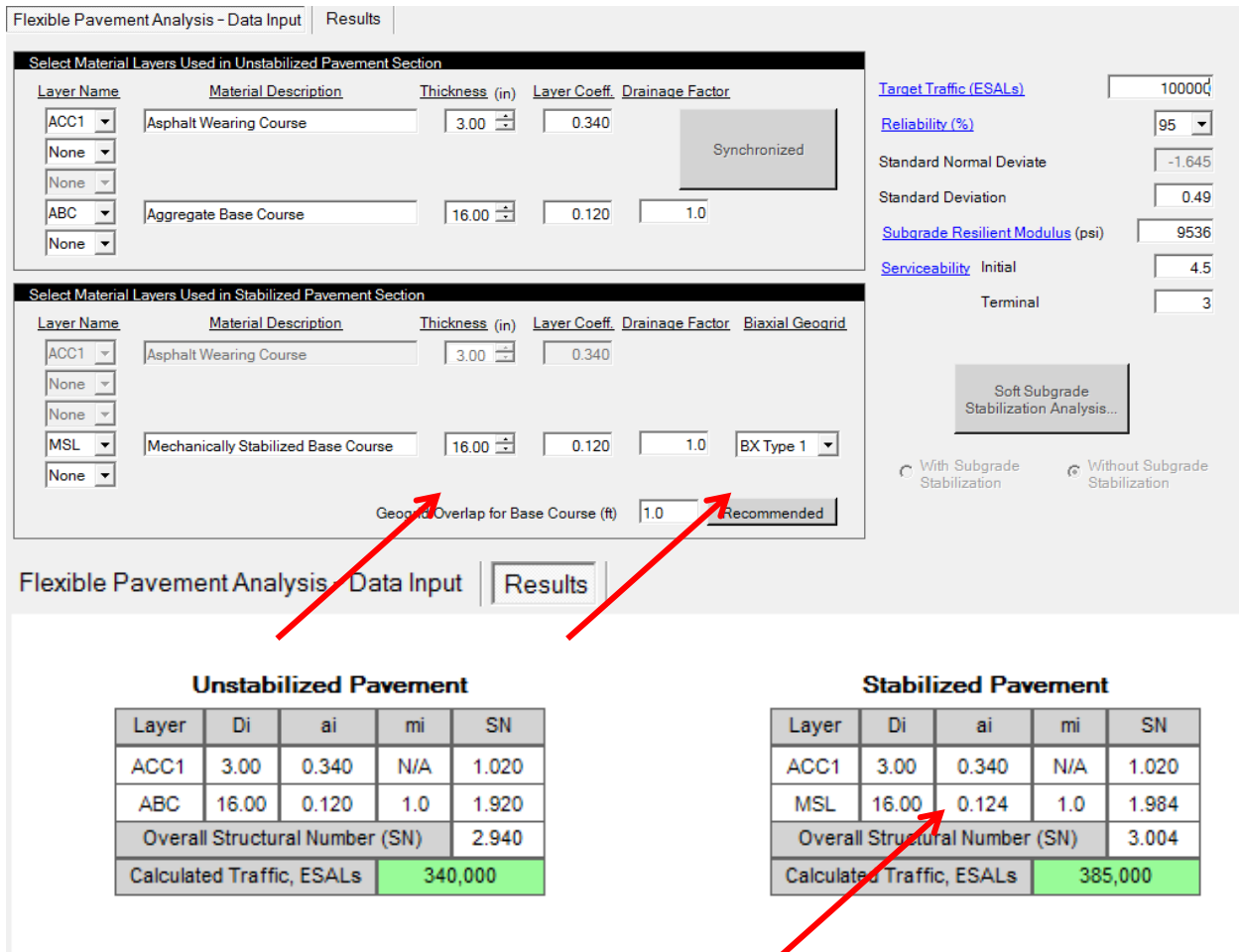


Figure IV.1: SpectraPave4-PRO software response to B16 test section

Pavement Optimization Design Analysis - Data Input | Results

Select Material Layers Used in Unstabilized Pavement Section

Layer Name	Material Description	Thickness (in)	Layer Coeff.	Drainage Factor
ACC1	Asphalt Wearing Course	3.00	0.340	
None				
None				
ABC	Aggregate Base Course	16.00	0.120	1.0
None				

Select Material Layers Used in Stabilized Pavement Section

Layer Name	Material Description	Thickness (in)	Layer Coeff.	Drainage Factor	TriAx Geogrid
ACC1	Asphalt Wearing Course	3.00	0.340		
None					
None					
MSL	Mechanically Stabilized Base Course	16.00	0.120	1.0	TX5
None					

Geogrid Overlap for Base Course (ft) 1.0

Target Traffic (ESALs) 1000000
 Reliability (%) 95
 Standard Normal Deviate -1.645
 Standard Deviation 0.49
 Subgrade Resilient Modulus (psi) 9536
 Serviceability Initial 4.5
 Terminal 3

With Subgrade Stabilization Without Subgrade Stabilization

Pavement Optimization Design Analysis - Data Input | Results

Unstabilized Pavement

Layer	Di	ai	mi	SN
ACC1	3.00	0.340	N/A	1.020
ABC	16.00	0.120	1.0	1.920
Overall Structural Number (SN)				2.940
Calculated Traffic, ESALs				340,000

Stabilized Pavement

Layer	Di	ai	mi	SN
ACC1	3.00	0.340	N/A	1.020
MSL	16.00	0.165	1.0	2.640
Overall Structural Number (SN)				3.660
Calculated Traffic, ESALs				1,206,000

Figure IV.2: SpectraPave4-PRO software response to T16 test section

Flexible Pavement Analysis - Data Input | Results

Select Material Layers Used in Unstabilized Pavement Section

Layer Name	Material Description	Thickness (in)	Layer Coeff.	Drainage Factor
ACC1	Asphalt Wearing Course	3.00	0.340	
None				
None				
ABC	Aggregate Base Course	12.00	0.120	1.0
None				

Select Material Layers Used in Stabilized Pavement Section

Layer Name	Material Description	Thickness (in)	Layer Coeff.	Drainage Factor	Biaxial Geogrid
ACC1	Asphalt Wearing Course	3.00	0.340		
None					
None					
MSL	Mechanically Stabilized Base Course	12.00	0.120	1.0	BX Type 1
None					

Geogrid Overlap for Base Course (ft) 1.0 Recommended

Target Traffic (ESALs) 100000
 Reliability (%) 95
 Standard Normal Deviate -1.645
 Standard Deviation 0.49
 Subgrade Resilient Modulus (psi) 9536
 Serviceability Initial 4.5
 Terminal

Soft Subgrade Stabilization Analysis...
 With Subgrade Stabilization Without Subgrade Stabilization

Flexible Pavement Analysis - Data Input | Results

Unstabilized Pavement

Layer	Di	ai	mi	SN
ACC1	3.00	0.340	N/A	1.020
ABC	12.00	0.120	1.0	1.440
Overall Structural Number (SN)				2.460
Calculated Traffic, ESALs		121,000		

Stabilized Pavement

Layer	Di	ai	mi	SN
ACC1	3.00	0.340	N/A	1.020
MSL	12.00	0.135	1.0	1.620
Overall Structural Number (SN)				2.640
Calculated Traffic, ESALs		183,000		

Figure IV.3: SpectraPave4-PRO software response to B12 test section

Pavement Optimization Design Analysis - Data Input | Results

Select Material Layers Used in Unstabilized Pavement Section

Layer Name	Material Description	Thickness (in)	Layer Coeff.	Drainage Factor
ACC1	Asphalt Wearing Course	3.00	0.340	
None				
None				
ABC	Aggregate Base Course	12.00	0.120	1.0
None				

Select Material Layers Used in Stabilized Pavement Section

Layer Name	Material Description	Thickness (in)	Layer Coeff.	Drainage Factor	TriAx Geogrid
ACC1	Asphalt Wearing Course	3.00	0.340		
None					
None					
MSL	Mechanically Stabilized Base Course	12.00	0.120	1.0	TX5
None					

Geogrid Overlap for Base Course (ft) 1.0

Target Traffic (ESALs) 1000000
 Reliability (%) 95
 Standard Normal Deviate -1.645
 Standard Deviation 0.49
 Subgrade Resilient Modulus (psi) 9536
 Serviceability Initial 4.5
 Terminal 3

With Subgrade Stabilization Without Subgrade Stabilization

Pavement Optimization Design Analysis - Data Input | Results

Unstabilized Pavement

Layer	Di	ai	mi	SN
ACC1	3.00	0.340	N/A	1.020
ABC	12.00	0.120	1.0	1.440
Overall Structural Number (SN)				2.460
Calculated Traffic, ESALs				121,000

Stabilized Pavement

Layer	Di	ai	mi	SN
ACC1	3.00	0.340	N/A	1.020
MSL	12.00	0.180	1.0	2.160
Overall Structural Number (SN)				3.180
Calculated Traffic, ESALs				535,000

Figure IV.4: SpectraPave4-PRO software response to T12 test section

REFERENCES

- (NDOT), N. D. (2011). *Uniform Standard Specifications*. Clark County Area.
- AASHTO. (1993). *AASHTO Guide for Design of Pavement Structures*. Washington, D.C: American Association of State Highway and Transportation Officials.
- AASHTO. (2009). *Standard Practice for Geosynthetic Reinforcement of the Aggregate Base Course of Flexible Pavement Structures*. Washington, D.C.: American Association of State Highway and Transportation Officials.
- Abd El Halim, A., Haas, R., & Chang, W. (1983). Geogrid reinforcement of asphalt pavements and verification of elastic layer theory. *Transp.Res.Rec.*(949), 55-65.
- Abu-Farsakh, M. Y., & Chen, Q. (2011). Evaluation of geogrid base reinforcement in flexible pavement using cyclic plate load testing. *International Journal of Pavement Engineering*, 12(03), 275- 288.
- Abu-Farsakh, M., Souci, G., Voyiadjis, G. Z., & Chen, Q. (2011). Evaluation of factors affecting the performance of geogrid-reinforced granular base material using repeated load triaxial tests. *Journal of Materials in Civil Engineering*, 24(1), 72- 83.
- Al-Qadi, I., Brandon, T., Valentine, R., Lacina, B., & Smith, T. (1994). Laboratory evaluation of geosynthetic-reinforced pavement sections. *Transportation Research Record 1439*, 21(2), 25-31.
- Al-Qadi, I., Dessouky, S., Kwon, J., & Tutumluer, E. (2008). Geogrid in flexible pavements: validated mechanics. *Transportation Research Record: Journal of the Transportation Board*, 2045, 102-109.
- Al-Qadi, I., Dessouky, S., Kwon, J., & Tutumluer, E. (2012, September). Geogrid-Reinforced Low-Volume Flexible Pavements: Pavement Response and Geogrid Optimal Location . *Journal of Transportation Engineering* , 138(9), 1083-1090.
- Al-Qadi, I., Dessouky, S., Tutumluer, E., & Kwon, J. (2011, April). Geogrid mechanism in low-volume flexible pavements: accelerated testing of full-scale heavily instrumented pavement sections. *International Journal of Pavement Engineering* , 12(2), 121-135.
- Aran, S. (2006). Base reinforcement with biaxial geogrid-long term performance. *Transportation Research Board 1975*, 115-123.

- ArchiEXPO. (2015). *Geomembranes*. Retrieved from THE ONLINE ARCHITECTURE AND DESIGN EXHIBITION: <http://www.archiexpo.com/architecture-design-manufacturer/geomembrane-3830.html>
- ArchiExpo. (2015). *Products*. Retrieved from Tensar: <http://www.archiexpo.com/prod/tensar-international/product-63203-245808.html>
- Barksdale , R., Brown, S., & Chan, F. (1989). *Potential Benefits of Geosynthetics in Flexible Pavement Systems*. National Cooperative Highway Research Program Report No 315, Transportation Research Board. Washigton D.C, USA: National Research Council.
- Bender, D. A., & Barenberg, E. J. (1978). Design and behavior of soil-fabric-aggregate systems. (671).
- Berg, R. R., Christopher, B. R., & Perkins, S. W. (2000). Geosynthetic reinforcement of the aggregate base course of flexible pavement structures. *GMA White Paper II, Geosynthetic Materials Association, Roseville, MN, USA, 130p*.
- Berg, R., & Association, G. M. (2000). *Geosynthetic reinforcement of the aggregate base/subbase courses of pavement structures*. Geosynthetic Materials Association. Retrieved from <http://www.textileconnect.com/documents/resources/WPIIFINALGMA.pdf>
- Bhatia, S., & Smith, J. (1996). Geotextile characterization and pore-size distribution: Part I. A review of manufacturing processes. *Geosynthetics International*, 3(1), 85-105.
- Binquet, J., & Lee, K. L. (1975). Bearing capacity analysis of reinforced earth slabs. *Journal of the geotechnical Engineering Division*, 101(12), 1257-1276.
- Bouazza, A., & Avalue, D. L. (2006). Effectiveness of rolling dynamic compaction on an old waste tip. *ISSMGE 5th International Congress on Environmental Geotechnics, Cardiff*, (pp. 1-7).
- Button, J., & Lytton, R. (2015). Guidelines for using geosynthetics with hot-mix asphalt overlays to reduce reflective cracking. *Transportation Research Record: Journal of the Transportation Research Board*.
- Cancelli, A., & Montanelli, F. (1999). In-ground test for geosynthetic reinforced flexible paved roads. *Proceedings of the Conference Geosynthetics '99* (pp. 863-878). Roseville, Minnesota, USA : IFAI.
- Carroll, R., Walls, J., & Haas, R. (1987). Granular base reinforcement of flexible pavements using geogrids. *Proceedings of Geosynthetics* (pp. 46-57). St Paul, Minnesota, USA: IFAI.

- Chen, Q., Abu-Farsakh, M., & Tao, M. (2009). Laboratory Evaluation of Geogrid Base Reinforcement and Corresponding Instrumentation Program. *Geotechnical Testing Journal*, 32(6).
- Cox, B., McCartney, J., Wood, C., & Curry, B. (2010). Performance evaluation of full-scale geosynthetic-reinforced flexible pavements using field cyclic plate load tests. *TRB 2010 Annual Meeting (CD-ROM)*, Transportation Research Board. Washington D.C, USA.
- Das, B. (2010). Use of Geogrid in Subgrade-Ballast System of Railroads Subjected to Cyclic Loading for Reducing Maintenance. *California State University, Sacramento, USA*.
- Dong, Y., Han, J., & Bai, X. (2010). A numerical study on the stress-strain responses of biaxial geogrids under tension at different directions. *ASCE G-I GeoFlorida Conference*.
- Dong, Y.-L., Han, J., & Bai, X.-H. (2011). Numerical analysis of tensile behavior of geogrids with rectangular and triangular apertures. *Geotextiles and Geomembranes*, 29(2), 83-91.
- Duncan-Williams, E., & Attoh-Okine, N. (2008). Effect of geogrid in granular base strength - An experimental investigation. *Journal of Construction and Building Materials*, 22, 2180-2184.
- Giroud, J., & Han, J. (2004). Design method for geogrid-reinforced unpaved roads. I: Development of design method. *Journal of Geotechnical and Geoenvironmental Engineering*, 130(8), 775-786.
- Giroud, J., & Noiray, L. (1981). Geotextile-reinforced unpaved road design. *Journal of Geotechnical Engineering*, 107(9), 1233-1254.
- Giroud, J.-P. (1984). *Geotextiles and Geomembranes definitions, Properties and design. Selected Papers, Revisions and Comments*.
- Göbel, C. H., Weisemann, U. C., & Kirschner, R. A. (1994). Effectiveness of a reinforcing geogrid in a railway subbase under dynamic loads. *Geotextiles and Geomembranes*, 13(2), 91-99.
- Haas, R., Wall, J., & Carroll, R. (1988). Geogrid reinforcement of granular bases in flexible pavements. *Transportation Research Record 1188*, 19-27.
- Helstrom, C., Humphrey, D., & Hayden, S. (2007). Geogrid reinforced pavement structure in a cold region. *Proceedings of the 13th International Conference on Cold Regions Engineering*, (pp. 1- 12).
- Henry, K. S. (1999). *Geotextile Reinforcement of Low-Bearing-Capacity Soils. Comparison of Two Design Methods Applicable to Thawing Soils*.

- Henry, K., Clapp, J., Davids, W., Humphrey, D., & Barna, L. (2009). *Structural improvements of flexible pavements using geosynthetics for base course reinforcement*. U.S. Army Corps of Engineers in conjunction with U.S. Department of Transportation, Pooled Fund, Federal Highway Administration, McLean, Virginia, USA.
- Hillier, S. a. (2008). *Bentonites*. Retrieved from The James Hutton Institute:
<http://www.claysandminerals.com/materials/bentonites>
- Holz, R., Christopher, B. R., & Berg, R. R. (1998). *Geosynthetic design and construction guidelines*.
- Inversiones, I. (2011). *Geomallas Uniaxiales*. Retrieved from Products:
<http://www.icainversiones.com/?cat=1013&title=Geomallas%20Uniaxiales%20&lang=es>
- Jersey, S., Tingle, J., Norwood, G., Kwon, J., & Wayne, M. (2012). Full-Scale Evaluation of Geogrid-Reinforced Thin Flexible Pavements . *Transportation Research Record: Journal of the Transportation Research Board*(2310), 61-71.
- Knapton, J., & Barber, S. (1979). THE BEHAVIOUR OF A CONCRETE BLOCK PAVEMENT. *ICE Proceedings*, 66, pp. 277-292.
- Koerner, R. M. (2015). *Designing with geosynthetics*. Xlibris Corporation.
- Koerner, R. M., & Soong, T.-Y. (2005). Analysis and design of veneer cover soils. *Geosynthetics International*, 12(1), 28-49.
- Kwon, J. (2007). Development of a mechanistic model for geogrid reinforced flexible pavements. *Dissertation Abstracts International*, 68(06).
- Kwon, J., Tutumluer, E., & Al-Qadi, I. L. (2009). Validated mechanistic model for geogrid base reinforced flexible pavements. *Journal of Transportation Engineering*.
- Leng, J., Ju, T., & Gabr, M. (2002). Characteristics of geogrid-reinforced aggregate under cyclic load . *Transportation Research Record* 1786, 29-35.
- Love, J., Burd, H., Milligan, G., & Houlsby, G. (1987). Analytical and model studies of reinforcement of a layer of granular fill on a soft clay subgrade. *Canadian Geotechnical Journal*, 24(4), 611-622.
- McCartney, J., Cox, B., Wood, C., & Curry, B. (2010). Evaluation of Geosynthetic-Reinforced Flexible Pavements using Static Plate Load Tests. *9th International Conference on Geosynthetics - Geosynthetics: Advanced Solutions for a Challenging World*, (pp. 1445-1450).

- Meccai, K. A., & Al Hasan, E. (2004). Geotextiles in transportation applications. *Proc. 2nd Gulf Conference on 'Roads*, (pp. 1-13).
- Moghaddas-Nejad, F., & Small, J. C. (2003). Resilient and permanent characteristics of reinforced granular materials by repeated load triaxial tests. *ASTM geotechnical testing journal*, 26(2), 152- 166.
- Montanelli, F., Zhao, A., & Rimoldi, P. (1997). Geosynthetic-Reinforced Pavement System: Testing and Design. *Proceedings of Geosynthetics '97. IFAI*, 2, pp. 619-632. Long Beach, California, USA.
- Morian, N. E. (2007). *Effect of geotextile fabrics on reflective cracking of hot mix asphalt overlays in Washoe County, Nevada*. University of Nevada, Reno.
- Nazzal, M. (2007). *Laboratory Characterization and Numerical Modeling of Geogrid Reinforced Bases in Flexible Pavements*. PhD Dissertation, Louisiana State University and Agricultural and Mechanical College, USA, Department of Civil Engineering.
- Palmeira, E. M., & Milligan, G. W. (1989). Large scale direct shear tests on reinforced soil. *土質工学会論文報告集*, 29(1), 18-30.
- Perkins , S. (1999). Mechanical response of geosynthetic-reinforced flexible pavements. *Geosynthetics International*, 6(5), 347-382.
- Perkins, S. (1999). *Geosynthetic Reinforcement of Flexible Pavements: Laboratory Based Pavement Test Sections*. Report No. FHWA/MT-99-001/8138, U.S. Department of Transportation, Federal Highway Administration, Washington D.C., USA .
- Perkins, S. (2002). *Evaluation of geosynthetic reinforced flexible pavement systems using two pavement test facilities*. Report No. FHWA/MT-02-008/20040, U.S. Department of Transportation, Federal Highway Administration, Washington D.C., USA .
- Perkins, S. W. (2001). *Mechanistic-Empirical Modeling and Design Model Development of Geosynthetic Reinforced Flexible Pavements: Final Report*. Montana Department of transportation, Helena, Montana.
- Perkins, S., Christopher, B., Cuelho, E., Eiksund, G., Hoff, I., Schwartz, C., . . . Watn, A. (2004). *Development of Design Methods for Geosynthetic Reinforced Flexible Pavements*. Report No. DTFH61-01-X-00068, U.S. Department of Transportation, Federal Highway Administration, Washington D.C., USA.
- Perkins, S., Ismerik, M., Fogelson, M., Wang, Y., & Cuelho, E. (1998). Geosynthetic-Reinforced Pavements: Overview and Preliminary Results. In Balkema (Ed.),

- Proceedings of the Fourth International Conference on Geotextiles, Geomembranes and Related Products, 1*, pp. 177-182. The Hague, The Netherlands.
- Qian, Y., Han, J., Pokharel, S., & Parsons, R. (2011). Stress Analysis on Triangular-Aperture Geogrid-Reinforced Bases over Weak Subgrade Under Cyclic Loading. *Transportation Research Record: Journal of the Transportation Research Board*(2204), 83-91.
- Saad, B., Mitri, H., & Poorooshab, H. (2006). 3D FE analysis of flexible pavement with geosynthetic reinforcement. *Journal of Transportation Engineering*, 132(5), 402-415.
- Shukla, S. K. (2002). *Geosynthetics and their applications*. Thomas Telford.
- Stadler, A. T. (2001). *Geogrid Reinforcement of Piedmont Residual Soil*. Charlotte: North Carolina Department of Transportation.
- Staff, C. C. (2012). *Roads and Highways*. Retrieved from Stabilizing Roads: <http://www.concreteconstruction.net/roads-and-highways/stabilizing-roads.aspx>
- (2004). *Standard Terminology for Geosynthetics*. American Society for Testing and Materials. ASTM International.
- (2013). *Standard Test Method for Index Puncture Resistance of Geomembranes and Related Products*. West Conshohocken, PA: ASTM International.
- (2014). *Standard Test Method for Stiffness of Fabrics*. West Conshohocken, PA: ASTM International.
- (2012). *Standard Test Methods for Linear Density of Textile Fibers*. West Conshohocken, PA: ASTM International.
- Stormont, J. C., Henry, K. S., & Evans, T. (1997). Water retention functions of four nonwoven polypropylene geotextiles. *Geosynthetics International*, 4(6), 661-672.
- Tensar. (2015). *Rib Testing*. Retrieved from TriAx: <http://www.tensar.co.uk/site/scientificall-proven/Rib-testing.aspx>
- Tensar. (2015). *RoadDrain™ Roadway Drainage System*. Retrieved from <http://www.tensarcorp.com/>: <http://www.tensarcorp.com/Systems-and-Products/Roadrain-roadway-drainage-system>
- Tensar. (2015). *Tensar Biaxial BX geogrids*. Retrieved from Tensar: <http://www.tensarcorp.com/Systems-and-Products/Tensar-geogrids/Tensar-Biaxial-BX-geogrids>

- Tensar. (2015). *Tensar TriAx (TX) Geogrids*. Retrieved from Tensar:
<http://www.tensarcorp.com/Systems-and-Products/Tensar-geogrids/Tensar-Triax-geogrid>
- Thompson, N. E. (2009). Small soil column investigation of soil-geotextile capillary barrier systems.
- Tingle, J., & Webster, S. (2003). Corps of Engineers Design of Geosynthetic-Reinforced Unpaved Roads. *Transportation Research Record: Journal of the Transportation Research Board*(1849), 193- 201.
- USFabrics. (2015). *Geotextiles, Geogrids & Geomembranes for the construction industry*. Retrieved from Geotextiles: <http://www.usfabricsinc.com/products/geotextiles>
- Uzan, J. (2004). Permanent deformation in flexible pavements. *Journal of Transportation Engineering*, 130(1), 6-13.
- Van Til, C., McCullough, B., Vallerga, B., & Hicks, R. (1972). NCHRP Report 128: Evaluation of AASHTO Interim Guides for Design of Pavement Structures. *Transportation Research Board, Washington, DC*.
- Wathugala, G., & Desai, C. (1993). Constitutive model for cyclic behavior of clays. I: Theory. *Journal of Geotechnical Engineering*, 119(4), 714-729.
- Wathugala, G., Huang, B., & Pal, S. (1996). Numerical simulation of geosynthetic-reinforced flexible pavements. *Transportation Research Record: Journal of the Transportation Research Board*(1534), 58-65.
- Webster, S. (1993). *Geogrid Reinforced Base Course for Flexible Pavements for Light Aircraft, Test Section Construction, Behavior under Traffic, Laboratory Test, Design criteria*. Technical Report GL-93-6, Waterways Experiment Station, U.S Army Corps of Engineers, Vicksburg, MS, USA.
- Zornberg, J. G., & LaRocque, C. J. (2008). Technical Report Documentation Page 1. Report No.



Nevada Department of Transportation
Rudy Malfabon, P.E. Director
Ken Chambers, Research Division Chief
(775) 888-7220
kchambers@dot.nv.gov
1263 South Stewart Street
Carson City, Nevada 89712